Understanding Observed and Projected Climate Changes in the Antarctic, and their Global Impacts

Mark England

Submitted in partial fulfillment of the

requirements for the degree of

Doctor of Philosophy

in the Graduate School of Arts and Sciences

COLUMBIA UNIVERSITY

2019

ABSTRACT

Understanding Observed and Projected Climate Changes in the Antarctic, and their Global Impacts

Mark England

The Antarctic climate has undergone complex changes over the last fifty years, driven largely by stratospheric ozone depletion. By the end of this century, under the current trajectory of anthropogenic emissions, the climate of Antarctica is projected to be significantly wetter, warmer and prone to the collapse of ice shelves and loss of sea ice cover. The overarching aim of this thesis is to increase our understanding of recent and projected Antarctic climate change and its drivers. We also investigate the potential global implications of these changes and show that the effects will not be limited to the southern high latitudes.

In the first half, we investigate the drivers of Antarctic climate change over the observational period. Specifically, we study the influence of the stratosphere on the southern high latitude surface climate, through stratosphere-troposphere dynamic coupling as well as stratospheric ozone depletion. We examine the impact of these on the Amundsen Sea Low, a key circulation feature near West Antarctica. We demonstrate using reanalysis that stratospheric heat flux extremes are linked to high latitude tropospheric anomalies in the Amundsen Sea region. During extreme negative (positive) events there is a westward (eastward) shift of the Amundsen Sea Low, a warming (cooling) and increase (decrease) of geopotential height over the Amundsen and Bellingshausen Seas. We find that most CMIP5 models are not able to capture this relationship. Next, we demonstrate that, since 1965, stratospheric ozone depletion has acted to deepen the Amundsen Sea Low in austral summer by 1 hPa per decade. This result was consistent across two different comprehensive climate models, each with very different model physics and climate sensitivity. It must be noted that the ozone depletion signal on the Amundsen Sea Low is small compared to the internal climate variability in this region. Using ensembles of model integrations and analysing them over the full period of ozone depletion (which started a couple of decades before the satellite era) is necessary to detect a robust signal.

In the second half, we investigate the effects of future Antarctic climate change, specifically the effects of projected sea ice loss over the coming century. Climate model simulations are used to isolate the effect of end-of-the-century Antarctic sea ice loss which is compared and contrasted with the effects of projected Arctic sea ice loss. We first study the effects of projected Antarctic sea ice loss used atmosphere-only simulations. As for the Arctic, results indicated that Antarctic sea ice loss will act to shift the tropospheric jet equatorward, an internal negative feedback to the poleward shift associated with increased greenhouse gases. Antarctic sea ice loss is shown to have an important effect throughout the year whereas Arctic sea ice loss will have more seasonally varying impacts. Building upon these results we the use the same climate model but in a fully coupled setup to study the effects of projected Antarctic sea ice loss on the climate system. We show that both Arctic and Antarctic sea ice loss will have important global effects, causing a 'mini global warming' signal. The tropical response to Antarctic sea ice loss is shown to be remarkably similar to that of Arctic sea ice loss, with enhanced warming in the Eastern Tropical Pacific and increased precipitation throughout much of the equatorial Pacific. These results highlight how intimately coupled the Antarctic climate is to the rest of the climate system.

CONTENTS

LIST OF TABLES

LIST OF FIGURES

Frequently used Acronyms

AMOC - Atlantic Meridional Overturning Circulation

ASL - Amundsen Sea Low

CESM - Community Earth System Model

CMIP5 - Coupled Model Intercomparison Project 5

E-P - Eliassen-Palm

ITCZ - Inter Tropical Convergence Zone

NAO - North Atlantic Oscillation

NH - Northern Hemisphere

NHT - Northward Heat Transport

ODS - Ozone Depleting Substance

RCP - Representative Concentration Pathway

SAM - Southern Annular Mode

SIC - Sea Ice Concentration

SIE - Sea Ice Extent

SH - Southern Hemisphere

SST - Sea Surface Temperature

WACCM - Whole Atmosphere Community Climate Model

Acknowledgements

First and foremost, I would like to express my deep gratitude to my advisor Dr. Lorenzo Polvani. He has been a fantastic mentor and helped me make tremendous progress over the last five years. I am also very appreciative of the other members of my committee: Dr. Adam Sobel, Dr. Michael Tippett, Dr. Michael Previdi and Dr. Robin Bell.

I would like to acknowledge the important contributions by my collaborators to the different projects I have worked on whilst at Columbia: Dr. Lantao Sun, Dr. Clara Deser, Dr. Alex Jahn, Dr. Karen Smith, Dr. Tiffany Shaw, Dr. Marika Holland and Dr. Laura Landrum. I would also like to thank Dr. Tiffany Shaw for her guidance during the first year of my PhD. Additionally, I would like to thank Dr. Vineel Yettella; the experience of publishing a paper with him, as two lowly graduate students, was very rewarding. Finally, I thank my family and friends for their encouragement and support.

I would like to dedicate this work to my wife-to-be Nina,

and my wonderful parents Joan and Steven England.

I would also like to dedicate this to my four loving grandparents,

all of whom started this journey with me,

but sadly are not around to see me graduate.

CHAPTER 1

INTRODUCTION

Antarctica is the most remote, and most extreme, continent on the planet. Its landmass is larger than both Europe and the continental United States. It contains the coldest *(-89.2°C recorded at Vostok station)*, windiest *(over 200 mph at Cape Denison)* and driest *(the Dry Valleys)* places on Earth. Antarctica was first sighted as late as 1820, being the last continent to be discovered. Due to its remote and inhospitable nature, few observational records exist in the interior of the continent; Stearns et al. (1997) refer to Antarctica as Earth's "largest meteorological void". Despite these challenges, it is imperative to understand how the climate of Antarctica has changed in the recent past and will change in the future. This is particularly important because changes in the Antarctic climate can impact the lower latitudes, and may even have important global implications.

There remain many challenges in trying to detect robust climate change signals at the southern high latitudes. The paucity of observational data makes it difficult to constrain and evaluate climate model simulations. Reanalysis products, which incorporate satellite data, extend back to 1979; however, there are large, known biases over Antarctica, especially in winter (Bracegirdle and Marshall, 2012). The climate variability of Antarctica and the surrounding Southern Ocean is one of the largest on Earth (Ting et al., 2009) and so the lack of a long observational record makes the detection and interpretation of climate trends especially difficult. In addition, there are less than 20 years of systematic, high quality observations from the Southern Ocean (Riser et al., 2016). This limits our ability to understand changes in ocean circulation and ocean heat uptake and has obvious implications for studying the

Antarctic.

To improve our understanding of Antarctic climate change we utilise state-of-the-art climate model simulations in an idealised manner. This is a powerful technique which allows us to isolate one important component or driver in the complex climate system. For example, we carry out simulations with or without an ozone hole, or with and without sea ice loss, and this enables us to understand their effects on the coupled climate system. Our results must be understood with the limitations previously outlined, as well as ability of the models to realistically simulate the climate of the southern high latitudes.

In the remainder of this chapter, we first outline the major observed changes in Antarctic climate over the past fifty years (Section 1.1). To provide context for this thesis, we focus on observed Antarctic sea ice trends (Section 1.1.1) and the Amundsen Sea Low (ASL) (Section 1.1.2) and discuss the potential drivers of recent Antarctic climate change (Section 1.1.3). We then transition to summarising how the Antarctic climate is projected to change in the coming century (Section 1.2). This chapter concludes with an outline of this thesis and its research goals (Section 1.3).

1.1 Observed changes in the Antarctic climate

Over the instrumental period (roughly the last fifty years), the most prominent and robust feature of circulation change around Antarctica has been an increase in the positive phase of the Southern Annular Mode (SAM) index (Turner et al., 2009a). The SAM is the major mode of atmospheric variability at the southern high latitudes which reflects the difference in zonal mean sea level pressure between the mid- and high-latitudes (Marshall, 2003). The trend towards a more positive SAM index is due to a drop in pressure around the coast of Antarctica and an increase in pressure at lower latitudes. This has a resulted in a poleward shift of the mid-latitude jet and a strengthening of the zonal wind by 15-20% (Turner et al., 2009a).

While most of the Earth's surface has warmed over the past half century, much of the

Antarctic continent has experienced either no warming or statistically significant cooling (Turner et al., 2009a; Smith and Polvani, 2017). The Antarctic Peninsula and Western Antarctica, however, have warmed substantially (Turner et al., 2009a; Smith and Polvani, 2017) and there has been an increase in surface mass loss due to glacier retreat in these regions (Konrad et al., 2017; Scambos et al., 2017; Rignot et al., 2019). In fact, there is new evidence to suggest that mass loss hasn't been confined to the Western Antarctic and that the Eastern Antarctic Ice Sheet is less stable than originally presumed (Rignot et al., 2019). These trends have potentially disastrous implications for sea level rise (Ritz et al., 2015; DeConto and Pollard, 2016).

1.1.1 Sea ice trends

Over the period 1979-2015, whilst Arctic sea ice has declined dramatically (Comiso et al., 2017b; Stroeve and Notz, 2018), Antarctic sea ice extent (SIE) experienced a small but statistically significant increase of 2% per decade. These Antarctic sea ice trends have a complex seasonal and spatial dependence (Fig. 1.1). The largest positive trend has occurred in the Western Ross Sea region, in every season, and there has also been a large increase of sea ice concentration (SIC) in the Weddell Sea in austral autumn. The only consistent decrease in SIC over this period has been in the Amundsen and Bellingshausen Seas in austral summer and autumn. Climate models, however, are not able to replicate an increase in SIE and instead simulate a substantial loss of Antarctic sea ice over this period (Eisenman et al., 2011; Rosenblum and Eisenman, 2017), as CO_2 concentrations have risen.

There have been a number of proposed explanations for why Antarctic SIE, in contrast with what climate models simulate, has not been declining. It has been suggested that accelerated mass loss from the Antarctic ice sheet (Wingham et al., 2009) has led to a freshening of the Southern Ocean (Jacobs et al., 2002) which may have slowed the pace of Antarctic sea ice loss (Bintanja et al., 2013). After performing model experiments with fresh water dynamically added in the Amundsen Bay, however, Swart and Fyfe (2013) find little effect on sea ice trends from mass loss from the Antarctic ice sheet. Alternatively,

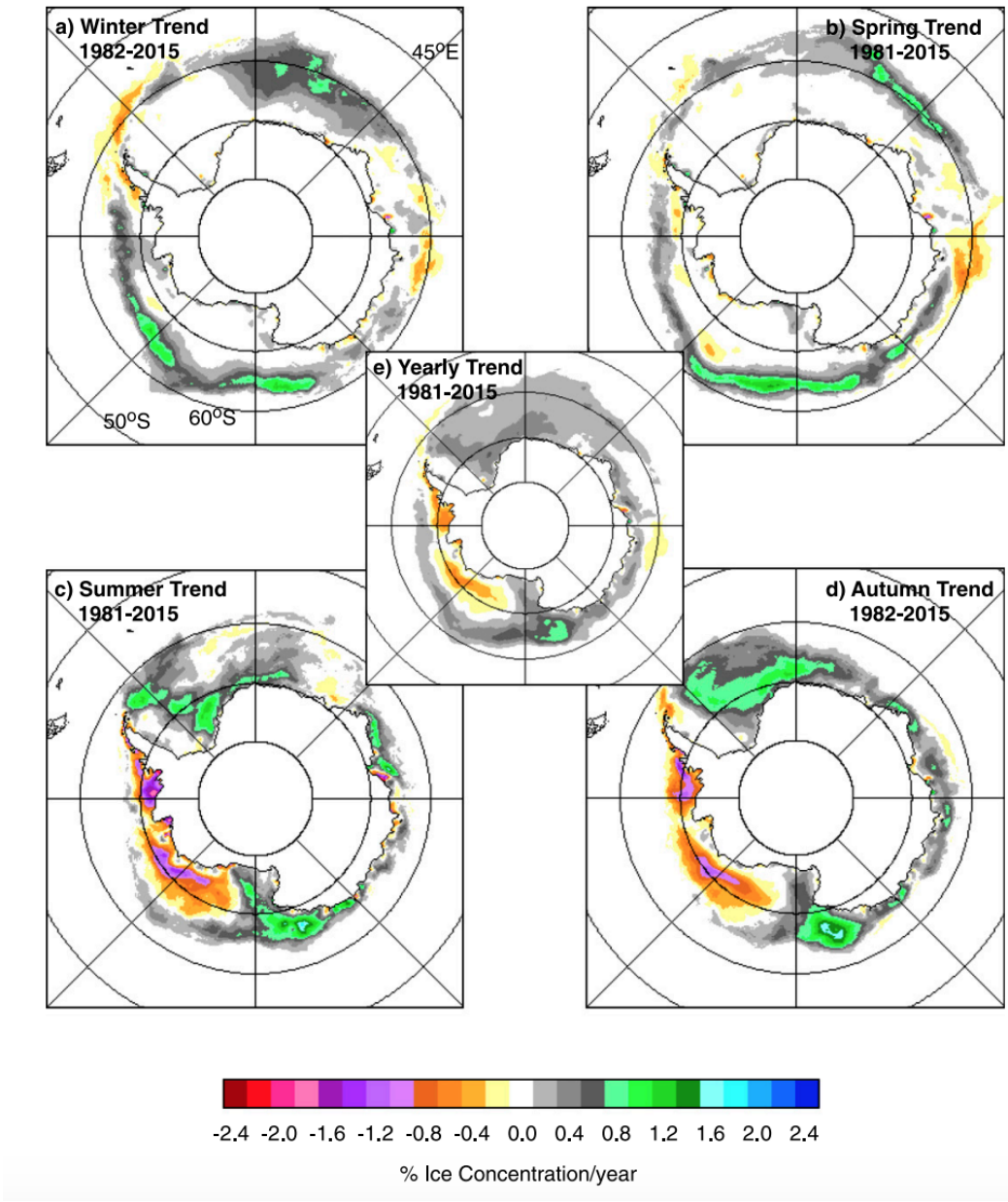

Figure 1.1: Trends in the sea ice cover during the austral (a) winter, (b) spring, (c) summer, and (d) autumn and (e) the entire year, during the period August 1981–December 2015, using SSM/I data. This is Figure 5 of Comiso et al. (2017a).

stratospheric ozone depletion over the Antarctic (Section 1.1.3), the major driver of Southern Hemisphere (SH) climate change over this period (Polvani et al., 2011), is often argued to cause this increase in sea ice ice extent, although modelling results do not agree (Landrum et al., 2017). The regional pattern of sea ice trends, which seems largely to be wind driven (Holland and Kwok, 2012), suggests a possible role for the ASL (Section 1.1.2) (Turner et al., 2015). Lastly, the dominance of internal variability has also been used to explain the discrepancy between models and observations (Polvani and Smith, 2013; Swart and Fyfe, 2013). These studies offer an important reminder to not directly match the observed record and the ensemble mean of climate simulations.

The last three years have marked a departure from the gradual trend of sea ice growth and Antarctic sea ice cover has diminished dramatically (Fig. 1.2). Sea ice conditions set record lows in austral spring of 2016, which were 3σ outside of the normal range of variability (Turner et al., 2017). The largest decrease in SIC occurred near the Antarctic peninsula (Turner et al., 2017; Wang et al., 2019); Turner et al. (2017) highlight the important role of the ASL in driving such changes. This sudden decrease in sea ice cover has been attributed to atmospheric variability at the southern high latitudes (i.e. an extremely negative SAM) (Stuecker et al., 2017; Turner et al., 2017) and a significant tropical influence (Stuecker et al., 2017; Wang et al., 2019). It is also possible that the stratospheric polar vortex played an important role (Wang et al., 2019). Whatever the cause of this recent record breaking low, it has been suggested that this may be a turning point toward a continued decrease in Antarctic sea ice cover over the coming decades (Ludescher et al., 2018). The effects of future Antarctic sea ice loss are investigated in Chapters 4 and 5.

1.1.2 The Amundsen Sea Low

The ASL, a low pressure centre in the Amundsen-Bellingshausen Seas region, is a key feature of the non-zonal circulation near Antarctica. To define the ASL, three metrics are normally used: the absolute central pressure, and its position in longitude and latitude. The location is determined from monthly sea level pressure data using the same method as Turner et al.

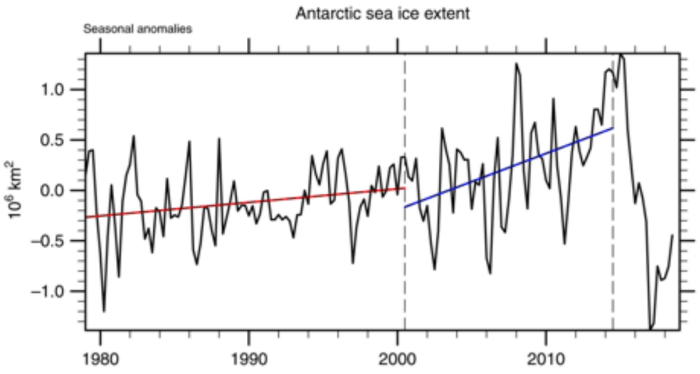

Figure 1.2: Observed seasonal anomalies of Antarctic sea ice extent from 1979 through JJA 2018, seasonal anomalies from the period 1979-August 2018; This is Figure 1a of Meehl et al. (2019).

(2013b): it is the location with the lowest mean sea level pressure in the region 50-180°W, 60-75°S. The location, and especially the depth of the ASL, has been shown to be important for understanding surface air temperature, precipitation and sea ice conditions around West Antarctica. Figure 1.3 shows, for the annual mean, the depth of the ASL between 1979 and 2017 (top row) from ERA-Interim data. We show the difference in sea ice conditions (bottom row) between composites of years with the deepest ASL (blue dots) and the shallowest ASL (red dots). This has been done for composites of different number of years to demonstrate the robustness. The results show that an anomalously deep ASL is associated with an increase in SIC in the Amundsen Sea and decrease in SIC in the Bellingshausen Sea and Antarctic Peninsula. This is consistent with the meridional wind-driven changes due to a deeper ASL and helps us understand the drivers of year-to-year variability of sea ice in the West Antarctic.

One obvious question, therefore, is how has the ASL been changing over the past four decades and has this contributed to the observed regional trends in Antarctic sea ice? Figure 1.4 shows the trend in the depth of the ASL in each season. There is a slight deepening of the ASL during austral summer and autumn however these trends are not statistically significant in any season, even using a 90% confidence level. The natural variability in the West Antarctic region is extremely high and hinders detection of any possible signal (Chapter 3). This suggests that the ASL is unlikely to be the driver of the recent trends in

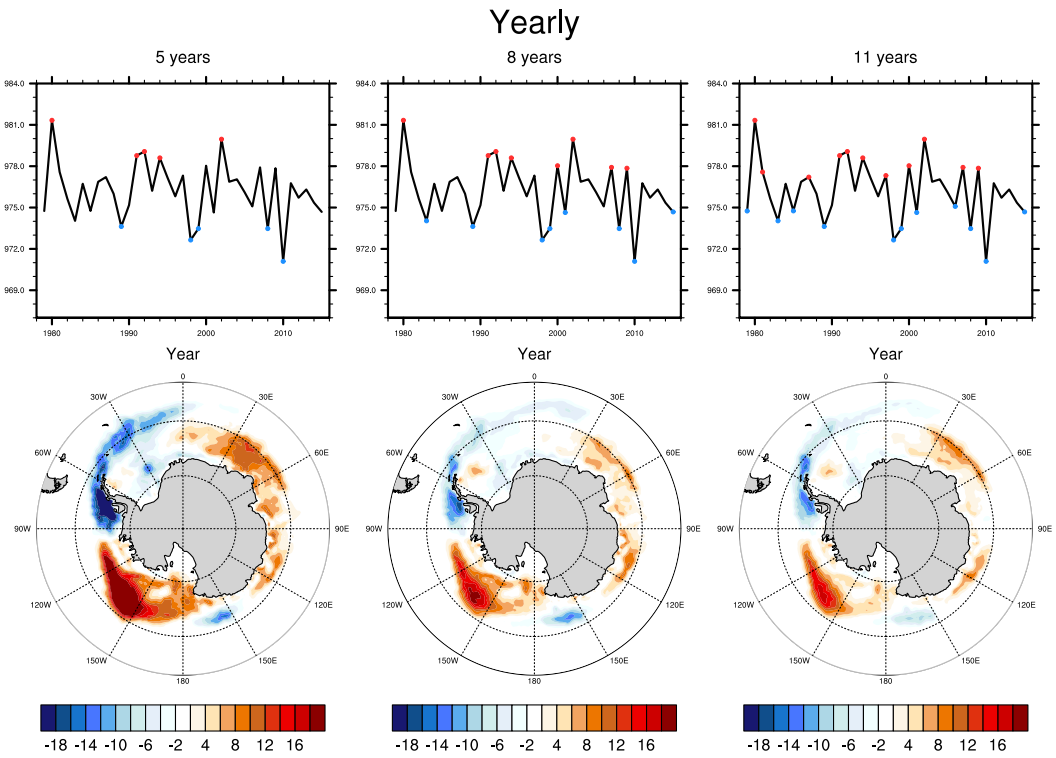

Figure 1.3: (Top row) The annual mean ASL depth in hPa from ERA-Interim, as defined in Turner et al. (2013b), between 1979-2017. (Bottom row) The difference in sea ice concentration (%) from NSIDC between a composite of years when the ASL is at its deepest (blue dots) and a composite of years when the ASL is at its shallowest (red dots). We show the results of using 5, 8 and 11 years per composite to test the robustness of the results.

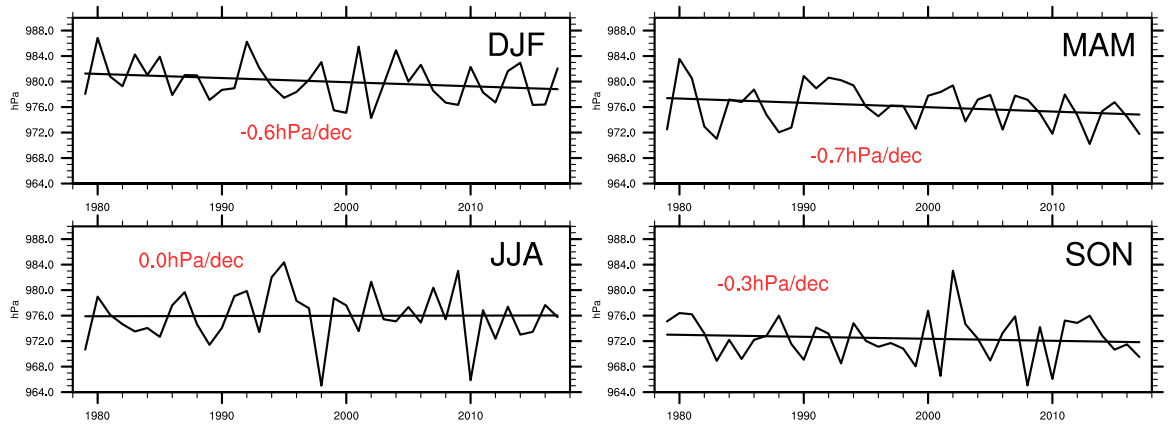

Figure 1.4: 1979-2017 trends in the ASL depth, from ERA-Interim data. The trend is reported in red.

SIC. Comparing the regions of observed sea ice growth and loss in Figures 1.1 and 1.4, it is clear that the sea ice trends are not consistent with an ASL signature. There has been an increase in the Ross Sea rather than the Amundsen Sea and, if the ASL was driving the changes, one would expect the opposite signed response in the Amundsen Sea and west of the Peninsula.

1.1.3 Potential drivers of Antarctic climate change

The main driver of Antarctic climate change over the last fifty years has been stratospheric ozone depletion (Polvani et al., 2011). A rapid increase in the amount of chlorofluorocarbons (CFCs) and other ozone depleting substances (ODSs) in the atmosphere (Fig. 1.5a) caused the concentration of stratospheric ozone to plummet (Fig. 1.5c). The largest loss of stratospheric ozone has been in the austral spring over Antarctica (Fig. 1.5d), commonly referred to as the ozone hole. Since 1960, levels of stratospheric ozone over the Antarctic polar cap have nearly halved. As a result of the Montreal protocol of 1987 (Catchpole et al., 2010), which phased out the production and use of ODSs, stratospheric ozone concentrations are projected to recover to 1980 levels by approximately 2060. Signs of the recovery of the ozone hole have already been detected (Solomon et al., 2016; Kuttippurath and Nair, 2017).

Stratospheric ozone depletion has had an important influence over many different aspects

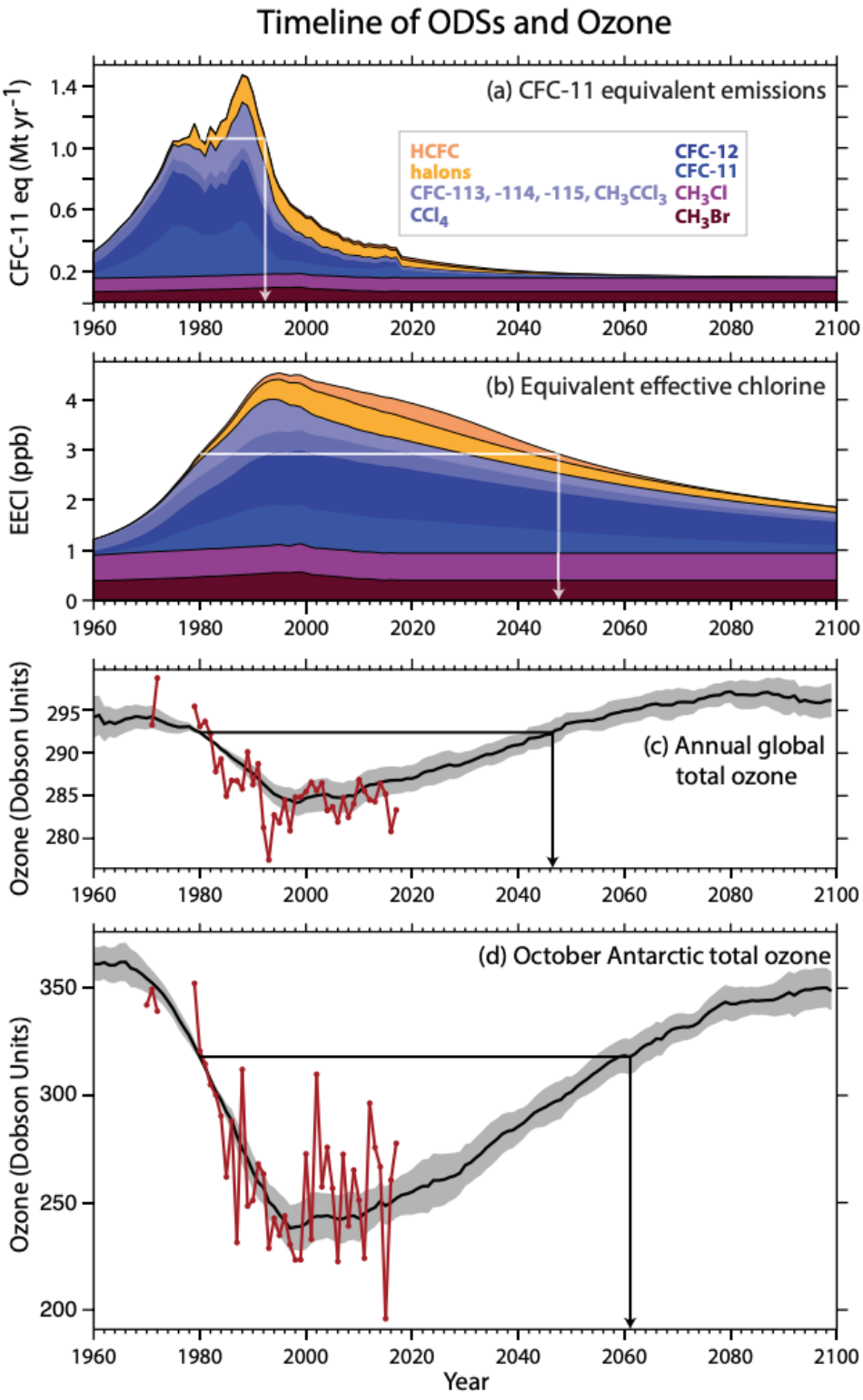

Figure 1.5: Timeline of: a) CFC-11-equivalent emissions, b) equivalent effective chlorine, c) global total ozone, and d) October Antarctic total ozone. This is Figure 1 of the executive summary of WMO (2018).

of SH climate. It has caused a cooling of the polar stratosphere (Ramaswamy et al., 1996; Son et al., 2010; WMO, 2018). In addition, the response to ozone depletion extends down into the troposphere. Stratospheric ozone depletion is strongest during austral spring and so tropospheric effects, which typically lag by 1-2 months, occur in early austral summer. These effects includes a southward expansion of the Hadley cell (Polvani and Kushner, 2002; Kang et al., 2011; Min and Son, 2013) and a poleward shift of the mid-latitude jet (Polvani et al., 2011) and its accompanying storm tracks (Purich and Son, 2012; Grise and Polvani, 2014). In fact, Polvani et al. (2011) demonstrate that over the second half of the 20th century, the effects of stratospheric ozone depletion on the SH mid-latitude jet were 2-3 times larger than those associated with greenhouse gases (Fig. 1.6, compare panels a and b). Stratospheric ozone depletion has also contributed to recent changes in Southern Ocean temperature and salinity (Solomon et al., 2015). Even without ozone depletion, variability in the stratosphere is closely linked to anomalous tropospheric weather patterns in the SH through planetary-scale waves (Gerber et al., 2012; Kidston et al., 2015). This can have an important regional signature in the West Antarctic (Chapter 2).

In the absence of stratospheric ozone depletion, the climate of the southern high latitudes would still have undergone significant change due to an increase in greenhouse gases. Roughly a third of the observed poleward shift of the austral summer mid-latitude jet can be explained by increased greenhouse gas emissions (Fig. 1.6). While the effects of stratospheric ozone are seasonally confined, the response to increased greenhouse gases can be seen throughout the year. Polvani et al. (2011) demonstrate that, unlike stratospheric ozone depletion which has had no detectable effect, increased greenhouse emissions have resulted in a poleward shift of the mid-latitude jet in austral winter. In addition to its effect on the jet, increased greenhouse gases have also reduced the mean sea level pressure around Antarctica (Polvani et al., 2011) and have played a more important role than ozone depletion in driving changes at the southern low latitudes. Over the coming century (Section 1.2), CO_2 and other greenhouse emissions will become the dominant driver of Antarctic climate change.

Although not technically a 'driver' of climate change, the Southern Ocean is key in

mediating the response of the southern high latitudes to ozone depletion and greenhouse gas increases. Firstly, the Southern Ocean is a large sink of carbon, accounting for over 40% of the amount of greenhouse gases sequestered into the world's oceans (Quere et al., 2018). As a result, the Southern Ocean has played a key role in mediating the effects of increased greenhouse emissions on the Antarctic (and the rest of the globe). Secondly, the Antarctic Circumpolar Current, the dominant circulation feature in the Southern Ocean which encircles the Antarctic continent, is understood to keep warm waters away from the Antarctic continent and partially isolate the climate of Antarctica from the effects of lower-latitude variability (Rintoul, 2000). Thirdly, the Southern Ocean has been shown to exhibit a two-timescale response (Ferreira et al., 2014) in response to stratospheric ozone depletion. The short timescale response is dominated by changes in the Ekman layer and leads to cooling around Antarctica and an expansion of the sea ice cover. The long timescale response is controlled by eddy diffusion and has the opposite effect: warming around the continent and a reduction of the sea ice cover. Lastly, in response to increased greenhouse emissions, the Southern Ocean has experienced a delayed warming (with important implications for Antarctic climate change) due in large part to the meridional overturning circulation of the Southern Ocean (Armour et al., 2016).

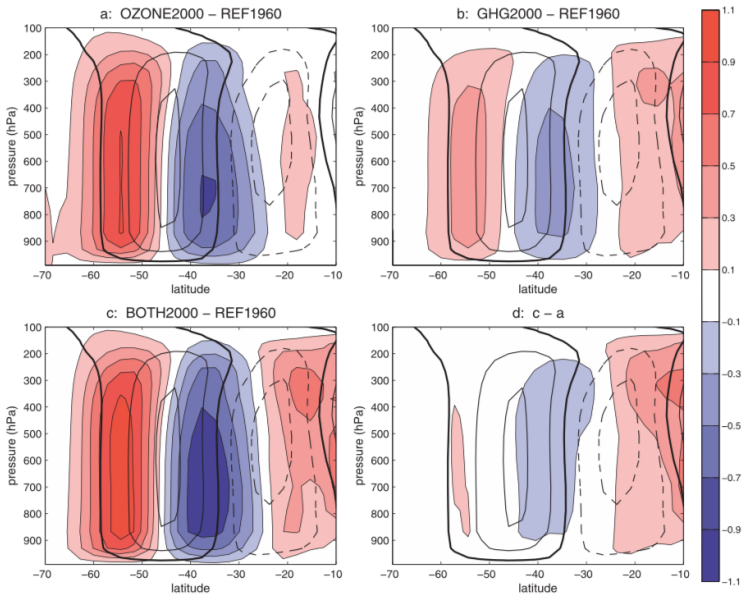

Figure 1.6: The change in DJF mass stream function over the period 1960-2000 due to (a) stratospheric ozone depletion, (b) greenhouse gases and (c) both stratospheric ozone depletion and greenhouse gases, with units of 1×10^{10} kg/s. The black contours show the 1960 climatology values, with contour intervals of 2×10^{10} kg/s. Solid lines indicate positive values and dashed lines indicate negative values. This is Figure 9 of Polvani et al. (2011).

1.2 Projected changes in the Antarctic climate

Determining how the Antarctic climate will change over the coming century, and the implications for the global climate system, is extremely important. Projections of Antarctic climate are made using a range of state-of-the art fully coupled climate models. These models, however, fail to capture many important features of the observed trends (Section 1.1). The literature is divided on whether these discrepancies are due to high levels of internal variability (Polvani and Smith, 2013; Zunz et al., 2013; Gagne et al., 2015) or to, yet to be robustly identified, major flaws in the models (Marshall et al., 2014; Kostov et al., 2017; Rosenblum and Eisenman, 2017). Whatever the reason, these projections are certainly associated with large uncertainties. These uncertainties can be divided into uncertainties arising from (i) internal variability (random fluctuations of the climate system unrelated to the response to anthropogenic forcing), (ii) model uncertainty (differences in model design and model physics causes models to produce different changes in climate in response to the same

forcing) , and (iii) scenario uncertainty (imperfect knowledge of the emissions pathway) (Hawkins and Sutton, 2009). By the end of this century, the uncertainties in projections arise largely from scenario uncertainty and model uncertainty. The projections outlined below come from a multi-model ensemble (to reduce model uncertainty) with many ensemble members per model (to minimise the effects of internal variability) and are heavily dependent on the emissions scenario.

Extensive surface warming is projected over Antarctica; models project a warming of between 1 and 4°C over the coming century (Turner et al., 2009a). The Antarctic has weaker projected polar amplification (where the poles warm faster than the rest of the globe) compared to the Arctic. One reason for this asymmetry is the towering surface height of the Antarctic continent, which is found to reduce the meridional heat transport and the water vapour feedback (Singh et al., 2016; Salzmann, 2017). Nevertheless, the average projected temperature increase over Antarctica is roughly an order of magnitude faster than previously seen in Antarctic ice cores (Turner et al., 2009a). Although confidence in precipitation projections are low, the most robust prediction is for an increase in net precipitation under a warmer, moister climate, as well as a continued poleward shift of the mid-latitude storm tracks (Uotila et al., 2007). As the world warms, the Antarctic ice sheets are expected to shrink in size. Of particular concern is the West Antarctic ice sheet (Joughin and Alley, 2011); most modelling studies suggest that much of the ice sheet will remain viable during this century but there is a tail risk of collapse which would be catastrophic for for global sea level rise.

All models project a significant reduction in Antarctic SIE under business as usual conditions, although the IPCC has *low confidence* in these projections. The annual average loss of Antarctic SIE is projected to be $2.5\times10^6\text{km}^2$, although most of the retreat is expected in austral spring (Fig. 1.7). This will reduce the seasonal cycle of Antarctic SIE (Eisenman et al., 2011), while, interestingly, the seasonal cycle of Arctic SIE will become more peaked. Bracegirdle et al. (2015) demonstrate that historical biases in Antarctic sea ice cover can project onto future projections of Antarctic climate. WACCM4, the model used in Chapters

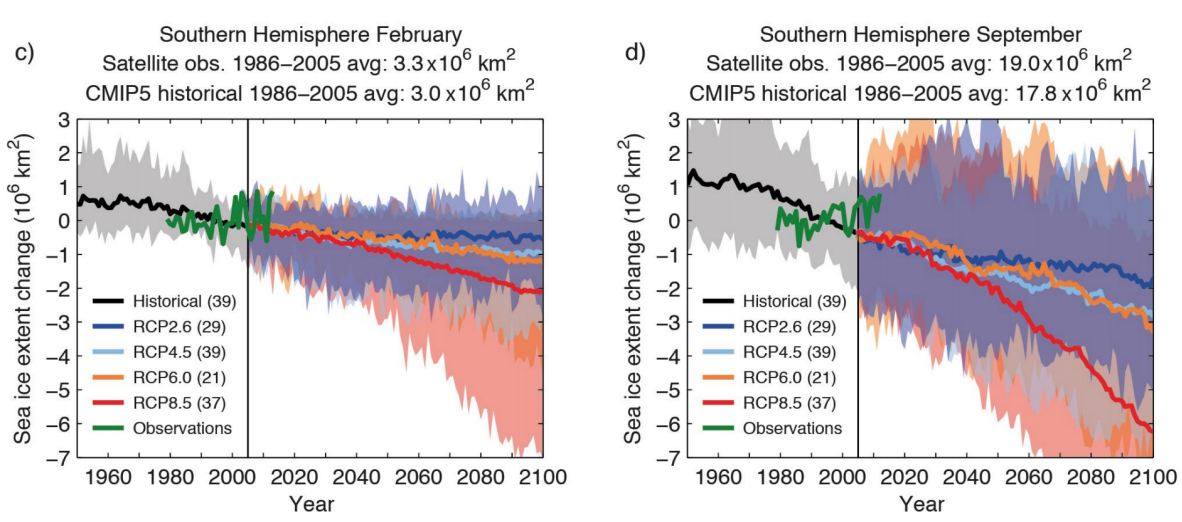

Figure 1.7: Projected change in Antarctic Sea Ice Extent for (left) February and (right) September under different RCP scenarios.The multimodel mean is indicated by the line and the shading shows the spread across the multimodel ensemble. This figure is taken from Topic 2 of the IPCC AR5 report (2014).

3, 4 and 5 simulates the seasonal cycle of Antarctic SIE well, which should increase confidence in our results. The effects of future Antarctic sea ice loss have been studied much less than the effects of future Arctic sea ice loss (e.g. Screen et al., 2018) so in Chapters 4 and 5 we explore the atmospheric response to projected Antarctic sea ice loss using sets of climate model simulations.

Over the last half century, the response to greenhouse emissions and the response to stratospheric ozone depletion combined together to create a robust effect on the climate system, especially in austral summer. Concentrations of stratospheric ozone, however, are expected to recover to pre-ozone hole levels by 2060 (Fig. 1.5). Therefore, over the next fifty years, the effect on the atmospheric circulation of stratospheric ozone recovery and increased greenhouse gases will oppose each other in austral summer (Arblaster et al., 2011; Polvani, 2011). This tug-of-war signal can also be seen in projected Antarctic sea ice loss, with ozone recovery slowing the projected rate of sea ice loss (Smith et al., 2012). We should therefore expect smaller trends in the SAM and the shift of the mid-latitude jet over the coming decades. By the end, of the century however, the projected changes of the southern high latitudes are driven almost entirely by increasing greenhouse emissions.

1.3 Research goals of this thesis

The overarching aim of this thesis is to increase our understanding of recent and projected Antarctic climate change and its drivers. We also investigate the potential global implications of these changes and show that the effects may not be limited to the southern high latitudes. In this section we briefly describe the results from each chapter and then highlight other projects which the author has been involved in during his PhD.

1.3.1 Thesis outline

Chapter 2, *Troposphere-stratosphere dynamical coupling in the Southern high latitudes, and its linkage to the Amundsen Sea*, was published in the Journal of Geophysical Research in 2016 (England et al., 2016b). In this chapter, we investigate the link between the stratospheric planetary-scale events and the surface climate of the southern high latitudes using reanalysis and CMIP5 models.

We find that extremes in the distribution of SH stratospheric heat flux are connected simultaneously to anomalous high-latitude tropospheric weather patterns in reanalysis, consistent with results from the Northern Hemisphere (NH). The dynamical links are revealed using a metric based on extreme stratospheric planetary-scale wave heat flux events, defined as the 10th and 90th percentiles of the daily high-latitude wave 1 heat flux distribution at 50 hPa. We show extreme negative (positive) heat flux events are linked to a westward (eastward) shift in the ASL and anomalous warming (cooling) over the Amundsen Bellingshausen Seas in reanalysis data. Since coupling to the stratosphere via planetary waves has significant impacts on the tropospheric circulation of both hemispheres, it is important to understand which coupled climate models can reproduce this phenomenon. The heat flux metric is used to evaluate troposphere-stratosphere coupling in CMIP5 models and compare their performance across hemispheres. The results show that models with a degraded representation of stratospheric extremes exhibit robust biases in tropospheric sea level pressure variability over the Antarctic Peninsula. Models which fail to capture the extremes in

stratospheric heat flux, significantly underestimate the variance of the distribution of mean sea level pressure anomalies over Western Antarctica.

Chapter 3, *Robust response of the Amundsen Sea Low to stratospheric ozone depletion*, was published in Geophysical Research Letters in 2016 (England et al., 2016a). In this chapter, using results from two different climate models, we demonstrate that stratospheric ozone depletion causes a deepening of the ASL during austral summer.

The effect of stratospheric ozone depletion on the ASL, a climatological low-pressure center important for the climate of West Antarctica, has been uncertain. Using state-of-the-art climate models, we show in this chapter that stratospheric ozone depletion can cause a statistically significant deepening of the ASL in summer with an amplitude of approximately 1 hPa per decade. We are able to attribute the modelled changes in the ASL to stratospheric ozone depletion by contrasting ensembles of historical integrations with and without a realistic ozone hole. In the presence of very large natural variability, the robustness of the ozone impact on the ASL is established by (1) examining ensembles of model runs to isolate the forced response, (2) repeating the analysis with two different climate models, and (3) considering the entire period of stratospheric ozone depletion, the beginning of which pre-dates the satellite era by a couple of decades.

Chapter 4, *Contrasting the Antarctic and Arctic atmospheric responses to projected sea ice loss in the late 21st Century*, was published in the Journal of Climate in 2018 (England et al., 2018). In this chapter, we use an atmospheric general circulation model with perturbed sea ice conditions to isolate the atmospheric response to projected Antarctic sea ice loss. We compare and contrast this with the atmospheric response to projected Arctic sea ice loss.

Models project that Antarctic sea ice cover will decline considerably by the end of this century, but the consequences remain largely unexplored. In this chapter, the atmospheric response to future sea ice loss in the Antarctic is investigated, and contrasted to the Arctic case, using the Community Earth Systems Model (CESM) Whole Atmosphere Coupled Climate Model (WACCM). Time-slice model runs with historic SIC are compared to runs with future concentrations, from the late twenty-first century, in each hemisphere separately.

As for the Arctic, results indicate that Antarctic sea ice loss will act to shift the tropospheric jet equatorward, an internal negative feedback to the poleward shift associated with increased greenhouse gases. Also, the tropospheric response to Antarctic sea ice loss is found to be somewhat weaker, more vertically confined, and less seasonally varying than in the case of Arctic sea ice loss. The stratospheric response to Antarctic sea ice loss is relatively weak compared to the Arctic case, although it is here demonstrated that the latter is still small relative to internal variability. In contrast to the Arctic case, the response of the ozone layer is found to be positive (up to 5 Dobson units): interestingly, it is present in all seasons except austral spring. Finally, while the response of surface temperature and precipitation is limited to the southern high latitudes, it is nonetheless unable to impact the interior of the Antarctic continent, suggesting a minor role of sea ice loss on recent Antarctic temperature trends.

Chapter 5, *Remarkably similar tropical response to Arctic and Antarctic sea ice loss*, is work currently in preparation. In this chapter, we use a fully coupled climate model with perturbed sea ice conditions to isolate the atmospheric response to projected Antarctic sea ice loss, building on work form Chapter 4. We focus on the response of the tropics to future Antarctic sea ice loss and find the tropical effects remarkably similar to that of Arctic sea ice loss.

Both Arctic and Antarctic SIE are projected to dramatically decline over the coming century. In this chapter we isolate the tropical response to end-of-century Antarctic sea ice loss and show it is as large as the response to end-of-century Arctic sea ice loss. Using climate model simulations with a dynamic ocean, we find that Antarctic sea ice loss, like Arctic sea ice loss will have important global effects, causing a 'mini global warming' signal. We show that the tropical response to Antarctic sea ice loss is remarkably similar to that of Arctic sea ice loss, with warming in the Eastern Tropical Pacific and increased precipitation throughout much of the equatorial Pacific. Ocean energy transport is found to be the main pathway for signals from both poles to reach the tropics. This chapter highlights the importance of projected Antarctic sea ice loss on the climate system.

1.3.2 Other work

During his PhD, the author has also worked on understanding the role of internal variability in driving historical regional Arctic sea ice trends (England et al., 2019) and investigating the role of internal variability in projected changes of the seasonal cycle of surface temperature (Yettella and England, 2018).

CHAPTER 2

TROPOSPHERE-STRATOSPHERE DYNAMICAL COUPLING IN THE SOUTHERN HIGH LATITUDES, AND ITS LINKAGE TO THE AMUNDSEN SEA

This work was published in Journal of Geophysical Research in 2016 (England et al., 2016b).

2.1 Introduction

Variability in the stratosphere is closely linked to anomalous tropospheric weather patterns in the SH (Gerber et al., 2012; Kidston et al., 2015). Coupling mainly occurs in SH spring time, when the breakdown of the stratospheric vortex influences the position of the tropospheric jet (Randel, 1988; Baldwin and Dunkerton, 2001; Baldwin et al., 2003; Gerber et al., 2012). Planetary scale waves, generated in the troposphere, represent one of the main modes of stratosphere troposphere coupling (Andrews et al., 1987; Plumb, 2010) and has significant impacts on the variability of the stratospheric polar vortex (Polvani and Waugh, 2004; Dunn-Sigouin and Shaw, 2015).

The primary mode of planetary wave coupling is upward wave coupling where signals in the troposphere propagate up into the stratosphere. Randel (1988) found that wave-1 exhibits an upward vertical propagation time scale of four days between the middle troposphere and the middle stratosphere and that its vertical structure is significantly different from waves

2 and 3. The upward propagation involves significant transfers of heat and momentum polewards (van Loon and Jenne, 1972; Randel, 1988). Shaw et al. (2010) demonstrate that, in addition to the upward coupling, wave-1 exhibits downward wave coupling (wave pattern in the stratosphere leads wave pattern in the troposphere with a propagation timescale around five days) from September to December when the zonal flow exhibits a bounded wave geometry. Over the past several decades, ozone depletion has increased downward wave coupling during November and December because the bounded wave geometry extends later into the year in reanalysis data and models (Harnik et al., 2011; Shaw et al., 2011).

Planetary wave coupling has a significant impact on the tropospheric circulation in the NH, associated with a distinct regional signal in the North Atlantic basin (Shaw et al., 2014) (subsequently referred to as S14). The tropospheric impact was revealed using an index based on extreme values of the high latitude heat flux at 50 hPa. The eddy heat flux is proportional to the vertical group velocity according to linear wave theory and is thus a measure of vertical coupling. Large positive eddy heat fluxes, indicating upward wave coupling, were simultaneously associated with anomalous high pressure over the North Atlantic reminiscent of the negative phase of the North Atlantic Oscillation (NAO) whereas large negative eddy heat flux, indicating downward wave coupling, involved opposite signed patterns. The simultaneous relationship reflected the peak time in the lifecycle of planetary wave events in the stratosphere (see Fig. 2 of Dunn-Sigouin and Shaw (2015)). S14 used the heat flux index to show that models with a biased stratospheric eddy heat flux distribution exhibited biases in eddy geopotential height and jet stream position in the North Atlantic troposphere. The models with the largest stratospheric heat flux bias were all low-top, following the definition of Charlton-Perez et al. (2013).

We investigate whether planetary wave coupling has a significant regional signature in the SH. One of the most important zonally-asymmetric features in the SH is the ASL. The ASL, a low pressure centre located in the region 60-75°S 170-290°E, is a key driver of of circulation variability over West Antarctica and has a large impact on the SIE in surrounding regions (Turner et al., 1997; Hosking et al., 2013). The formation of the ASL

is attributable to a combination of (i) flow separation over the coastal line of the Ross Sea embayment and the steep orography inland (Baines and Fraedrich, 1989), and (ii) the strong baroclinicity resulting from the irregular coastline of Antarctica, which intensifies the cyclogenesis patterns in the region (Walsh et al., 2000; Fogt et al., 2012b). It is an essentially barotropic phenomenon and its climatology is well documented by Turner et al. (2013b).

We seek to address the following questions: Are stratospheric heat flux extremes linked to a regional circulation in the troposphere in the SH? What is the impact of the coupling in the Amundsen Sea region? Does troposphere-stratosphere planetary wave coupling play as dominant a role in setting the mean state and variability of the tropospheric circulation as it does in the NH? Can tropospheric biases in the Amundsen Sea region in CMIP5 models be linked to the ability to represent extreme stratospheric heat flux events?

This chapter is organised as follows. Section 2.2 describes the reanalysis data set and CMIP5 simulations analysed in this study. In section 2.3 the links between stratospheric planetary-scale wave heat flux extremes and SH tropospheric weather and climate patterns in reanalysis data are examined. In section 2.4 the representation of stratospheric heat flux extremes in CMIP5 models is studied and coupling with the tropospheric circulation is compared in models with large and small biases in stratospheric heat flux extremes. Section 2.5 concludes the chapter with a summary and discussion.

2.2 Data and Methods

This study uses daily data from the European Centre for Medium-Range Weather Forecasts (ECMWF) Interim (ERA-Interim) reanalysis for the years 1979-2005 (Dee et al., 2011). In addition, we make use of daily and monthly data from 30 CMIP5 historical simulations (Table 2.1) (Taylor et al., 2012). In this study anomalies are computed by removing the climatological seasonal cycle (1979-2005).

The following analysis is based on the daily wave-1 (meridional) heat flux i.e. $\overline{v'T'}_{k=1}$ at 50 hPa where the overbar represents a zonal average, the prime indicates a deviation

Table 2.1: CMIP5 historical data used in this study model ensemble. The * and † indicate models included in the small and large bias ensembles.

Model	Ensemble member[1]	Model	Ensemble member[1]
bcc-csm1-1	r1i1p1	bcc-csm1-1-m*	r1i1p1
BNU-ESM	r1i1p1	CanESM2	r1i1p1
CCSM4	r1i1p1	CMCC-CESM	r1i1p1
CMCC-CM	r1i1p1	CNRM-CM5†	r1i1p1
FGOALS-g2†	r1i1p1	FGOALS-s2	r1i1p1
GFDL-ESM2G†	r1i1p1	GFDL-ESM2M†	r1i1p1
HadCM3†	r1i1p1	inmcm4†	r1i1p1
MIROC5	r1i1p1	NorESM1-M*	r1i1p1
CESM1-WACCM	r1i1p1	CMCC-CMS*	r1i1p1
GFDL-CM3	r1i1p1	HadGEM2-CC	r1i1p1
IPSL-CM5A-LR*	r1i1p1	IPSL-CM5A-MR*	r1i1p1
MIROC-ESM†	r1i1p1	MIROC-ESM-CHEM	r1i1p1
MPI-ESM-LR	r1i1p1	MPI-ESM-MR*	r1i1p1
MPI-ESM-P	r1i1p1	MRI-CGCM3*	r1i1p1

from the zonal average and k is the zonal wave number, which is extracted using Fourier decomposition. We use the wave-1 heat flux, which represents 80% of the eddy (deviation from the zonal mean) heat flux variability, as a measure of vertical wave coupling (Charney and Drazin, 1961). The 50 hPa level, located in the mid to lower region of the stratosphere, is chosen because it is a standard output level in the ERA-Interim and CMIP5 data sets. The wave-1 heat flux is averaged between 60° and 90°S creating a daily time series, which is hereafter referred to as the high-latitude stratospheric heat flux. This latitudinal band is where the temporal variability of the heat flux is maximum. The sensitivity of the results to the choice of latitudinal average and the effect of weighting by the cosine of the latitude are negligible.

The study focusses on September, October and November (SON), which is the period of maximum wave coupling between the troposphere and stratosphere in the SH (Fig. 2.1a., blue) (Shaw et al., 2010). S14 analysed the period January, February and March (JFM), the period of maximum wave coupling in the NH (Fig. 2.1a., red).

The eddy field is found by calculating the deviation from the zonal mean. The eddy field is broken down into its components of different wave-numbers using Fourier decomposition.

2.3 Links Between Stratospheric Wave-1 Heat Flux Extremes and the Tropospheric Circulation in Reanalysis Data

The daily distributions of high latitude wave-1 heat flux at 50 hPa for both the NH (averaged 60° to 90°N, JFM) in red and the SH (averaged 60° to 90°S, SON) in blue are shown in Figure 2.1b. Note that the NH distribution has been multiplied by -1, so that the mean has been flipped from positive to negative, to allow for an easy comparison of the phenomenon in the two hemispheres. In the SH (NH) the mean is negative (positive) meridional heat flux values, consistent with upward propagating waves. The SH wave-1 heat flux distribution has

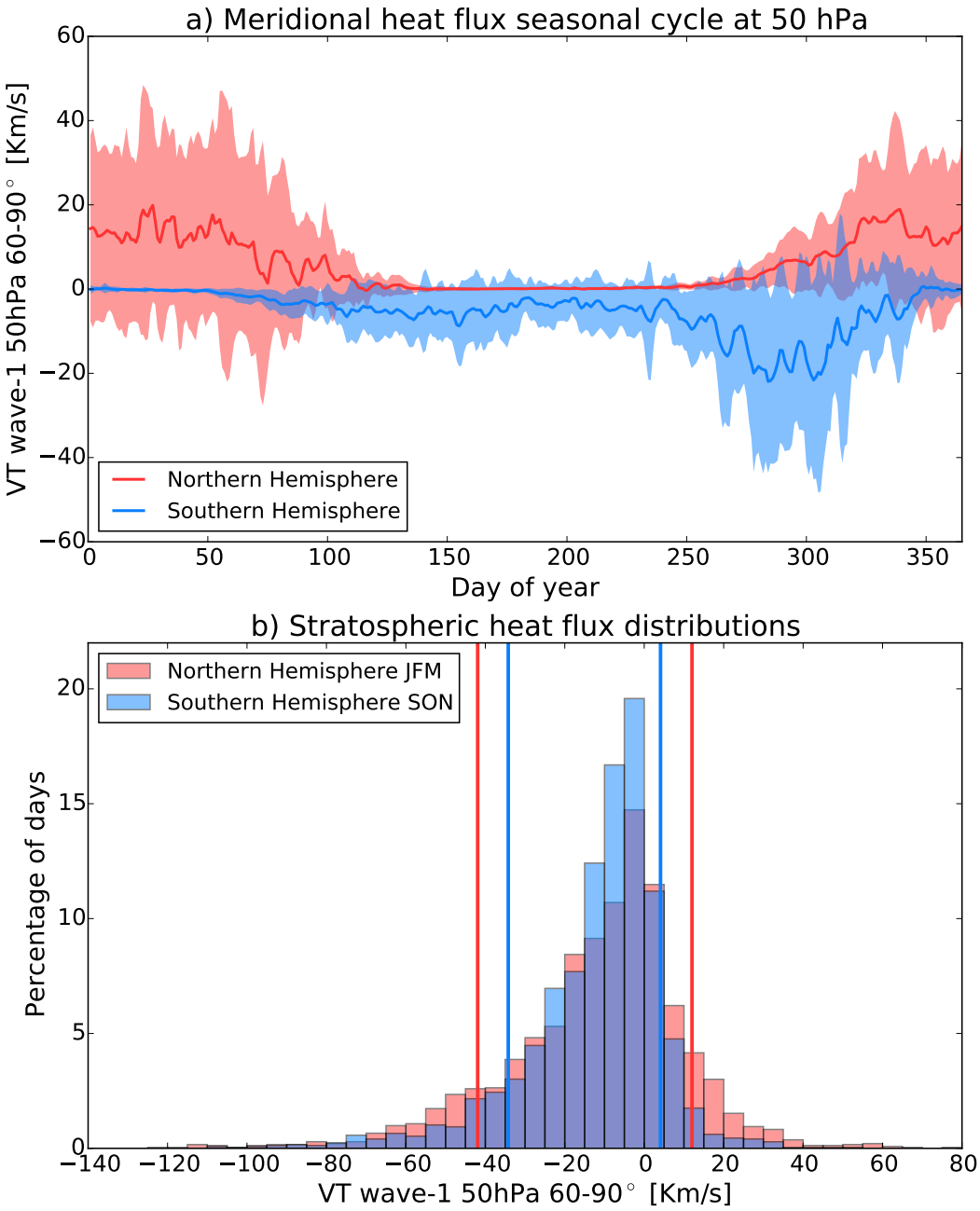

Figure 2.1: The 60°-90°S and 60°-90°N wave-1 meridional heat flux at 50 hPa in ERA-Interim for 1979-2005. a) Seasonal cycle in both hemispheres. The line shows the mean value of the heat flux and the shaded envelope gives one standard deviation interval either side. b) Daily distribution averaged 60°-90°S during SON and 60°-90°N during JFM from 1979 to 2005. The distribution from the NH has been multiplied by -1. The vertical lines represent the 10th and 90th percentiles of the distributions.

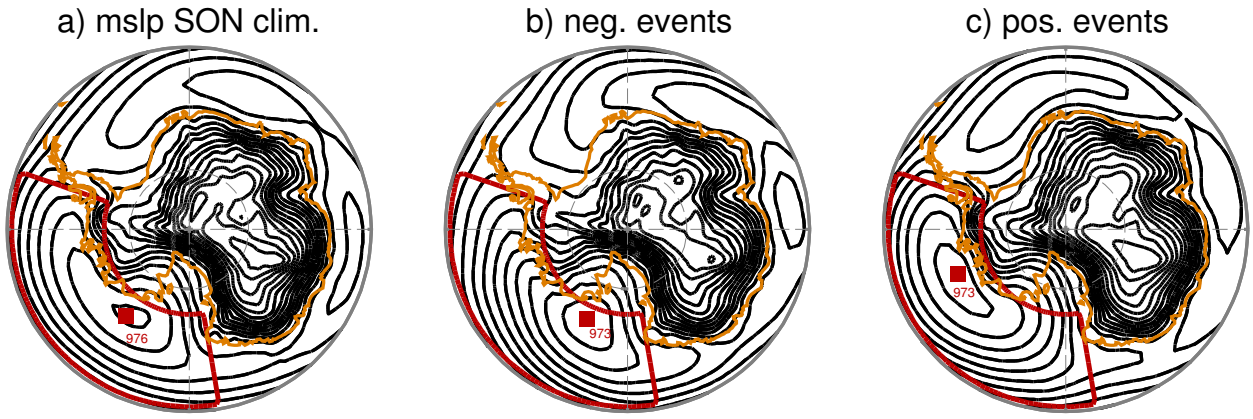

Figure 2.2: The ERA-Interim mean sea level pressure (a) SON climatology, and a composite of (b) extreme negative and (c) positive heat flux events. See text for definition of extreme positive and negative heat flux events. The contour interval is 2 hPa. The Amundsen Sea region (60-75°S 170-290°E) is shown by the red box. The location of the ASL (the point with the lowest mean sea level pressure in the region) is represented by the red square and the ASL central pressure is indicated in hPa.

a smaller mean and standard deviation than that of the NH, consistent with the SH having a weaker wave source. The NH wave-1 heat flux distribution therefore has thicker tails; the 10th percentile is 41.7 Kms^{-1} compared to -32.5 Kms^{-1} for the SH, and the 90th percentiles is of -10.8 Kms^{-1} and 4.3 Kms^{-1} for the SH.

From now on we will focus on the SH and any mention of the heat flux distribution refers to that in the SH. The mean of the distribution is negative and equal to -11.7 Kms^{-1}, indicating upward propagation. The standard deviation is equal to 17.2 Kms^{-1}. Days with stratospheric heat flux lower than the 10th percentile of the distribution (-32.5 Kms^{-1}) will be labelled as 'extreme negative heat flux days' and days with values larger than the 90th percentile of the distribution (4.3 Kms^{-1}) will be labelled as 'extreme positive heat flux days'. According to linear wave theory, extreme negative days are associated with upward wave propagation and extreme positive days are associated with downward wave coupling. As mentioned in the introduction, our eddy heat flux index exploits the near simultaneous stratospheric and tropospheric signals seen in the planetary wave lifecycle.

We assess the link between extreme stratospheric heat flux events and the troposphere by comparing the climatological pattern to the patterns during extreme stratospheric events. The climatology of the mean sea level pressure (mslp) from ERA-Interim during SON is

shown in Figure 2.2a from the years 1979-2005. The location and depth of the ASL is indicated in red, in agreement with Figure 1 of Turner et al. (2013b). Figure 2.2b and 2.2c show mslp for composites of extreme negative and positive stratospheric heat flux events respectively. During extreme negative events the ASL centre migrates westwards by 12° whereas during extreme positive events it shifts eastwards by 32°. This is a significant longitudinal change given the amplitude of the seasonal cycle (taking monthly mean position) is only 40° (Turner et al., 2013a). These shifts are in the lowest and highest 20th percentiles of the distribution of monthly ASL longitude positions respectively. Hosking et al. (2013) demonstrate how the longitudinal position of the ASL can have a large impact on SIC; when the ASL is displaced westward there is a decrease in SIC in the Amundsen and Bellingshausen Seas and vice versa.

Figure 2.3 shows the anomalous mslp (2.3a,b), anomalous temperature at 850 hPa (2.3c,d) and anomalous meridional wind (2.3e,f) during extreme positive and negative heat flux days in SON. During extreme negative heat flux events there is anomalously high mslp over the Bellingshausen Sea, with equatorward flow over the Antarctic Peninsula and strong poleward flow over the Amundsen Sea. Furthermore, there is anomalous warming over the Amundsen and Bellingshausen Seas, due to advection from the north east (anticyclonic flow around the anomalous high surface pressure). In contrast, for days with extreme positive heat flux values, anomalously low mslp over the Bellingshausen Sea advects cold air from over Antarctica equatorward and westward through cyclonic flow, causing anomalously cold temperatures in this region. These patterns drive the longitudinal movement of the ASL during SON seen in Figure 2.2.

The stratospheric events are also linked to patterns in the mid troposphere and upper stratosphere. Figure 2.4 shows the climatological 500 hPa (black) and 10 hPa (shaded) wave-1 and anomalous geopotential height, which both exhibit a clear wave-1 structure for composites of extreme negative and positive events. During extreme negative heat flux days (Fig. 2.4b,e) geopotential height patterns resemble those near the surface but with a westward shift and tend to reinforce the climatology in high latitudes (Fig. 2.4a,d). In

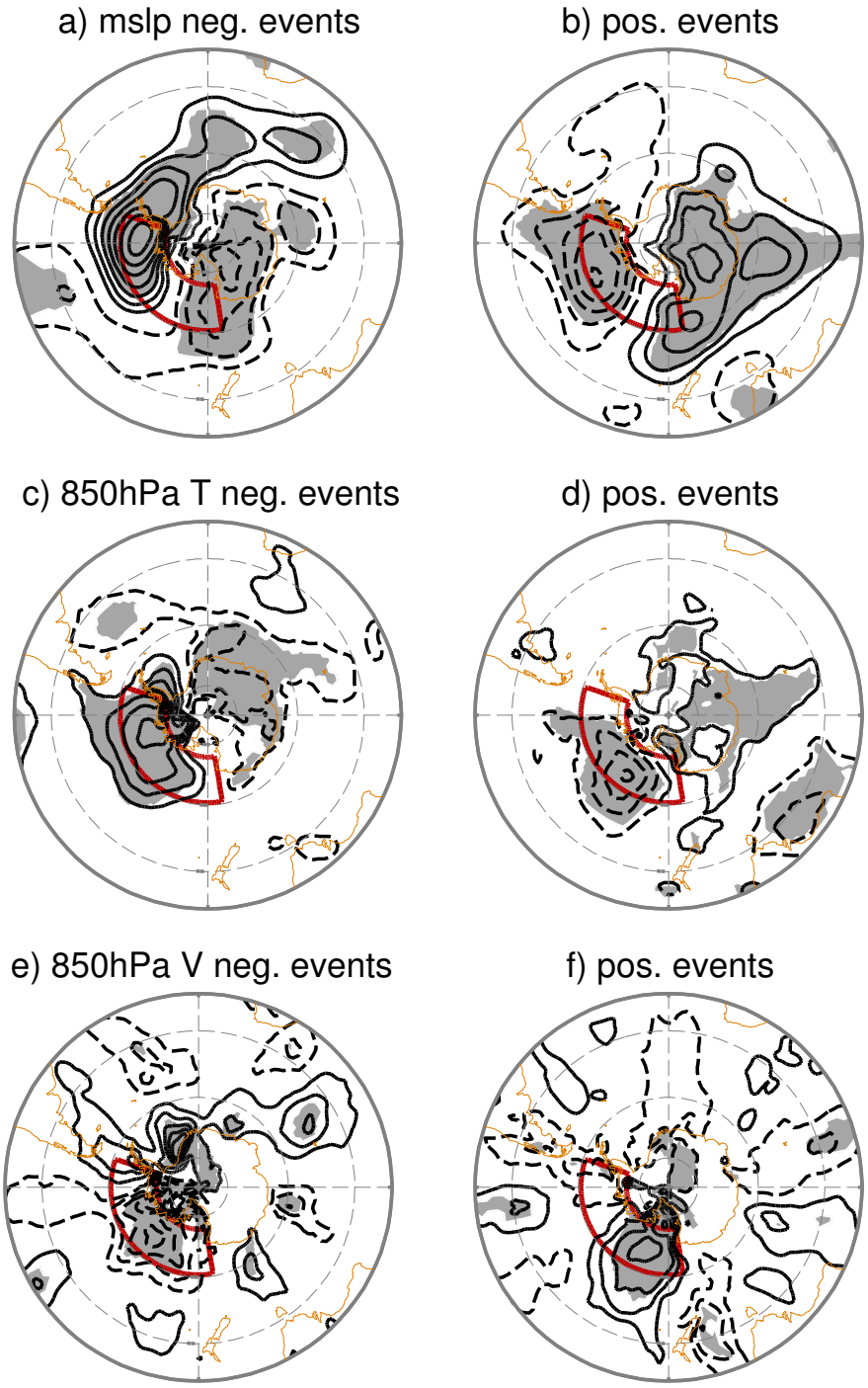

Figure 2.3: ERA-Interim composite of (a,b) mean sea level pressure, (c,d) 850 hPa temperature and (e,f) 850 hPa meridional wind anomalies during extreme (left) negative and (right) positive heat flux events. The contour interval is 1 hPa for mean sea level pressure, 0.5 K for temperature and 0.5 ms^{-1} for the meridional wind. Grey shading shows anomalous values statistically significant at 99% (see Appendix 2.6 for details). Black contours show positive values, and dashed contour lines correspond to negative values. The zero contour is omitted. The continents are plotted in brown.

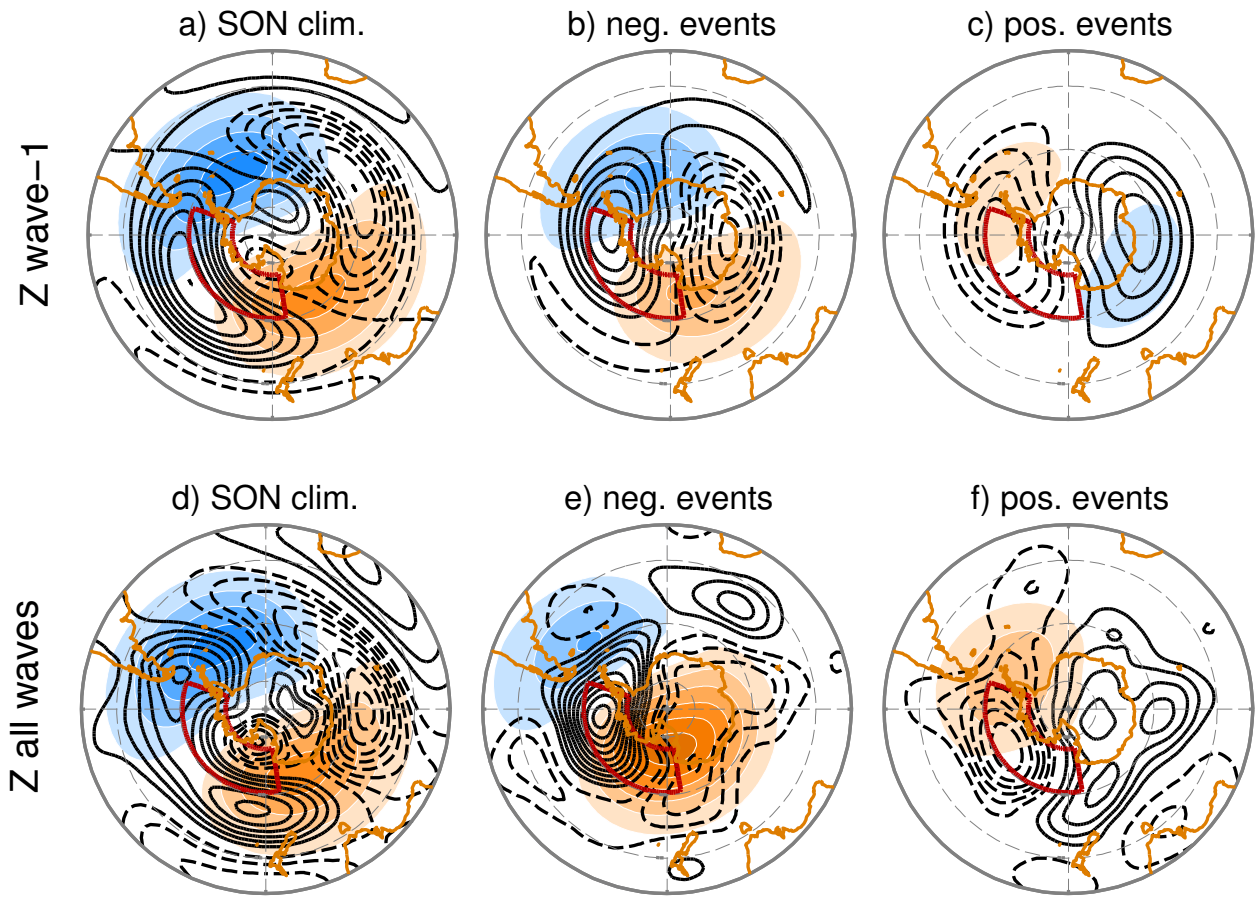

Figure 2.4: The ERA-Interim (top) wave-1 and (bottom) rededdy geopotential height for (a,d) SON eddy climatology from 1979 to 2005 and composites of anomalous values for extreme (b,e) negative and (c,f) positive heat flux events, at 500 hPa (black) and 10 hPa (shaded). See text for definition of extreme positive and negative heat flux events. Contour interval is 10 m (black) and 100 m (shaded). Black contours and orange shading show positive values, and contours lines and blue shading correspond to negative values. The zero contour is omitted. The continents are plotted in brown and the Amundsen Sea region is shown in red.

the troposphere, the wave-1 component (Fig. 2.4b) explains nearly 70% of the anomalous geopotential height pattern in the high latitudes with wave-2 and -3 making up the remainder. The wave pattern between 500 and 10 hPa exhibits a westward phase tilt with height, consistent with upward propagation of wave activity from the troposphere to the stratosphere (Andrews et al., 1987).

During extreme positive heat flux days the geopotential height anomalies are opposite in sign to those during negative heat flux days (Fig. 2.4c,f), which moves the ASL eastward (towards the Antarctic Peninsula, Fig.2.2b). There is an eastward phase tilt with height between 500 and 10 hPa consistent with the idea of wave reflection. Similar to the extreme negative case, wave-1 (Fig. 2.4c) explains roughly 80%. of the anomalous geopotential height pattern (Fig. 2.4f).

These reanalysis results show that extreme variations of the stratospheric wave-1 heat flux are linked to the Amundsen Sea region. The next step is to use the high-latitude heat flux metric to evaluate the representation of stratospheric heat flux events in CMIP5 models including their coupling to the troposphere.

2.4 Links Between Stratospheric Wave-1 Heat Flux Extremes and the Tropospheric Circulation in CMIP5 Models

2.4.1 Representation of Stratospheric Heat Flux Extremes

Here we use the stratospheric heat flux extremes metric to evaluate how well CMIP5 climate models simulate planetary-scale wave coupling between the troposphere and stratosphere. The daily high latitude heat flux distributions at 50 hPa is calculated for the CMIP5 models listed in Table 2.1. Figure 2.5 shows the percentage of days in SON for the years 1979 to 2005 that were classified as extreme negative heat flux days (values less than the 10th percentile of the ERA-Interim distribution, -34.2 Kms^{-1}) against the percentage of days labelled as

Table 2.2: Classification of models as small or large bias as indicated by Figure 2.5. Low-top models are shown by (L) and high-top models are shown by (H).

Small bias model set	Large bias model set
bcc-csm1-1-m (L)	CNRM-CM5 (L)
NorESM1-M (L)	FGOALS-g2 (L)
CMCC-CMS (H)	GFDL-ESM2G (L)
IPSL-CM5A-LR (H)	GFDL-ESM2M (L)
IPSL-CM5A-MR (H)	HadCM3 (L)
MPI-ESM-MR (H)	inmcm4 (L)
MRI-CGCM3 (H)	MIROC5 (L)

extreme positive heat flux days (values greater than the 90th percentile of the ERA-Interim distribution, 4.1 Kms^{-1}). The models have been colour coded in the same manner as S14 with circles representing low-top models and squares showing high-top models, following the definition of Charlton-Perez et al. (2013).

The percentage of extreme negative heat flux days and the percentage of extreme positive heat flux days at 50 hPa for the CMIP5 models are significantly correlated ($r = 0.64$, $p = 0.01$). The correlation suggests that models which under-predict the number of extreme positive heat flux days also under-predict the number of extreme negative heat flux days. This is to be expected because downward wave coupling is preceded by upward wave coupling. The majority of CMIP5 models under-predict the stratospheric extremes (both positive and negative) at 50 hPa in the SH (models in the lower left quadrant).

Two model ensembles are constructed based on the bias relative to the 10th and 90th percentiles of the ERA-Interim heat flux distribution. Models are labelled as 'small bias' if the combined bias of positive and negative extremes at 50 hPa is less than 3.5% (models contained within red circle of radius 3.5% in Figure 2.5). Models are labelled as 'large bias' if the percentage of either the extreme negative or extreme positive heat flux days is under 4.0% (models contained within blue square in Figure 2.5). This classification system produces

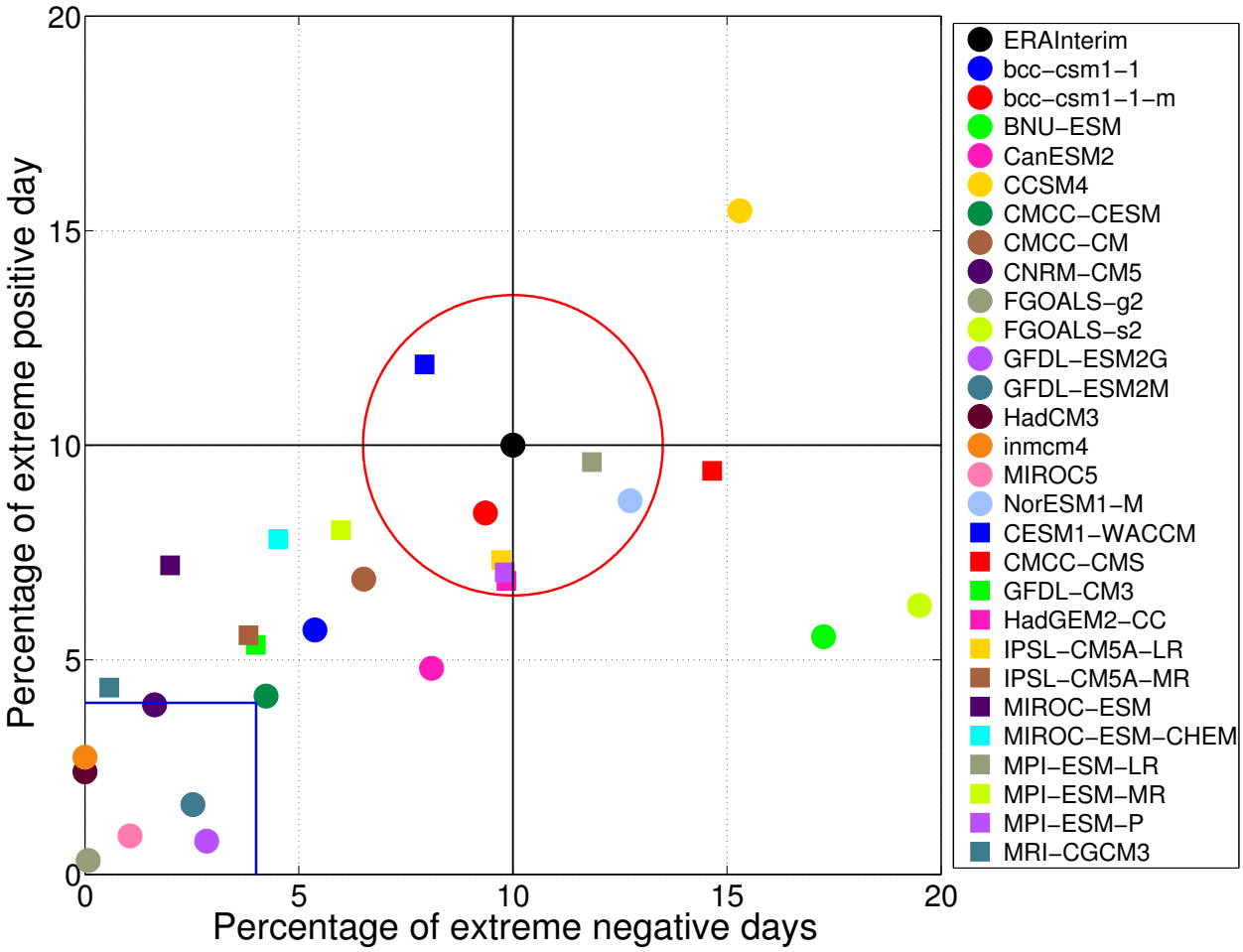

Figure 2.5: Percentage (frequency) of extreme negative wave-1 heat flux events versus extreme positive events at 50 hPa averaged 60°-90°S during SON. Here, negative and positive extreme events are defined as the 10th and 90th percentiles of the ERA-Interim distribution for SON 1979 to 2005 with values of $<$ -34.2 Kms^{-1} and $>$ 4.1 Kms^{-1} respectively. CMIP5 models, with circles representing low-top models and squares representing high-top models, along with the ERA-Interim data are plotted averaged over 1979 to 2005. The blue square is used to define the large bias models and the red circle is used to define the small bias models.

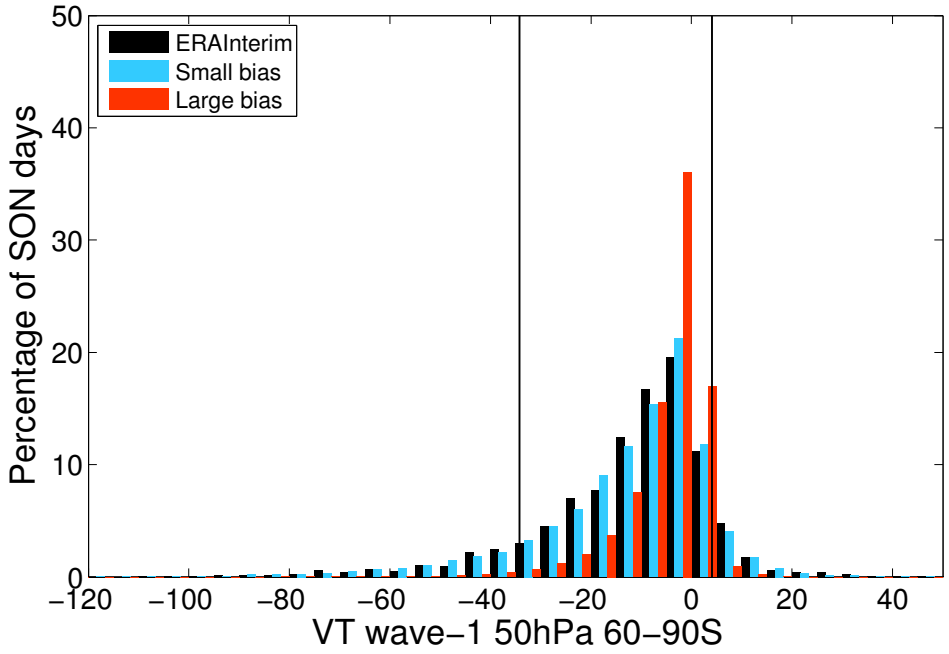

Figure 2.6: Distribution of 50 hPa wave-1 meridional heat flux averaged 60°-90°S during SON from 1979 to 2005 for ERA-Interim (black) and ensemble of CMIP5 models with the small (blue) and large (red) biases relative to ERA-Interim, with model ensembles defined in Table 2.2. The vertical black lines represent the 10th (-32.5 Kms^{-1}) and the 90th (4.3 Kms^{-1}) percentile values of the daily ERA-Interim distribution.

seven small bias models and seven large bias models (Table 2.2). The results presented below are largely insensitive to the addition or removal of one model from the ensembles.

The distribution of the large bias ensemble is significantly different from the ERA-Interim distribution at 95% significance (compared red and black in Fig. 2.6) whereas the distribution of the small bias ensemble is significantly similar (compared blue and black in Fig. 2.6), according to a random sampling Kolmogorov-Smirnov test (Table 2.3). Note, a regular Kolmogorov-Smirnov test was not used because of the known biases introduced into the statistical test when applied to populations of significantly different sizes. The statistical analysis shows that the large bias models do not capture the mean or higher order moments of the ERA-Interim distribution.

All large bias models are low-top models, consistent with S14's findings in the NH. All six models identified in S14 as large bias for the NH are also part of the large bias model ensemble in the SH. Models which fail to replicate the heat flux extremes at 50 hPa in one hemisphere, also under-represent the extremes in the other hemisphere which seems to imply

Table 2.3: Statistics of the daily distribution of wave-1 heat flux averaged 60°-90°S at 50 hPa during SON for ERA-Interim data, the small bias model set and the large bias model set for the years 1979-2005. The Kolmogorov-Smirnov test is relative to ERA-Interim data. For this run no large bias samples had a KS test p value over 0.05 whilst small bias samples had a KS test p value over 0.05 95.4% of the time. This was implemented using method in S14 appendix A.

		Mean	Std	10th perc.	90th perc.	KS test p value
	ERA-Interim	-12.05	17.62	-34.23	4.10	1.00
50 hPa	Small bias	-12.39	17.81	-34.50	3.17	> 0.05
	Large bias	-4.51	8.13	-14.89	1.17	< 0.05 (95%)

there are mechanisms intrinsic to these models. Although the majority of the models in the small bias ensemble are high-top, two models (bcc-csm-1-m and NorESM1-M) are low-top. Only two models (MPI-ESM-MR and MPI-ESM-P) are contained in the small bias model ensembles in both hemispheres. It can be seen from Figure 2.5 that although high-top models are generally better at capturing the extremes in the heat flux distribution, there are some low-top models which perform well by this criterion, and there are some high-top models which do much worse.

The large bias models also under-estimate negative and positive heat flux extremes at 10 hPa (not shown), with a tendency of the low-top models to fall above the 1-to-1 line, as found by S14. Shaw and Perlwitz (2010), motivated by previous work by Boville and Cheng (1988), investigated planetary wave biases associated with low-top models. They found that at 10 hPa low-top models either under-predict upward wave coupling because of excessive damping or over-predict downward wave coupling due to unphysical wave reflection from the model lid.

Figure 2.7 compares the error at 10 hPa (defined as the radial distance from the ERA-Interim, for which both types of extreme events occur 10 percent of the time) in the NH during JFM versus the same bias in the SH during SON. The correlation value between the extremes of CMIP5 in the NH JFM and the SH SON is 0.71, consistent with the idea that a model's performance according to this metric is roughly the same between hemispheres, especially higher up in the stratosphere. The high-top models, in general, are better able

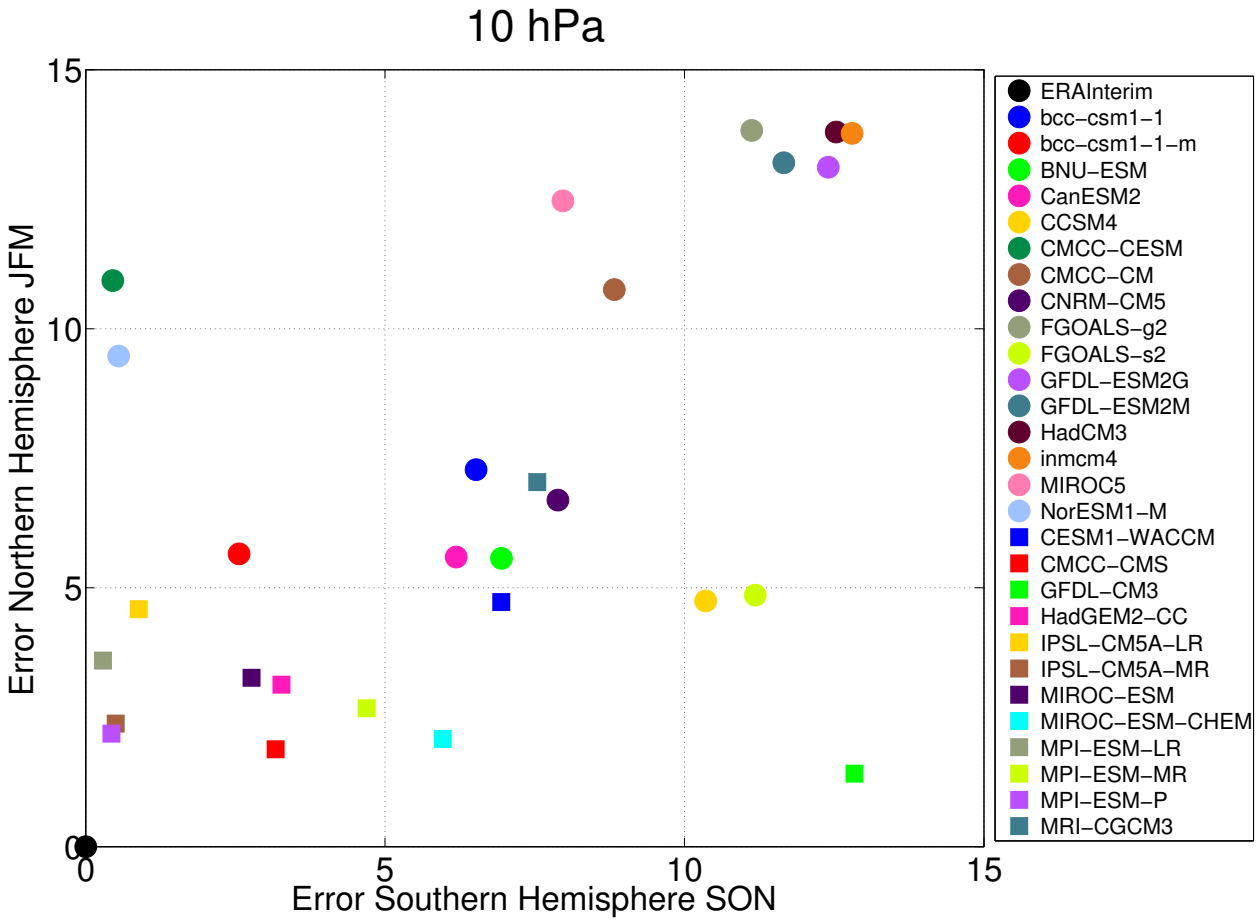

Figure 2.7: Error of the NH JFM high latitude eddy heat flux versus SH SON high latitude eddy heat flux at 10 hPa for the CMIP5 models. The error has been defined as the radial distance to ERA-Interim for percentage of extreme negative and positive days ($<$ -71.34 Kms^{-1}and $>$ 2.81 Kms^{-1} for the SH and $<$ -10.41 Kms^{-1} and $>$ 148.10 Kms^{-1} for the NH). CMIP5 models, with circles representing low-top models and squares representing high-top models, along with the ERA-Interim data (which has zero error) are plotted.

to capture the extremes of the planetary-wave stratospheric heat flux at 10 hPa in both hemispheres (with the error close to zero in both hemispheres). The low-top models consistently show larger biases in representing the heat flux extremes at 10 hPa. We can see that the majority of models fall on the 1-to-1 line, but with some noticeable exceptions such as GFDL-CM3, a high-top model which performs significantly better at this metric at 10 hPa in the NH, and vice versa for the low top model CMCC-CESM.

2.4.2 Representation of Links to Troposphere

In this section we explore whether model biases in high latitude stratospheric heat flux extremes are connected to the tropospheric circulation in CMIP5 models. In the NH biases in stratospheric eddy heat flux were largest for extreme negative events and this led to model biases in the North Atlantic jet stream and geopotential height. An important difference between the SH and NH is that the modelled mslp and eddy geopotential height exhibit large climatological biases compared to ERA-Interim. Figure 2.8 shows the difference between the CMIP5 models and ERA-Interim SON climatological mslp (top row) and climatological eddy geopotential height (bottom row), at 500 hPa (black) and 10 hPa (shaded). Individual models cannot capture the longitudinal position seasonal cycle of the ASL and the central pressure is high compared to reanalysis (Hosking et al., 2013). Only the small bias models are able to capture the wave-1 high latitude pattern at 10 hPa. Neither of the model ensembles are able to replicate the 500 hPa ERA-Interim SON climatology (Fig. 2.4a,d) sufficiently, with the differences as large as between the model ensembles themselves. Since the mean state of the models are so biased, compared to ERA-Interim, we cannot use the CMIP5 models to detect the impact of biased stratospheric wave-1 heat flux extremes (Fig. 2.5 on the mean tropospheric climate in the SH, in contrast to the NH.

We find that the biased eddy geopotential height variance at 500 hPa ($\sqrt{\overline{z'^2}}$) is significantly correlated with the position of the jet stream relative to reanalysis (defined as the difference in latitude of maximum zonal-mean zonal wind at 850 hPa) as shown in Figure 2.9. The biased position of the SH jet is well known (Kidston and Gerber, 2010). The cor-

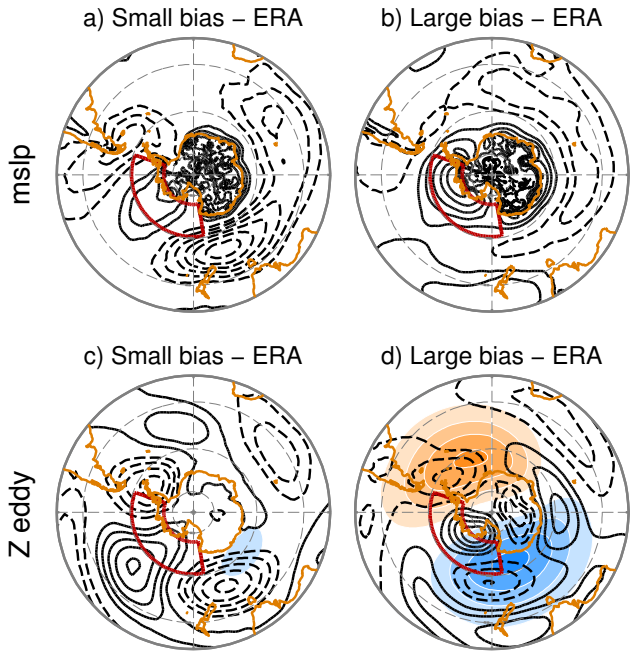

Figure 2.8: Difference in climatological mean sea level pressure (top), and eddy geopotential height (bottom) at 500 hPa (black) and 10 hPa (shaded), during SON from 1979 to 2005 between ERA-Interim and (left) small, (right) large bias ensembles. Contour interval is 1hPa for mslp and 10 m (black) and 100 m (shaded) for eddy geopotential height. The zero contour is omitted.

relation coefficient is $r = -0.54$ and a linear regression explains 30% of the model variance. This suggests that reducing the bias in geopotential height is important.

The link between the representation of stratospheric heat flux extremes in CMIP5 historical simulations to tropospheric conditions can be quantified after removing the biased climatological mean state. Figure 2.10 compares the mslp anomaly of the small bias and large bias model ensembles with ERA-Interim. The small bias models are able to capture the strength and position of the anomalous mslp seen during the extreme events whereas the large bias models are unable to replicate this tropospheric variability. We obtain similar results for 500 hPa geopotential height and 850 hPa temperature (not shown). The issue of differences in the length of time series, with considerably fewer extreme days for large bias compared with small bias models, is discussed in Section 2.6.

The large bias models do not capture the anomalous mslp over the Antarctic Peninsula during stratospheric extreme events. Figure 2.11 shows the SON distribution of anomalous daily mslp over the Antarctic Peninsula for ERA-Interim and the CMIP5 model ensembles.

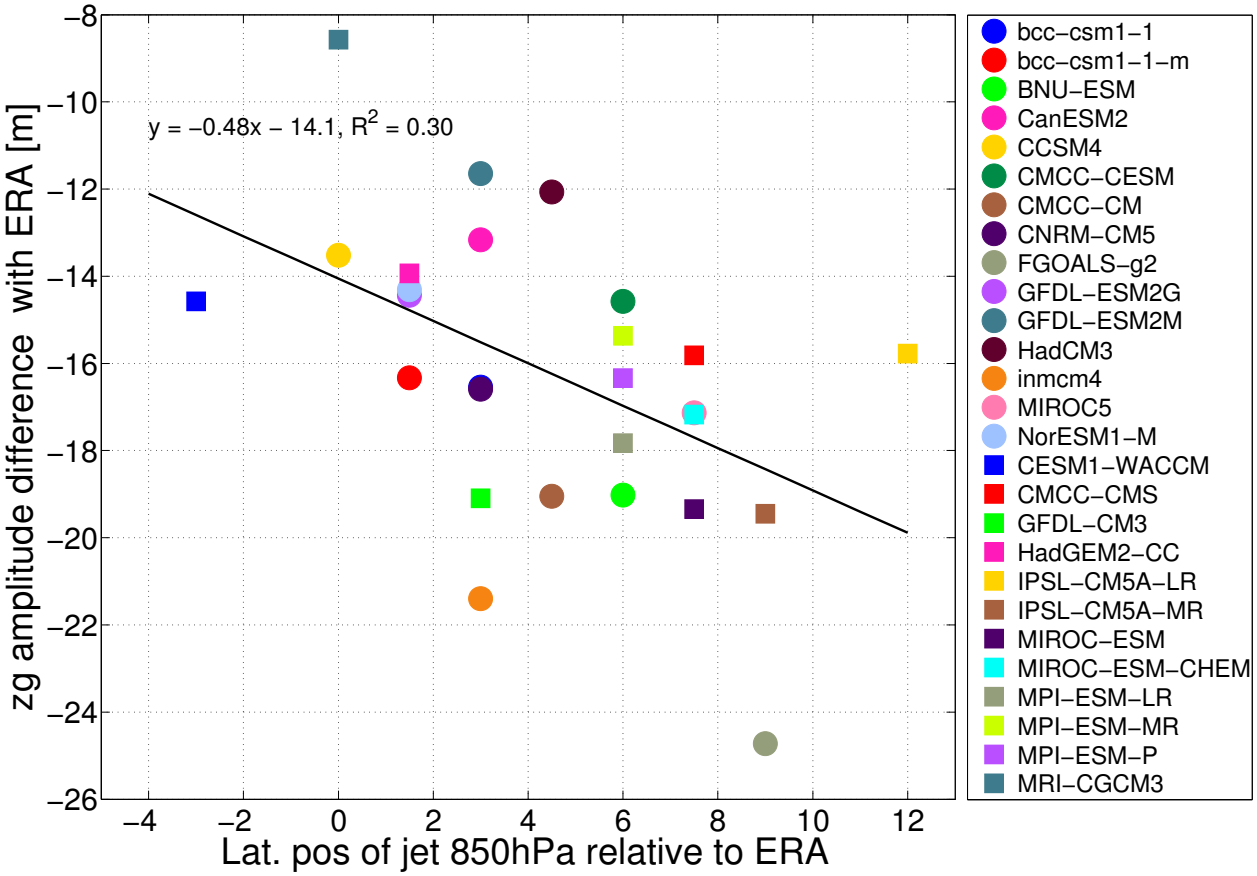

Figure 2.9: CMIP5 high-latitude 500 hPa eddy geopotential height amplitude bias relative to ERA-Interim versus bias in SH tropospheric jet at 850 hPa relative to ERA-Interim during SON. See section 2.4.2 for explanation of how each quantity was calculated. Circles represent low-top CMIP5 models and squares represent high-top CMIP5 models. A linear fit is added, along with its regression coefficients and the R^2 value.

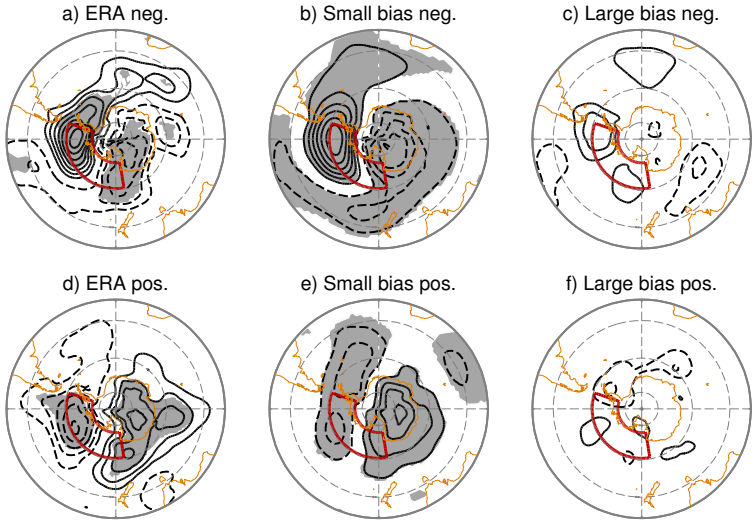

Figure 2.10: Mean sea level pressure field for extreme (top) negative days and extreme (bottom) positive days during 1979 to 2005. See section 2.3 for definition of extreme event days. The anomalies found for (a,b) ERA-Interim are compared with those for the (b,e) small bias model set and the (c,f) large bias model set. Positive anomalies are shown with full lines and negative anomalies are indicated by dashed lines, with contour levels of 10 m. The zero contour has been omitted in all plots. Grey shading shows anomalous values statistically significant at 99% (see Appendix 2.6 for details).

The region 60°-75°S, 240°-330°E was chosen to coincide with the centre of the wave-1 anomalous pattern seen in Figure 2.3a,b. The large bias models (unlike the small bias models) do not capture the extent of the variability seen in reanalysis. In particular, the large bias ensemble distribution is significantly different from the ERA-Interim distribution at 99% significance according to a random sampling Kolmogorov-Smirnov test. The mean and variability of the small bias models agree well with ERA-Interim. Although the topography of the region makes the comparison harder, similar assertions can be made for Eastern Antarctica. The representation of stratospheric wave events appears to be an important factor in the variability of Antarctic weather and climate patterns during spring.

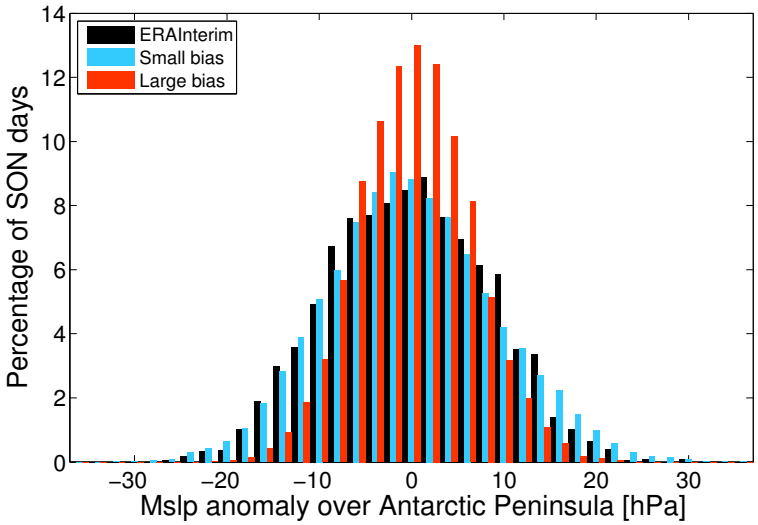

Figure 2.11: Daily distribution of anomalous mean sea level pressure averaged from 60°-75°S, 240°-330°E during SON from 1979 to 2005 for ERA-Interim (black) and small (blue) and large (red) bias CMIP5 model ensembles, with ensembles defined in Table 2.2.

2.5 Summary and Discussion

2.5.1 Summary

A dynamical metric of troposphere-stratospheric planetary-wave heat flux events, defined as the 10th and 90th percentiles of the daily 50 hPa wave-1 heat flux originally developed for the NH, is applied to the SH. These extreme events in the stratosphere are associated with upward and downward wave-coupling between the troposphere and the stratosphere. To investigate which CMIP5 models have realistic troposphere-stratosphere coupling in the SH, a 'small bias' and a 'large bias' ensemble are created containing models which can and cannot replicate the stratospheric heat flux extremes seen in ERA-Interim data, respectively. The main findings of this study on SH stratosphere-troposphere coupling are as follows:

- In reanalysis, SH stratospheric heat flux extremes are linked to high latitude tropospheric anomalies in the Amundsen Sea region. During extreme negative (positive) events there is a westward (eastward) shift of the ASL, a warming (cooling) and increase (decrease) of geopotential height over the Amundsen and Bellingshausen Seas.

These findings complement those from the NH where the largest impacts occurred in the North Atlantic (Shaw and Perlwitz, 2013, S14).

- CMIP5 models exhibit a large climatological eddy geopotential height bias during SON which is connected to the well-known bias of the jet position. This climatological bias prevents an assessment of any potential impact of stratospheric heat flux extremes on tropospheric climate.

- The impact of stratospheric heat flux extremes on tropospheric variability can be assessed after the climatological bias is removed. The results show that CMIP5 models with biased stratospheric heat flux extremes significantly under-estimate mslp variabilty over the Antarctic Peninsula.

2.5.2 Discussion

We have demonstrated that stratospheric variability is linked to tropospheric variability over the ASL. However, large climatological mean biases in the SH circulation (Kidston and Gerber, 2010; Ceppi et al., 2012; Bracegirdle et al., 2013) mask any impact of troposphere-stratosphere coupling on the tropospheric mean state.

We investigated potential sources of tropospheric bias including biased sea surface temperature (SST) and model resolution. However, we found no significant difference between the eddy geopotential height simulated in atmosphere-only models, AMIP (Atmospheric Model Intercomparison Project), and CMIP models. There are, however, a limited number of models available with AMIP runs so the size of the ensembles were restricted to two models in this analysis. We also found no relationship between the model bias and model resolution across CMIP5 models.

The distribution of Antarctic sea ice has been shown to influence the tropospheric circulation at high latitudes (Raphael, 2001). The link to extreme changes in sea ice can be seen in mslp (Wu et al., 1996) and 500 hPa geopotential height(Renwick, 2002). Sea ice variability has a large radiative effect, as well as an impact on mass flux in the polar region

(Budd, 1991).

Ozone has had a significant impact on regional climate in the SH during 1979-2005 (Thompson and Solomon, 2002). There have been no significant changes in the 50 hPa heat flux distributions during SON, however there are impacts later in the seasonal cycle (Shaw et al., 2011). How troposphere-stratosphere coupling in the SH will change during the period of ozone recovery is a question for further research.

We have shown that planetary wave coupling is linked to climate variability of the Amundsen Sea region. The vast majority of coupled climate models are not reproducing the observed trends in Antarctic SIE (Eisenman et al., 2011; Maksym et al., 2012; Turner et al., 2013a) so improving simulation of Antarctic climate variability and connections to the ASL is an important question for future research (Raphael et al., 2016). Our results suggest an accurate simulation of stratospheric variability is important for the ASL. Understanding the dynamical mechanism responsible for the link between troposphere-stratosphere planetary-scale wave coupling and the ASL and Antarctic tropospheric climate variability is an area for future research.

2.6 Appendix: Statistical significance of anomalous values

The grey shading in Figures 2.3 and 2.10 indicates that the anomalous values are statistically significant at 99%. This analysis was completed, for every latitude and longitude gridpoint, by taking 10,000 random composite subsamples, with each subsample the same size as the composite of extreme events, from the whole SON time series to create a distribution. The shaded areas occur outside of the 0.5th and 99.5th percentile of this distribution and so can be thought of as statistically distinct from the natural variability of the region. This also solves the issue of differing length of time series and uses the entire period of data available.

CHAPTER 3

ROBUST RESPONSE OF THE AMUNDSEN SEA LOW TO STRATOSPHERIC OZONE DEPLETION

This work was published in Geophysical Research Letters in 2016 (England et al., 2016a).

3.1 Introduction

Stratospheric ozone depletion, and the occurrence of the ozone hole during spring, has been the dominant forcing of SH climate change in recent decades (Polvani et al., 2011) and its effects on large-scale features of the atmospheric circulation have been well documented (Marshall, 2003; Son et al., 2010; Thompson et al., 2011; Previdi and Polvani, 2014). Recent research has attempted to document how ozone depletion has driven changes in the ASL, one of the most important regional features in the southern high latitudes (Turner et al., 2013b). The ASL is a low pressure centre located in the region 60-75°S 170-290°E. The depth and location of the ASL have been shown to have a significant impact on the surface air temperature, precipitation and the distribution of sea ice around West Antarctica (Turner et al., 1997; Massom et al., 2008; Holland and Kwok, 2012; Hosking et al., 2013), the region with the largest trends in SIE (Parkinson and Cavalieri, 2012). More detail on the ASL for the period 1979-2017 is given in Section 1.1.2. Due to the ASL's influence over the climate of West Antartica, it is important to understand how it has been affected by the forcing of stratospheric ozone depletion in the twentieth century.

Turner et al. (2013b) examine the monthly trends in central pressure and location of the ASL in the years 1979-2008 using ECMWF reanalysis data, and find that they are highly variable, with no robust trend in any season. Nonetheless, Turner et al. (2009b) have proposed that a slight deepening of the autumn ASL in models might be linked to stratospheric ozone depletion. Furthermore Fogt and Zbacnik (2014) offered modelling evidence for the importance of ozone depletion in deepening the summertime ASL, although were not able to demonstrate this at the 95% significance level.

The difficulty in establishing ozone-forced trends in the ASL arises from the very large natural variability in that region (Lachlan-Cope et al., 2001; Turner et al., 2015). Interannual variations of the ASL has been linked to several drivers of climate variability: the phase of El Nino-Southern Oscillation is important for the ASL central pressure (Fogt et al., 2011; Pezza et al., 2012; Turner et al., 2013b), and the phase of the SAM influences the ASL central pressure and longitudinal location (Lefebvre et al., 2004; Fogt et al., 2012a; Turner et al., 2013b). Furthermore, recent model studies (Ding et al., 2011; Ding and Steig, 2013; Fogt and Wovrosh, 2015; Li et al., 2015; Raphael et al., 2016) have highlighted the importance of tropical SSTs on the ASL and West Antarctic temperatures (Comiso, 2000; Marshall, 2003; Schneider et al., 2012). Finally, a stratospheric influence has been shown to be important for the location of the ASL (England et al., 2016b). The goal of this paper is to bring out the ozone-forced response of the ASL and distinguish it from this large and complex natural variability.

We here isolate the effect of ozone forcing by comparing an ensemble of climate model runs with a realistic ozone hole evolution to an ensemble with stratospheric ozone concentrations fixed at 1955 levels. This comparison allows a direct attribution of the differences to stratospheric ozone depletion, and the use of ensembles allows us to extract the forced response from the large natural variability. To establish a robust result, we repeat this analysis with two different, fully coupled general circulation models: although both of these models are from the CESM family, they have very different physical processes and configurations. Both models show a robust deepening of the summertime ASL forced by stratospheric ozone

depletion over the second half of the twentieth century

3.2 Data and Methods

In this study we employ two configurations of a state of the art model, the CESM1, to investigate the effect of stratospheric ozone depletion on the ASL. WACCM4, documented by Marsh et al. (2013), is the high-top atmosphere model configuration included in CESM1. It has a horizontal resolution of 1.9° latitude by 2.5° longitude, with 66 vertical levels and a model lid height extending up to the lower thermosphere, 140 km. WACCM4 has fully interactive middle atmosphere chemistry, so is able to realistically capture the development of the Antarctic ozone hole in austral spring. The Community Atmosphere Model (CAM5) is the low top atmosphere model configuration of CESM1 (Kay et al., 2015). It has a higher horizontal resolution of 0.9° latitude by 1.25° longitude. There are 30 levels in the vertical direction, with a rigid lid at 50 km above the surface. Both models are coupled to fully prognostic ocean, sea ice, and land components (Gent et al., 2011).

For each model configuration, we analyse two ensembles of 51-year runs 1955-2005, differing only in the levels of stratospheric ozone depletion. The first ensemble comprises standard 'historical' Coupled Model Intercomparison Project Phase 5 (CMIP5) integrations (Taylor et al., 2012), including all known natural and anthropogenic forcings. These runs will be referred to as 'Ozone Hole' runs. The second ensemble is identical in every respect, except that ODSs and, for CAM5, the levels of stratospheric ozone, are held fixed at 1955 levels (pre-ozone hole). These runs will be referred to as 'Fixed Ozone' runs because no ozone hole develops in the springtime. Since the ozone concentrations in CAM5 are specified from the mean of the WACCM4 historical runs, the amplitude and evolution of stratospheric ozone depletion is practically identical between the WACCM4 and CAM5 runs. Spring polar cap ozone levels for the individual WACCM4 members (Fig. 3.1), and these were found by Marsh et al. (2013) to compare very well with observations. There are six members contained in both WACCM4 ensembles, previously analysed by Solomon et al. (2015) in the context of the

Southern Ocean response to changing ODSs, and eight members contained in both CAM5 ensembles.

To put the model results in the context of observations, monthly mean sea level pressure is analysed from two reanalysis datasets, the Interim European Centre for Medium-Range Weather Forecasts (ECMWF) reanalysis (ERA-Interim) (Dee et al., 2011) and the National Centre for Environmental Prediction: U.S. Department of Energy (NCEP-DOE) AMIP-II reanalysis (Kanamitsu et al., 2002) over the period 1979-2005. As in other investigations of the ASL (eg.Fogt et al. (2012b)), the usage of reanalysis products is limited to the years following 1979, after the assimilation of satellite data.

Finally, we introduce the three metrics used to define the ASL: the absolute central pressure, and its position in longitude and latitude. The location is determined from monthly sea level pressure data using the same method as Turner et al. (2013b): it is the location with the lowest mean sea level pressure in the region 50-180°W, 60-75°S. Figure 3.2 shows the climatological seasonal cycle of the three ASL metrics for the historical runs of CAM5 and WACCM4. The seasonal cycle of the ASL for the ensemble average WACCM4 (green) and CAM5 (red) 'Ozone Hole' runs are compared to reanalysis (black) as well as a range of 26 CMIP5 models (shaded envelope). Both WACCM4 and CAM5 display better skill in simulating the seasonal cycle of these three ASL properties compared to the majority of the models (Hosking et al., 2013), especially the location.

Building upon previous work by Fogt and Zbacnik (2014) and Fogt and Wovrosh (2015), we are able to detect a robust signal of ozone depletion on the ASL. By employing large ensembles of runs from two state of the art climate models, which are able to well represent the ASL climatology (Figure 3.2), we are able to isolate the forced signal from the large natural variability (Lachlan-Cope et al., 2001). Moreover, comparing 'Fixed Ozone' and 'Ozone Hole' ensembles allows us to directly attribute any differences in the ASL to stratospheric ozone depletion because all other factors are held fixed.

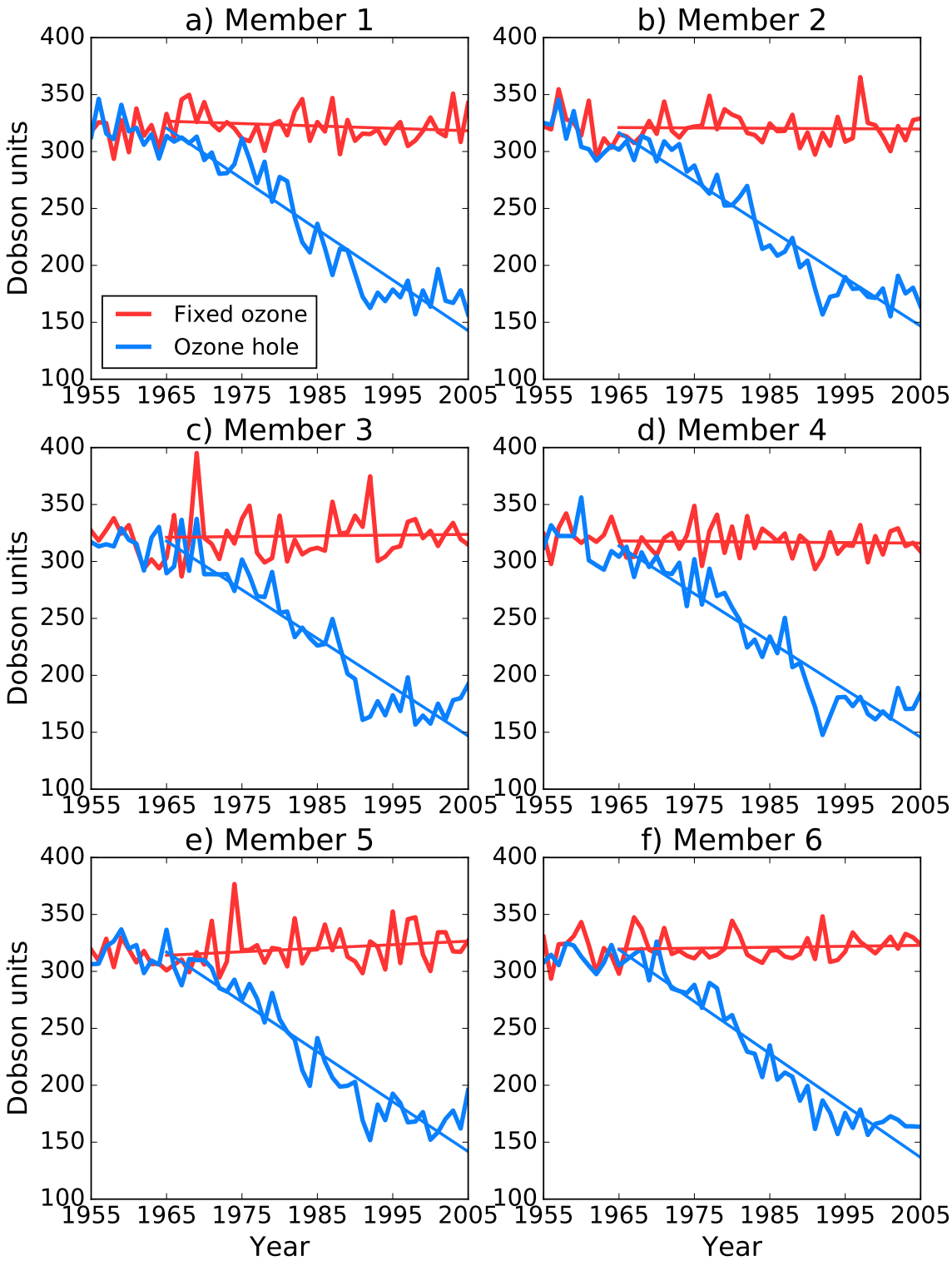

Figure 3.1: Polar cap 70-90°S integrated ozone, SON, for six WACCM4 runs (a-f) with fixed ozone (red) and historic ozone levels (blue).

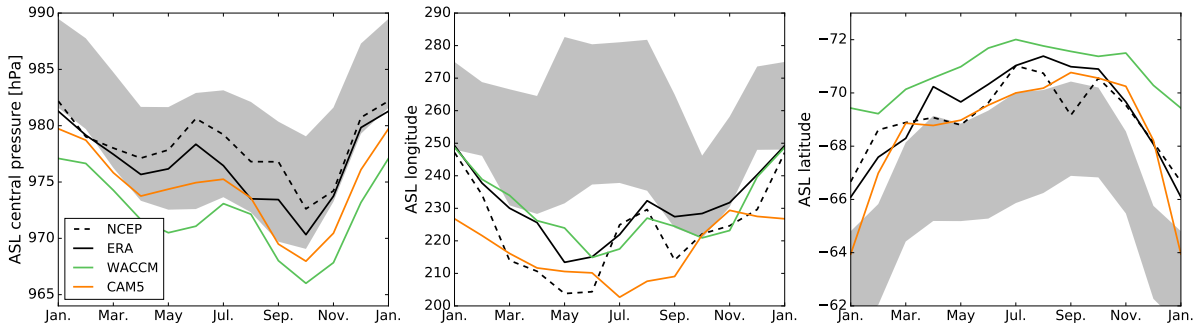

Figure 3.2: Seasonal cycle (average over 1979-2005) of three key metrics that define the Amundsen Sea Low: central pressure (left), longitude (centre) and latitude (right). An ensemble average of six WACCM4 (green) and eight CAM5 (orange) historical integrations are compared with NCEP-DOE II (dashed black) and ERA-Interim (solid black). The grey shading indicates the $+/-1\sigma$ envelope for 26 CMIP5 models.

3.3 Results

Figure 3.3a shows the column integrated polar cap ozone levels during spring; levels of stratospheric ozone are seen to start depleting after 1965, reaching a minimum value by 2005. Whilst the Antarctic ozone hole forms in spring, it takes time for the signature to migrate down to the surface resulting in the largest effects of ozone depletion in the troposphere occurring in summer (Thompson et al., 2011). Consistent with this, we find that stratospheric ozone depletion only has an impact on the ASL in DJF (Dec., Jan. and Feb.).

When forced with a realistic ozone hole the ASL is seen to deepen by 1 hPa per decade in DJF over a 41-year period of stratospheric ozone depletion in both WACCM4 and CAM5 (Figures 3.3b,c blue curves). In contrast, the 'Fixed Ozone' ensembles (red curves) display no trends in the central pressure of the ASL over the same time period (Figures 3.3b,c red curves). The difference between the two ensembles becomes statistically significant at 95% levels by 1993 in WACCM4 and 1999 in CAM5. It must be noted that the magnitude of the change is smaller than the natural variability of the ASL as depicted by the large spread across the individual ensemble members (thin blue and red curves). The presence of the ozone effect in two very different models provides confidence in the result. Of the three ASL metrics, stratospheric ozone depletion only has an effect on the ASL central pressure;

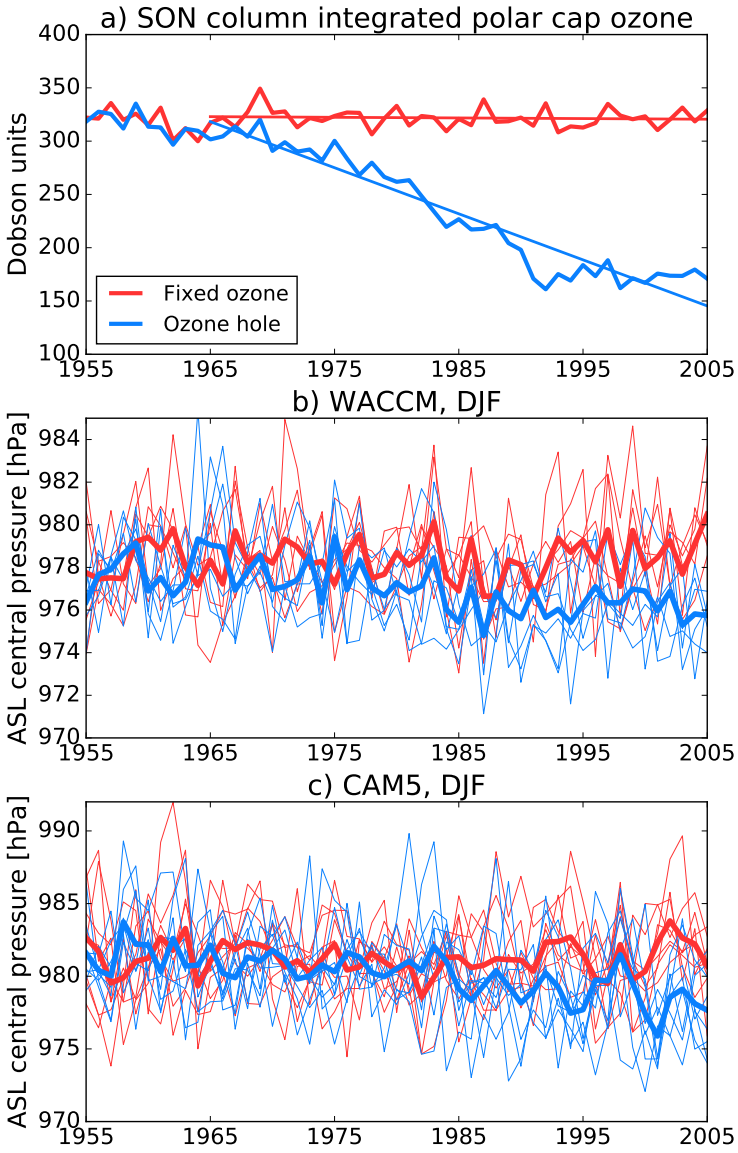

Figure 3.3: a) Column integrated polar (60-90°S) ozone in the Southern Hemisphere, averaged over SON, used for the CAM5 runs with fixed ozone (red) and historic ozone levels (blue). The trendlines show trends over the period 1965-2005. Ozone levels for the individual WACCM members are shown in supplementary figure S1. b) The ASL central pressure during DJF for six 'Fixed Ozone' runs and six 'Ozone Hole' runs in WACCM4 with the bold lines indicating the ensemble averages. c) The ASL central pressure during DJF for eight 'Fixed Ozone' runs and eight 'Ozone Hole' runs in CAM5 with the bold lines indicating the ensemble averages.

in agreement with Fogt and Wovrosh (2015), we find no statistical difference between the 'Fixed Ozone' and 'Ozone Hole' ensembles when examining the latitudinal or longitudinal position of the ASL over the same time period (not shown).

To illustrate that the ozone effect on the ASL is confined to summer, we show in Figure 3.4 the full seasonal cycle of ASL central pressure in WACCM4 (a,c) and CAM5 (b,d) averaged over the 15 years before the dramatic depletion of stratospheric ozone (1955-1969) and the 15 years when stratospheric ozone levels reached their minimum (1991-2005). The 15-year averaging window was chosen to maximise the signal to noise ratio. Although Turner et al. (2009b) and Fogt and Zbacnik (2014) suggested there was a possible relationship between ozone depletion and the ASL in austral autumn, our models show no evidence for this. For the 'Ozone Hole' ensemble there is a pronounced deepening in summer, most notably in January, found in the years after the ozone hole has peaked. In contrast, the seasonal cycle of ASL for the 'Fixed Ozone' ensemble remains unchanged between the two periods.

Recent studies into the link between ozone depletion and changes in the ASL (Turner et al., 2009b; Fogt and Zbacnik, 2014) only looked at the years following 1979, constrained by available reanalysis and model data. However, it is well established that levels of stratospheric ozone started to significantly decrease from the mid 1960s, so these studies miss out on roughly 15 years of ozone forced trends. Figure 3.5 compares DJF trends in ASL central pressure for the WACCM4 and CAM5 ensembles found over the truncated period 1979-2005 and those from the full period 1965-2005. Trends for the ensemble means (left panels) are calculated by examining the distribution of trends of the individual members (centre and right panels). Trends are statistically different from zero at 95% significance if the errorbars do not cross the zero line. The deepening of the ASL in DJF due to ozone depletion can be seen in Figure 3.5 from the trend in the difference (green) between the 'Ozone Hole' (blue) and 'Fixed Ozone' (red) ensembles.

For the WACCM4 runs, even with the large number of members used, this non-zero trend is only statistically significant at a 95% level using the longer time period. This would explain why previous studies found it difficult to diagnose a robust ozone effect on the ASL.

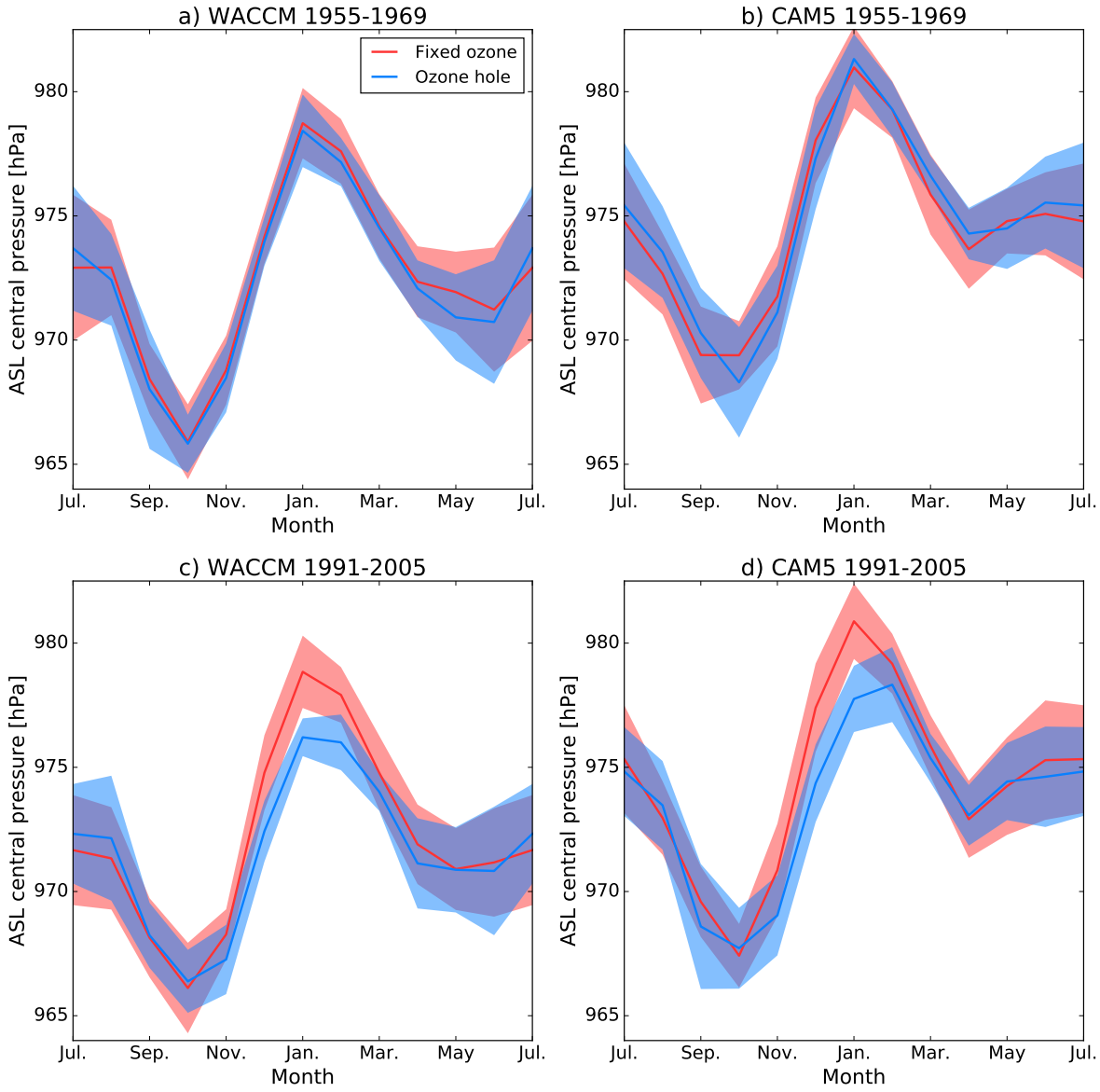

Figure 3.4: Seasonal cycle of ASL central pressure taken over fifteen-year periods: a) and b) the early period (1955-1969) before the effects of ozone depletion, and c) and d) the late period (1991-2005) with the effects of ozone. Fixed ozone (red) and realistic ozone (blue) runs from, a) and c), WACCM4 and, b) and d), CAM5 are compared. The lines indicate the ensemble average and the shading represents the $+/-1\sigma$ of the yearly variability across the ensemble over the fifteen-year period.

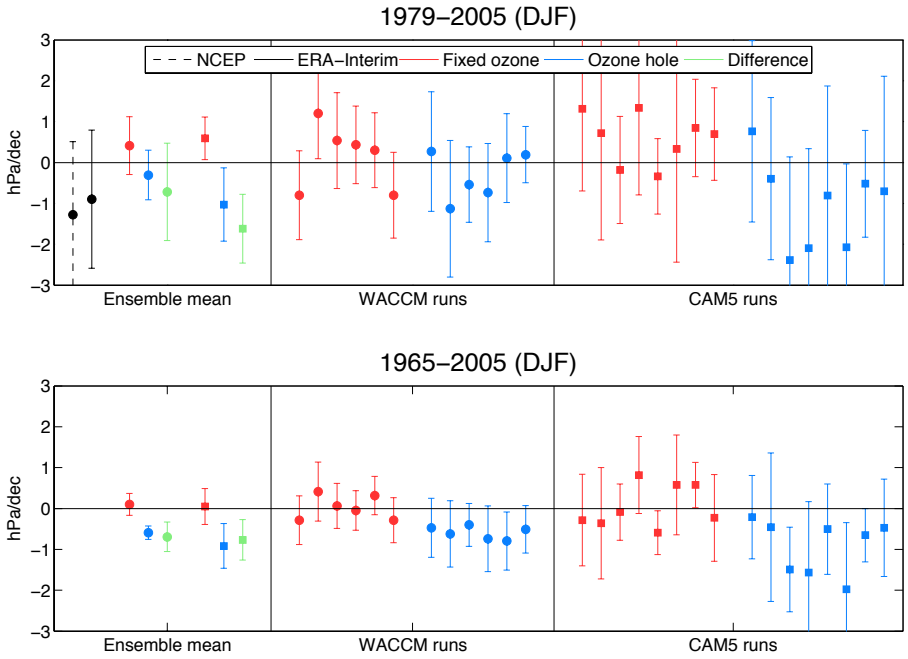

Figure 3.5: Trends in ASL central pressure in DJF during years 1979-2005 (top) and 1965-2005 (bottom). The ensemble average for both WACCM4 (circles) and CAM5 (squares) runs, as well as the individual members, are displayed with error bars indicating 95% significance. NCEP-DOE II and ERA-Interim are plotted for the shorter time period. Red indicates runs with fixed ozone levels, blue indicates runs with realistic ozone and green shows the difference between them.

Trends for individual members of each ensemble are also shown; broadly, the individual 'Ozone Hole' runs have negative trends, whilst the individual 'Fixed Ozone' runs have no trends. Averaging over all members of the ensemble, as well as the full time period 1965-2005, is required to clearly see that stratospheric ozone depletion causes a deepening of the ASL in summer.

3.4 Summary and Discussion

Using two CESM1 models, CAM5 and WACCM4, we have demonstrated that stratospheric ozone depletion causes a deepening of the summertime ASL of roughly 1 hPa/dec. Previous studies have struggled to isolate the impact of stratospheric ozone on the ASL, mostly due to the large natural variability of the ASL itself. This study makes it clear, however, that using ensembles of model integrations and analysing them over the full period of ozone depletion (which started a couple of decades before the satellite era) are crucial in determining the

ozone impact on the ASL.

In contrast with similar studies (Turner et al., 2009b; Fogt and Wovrosh, 2015; Hosking et al., 2016) which only analysed integrations with all known forcings present, the changes seen here can be unequivocally attributed to stratospheric ozone depletion since we have explicitly run the model with and without ozone depletion. One might question, however, whether two models are enough to draw robust conclusions. It should be emphasised that these are two very different models, with markedly different climate sensitivities (Gettelman et al., 2013). Furthermore, impacts of stratospheric ozone depletion being confined to summer is consistent with the observational study by Thompson et al. (2011), and we are able to build upon the modelling study by Fogt and Zbacnik (2014) to more cleanly isolate the signal.

Although beyond the scope of this study, the next step would be to establish the precise mechanism connecting stratospheric ozone depletion and the ASL. One reasonable hypothesis pertains to changes in synoptic scale activity around West Antarctica. High latitudes cyclones in the Amundsen and Bellingshausen Seas have been shown to be important for the formation of the ASL (Walsh et al., 2000; Fogt et al., 2012b). Grise et al. (2014) demonstrate that stratospheric ozone depletion has induced a significant poleward shift in cyclone frequency in summer, with a marked increase in the frequency of the strongest cyclones in the Amundsen and Bellingshausen Seas region. Therefore an intensification of cyclonic activity around West Antarctica, as a result of stratospheric ozone depletion, is a potential mechanism which would cause the ASL to deepen in summer.

CHAPTER 4

CONTRASTING THE ANTARCTIC AND ARCTIC ATMOSPHERIC RESPONSES TO PROJECTED SEA ICE LOSS IN THE LATE 21ST CENTURY

This work was published in Journal of Climate in 2018 (England et al., 2018).

4.1 Introduction

Although Antarctic SIE has been increasing steadily (Section 1.1.1) at a small but significant rate of nearly 2% per decade over the last forty years (Comiso et al., 2017a), it is hard to imagine, under the current trajectory of greenhouse gas emissions, a scenario without a significant reduction in SIE by the end of this century. In fact, 2017 and 2018 were at, or near, record lows for Antarctic March SIE (NSIDC, 2019). In all of the Representative Concentration Pathways (RCPs) examined by the Intergovernmental Panel on Climate Change Fifth Assessment Report, both Arctic and Antarctic SIE are projected to decrease by 2100 (Collins et al., 2013). The atmospheric response to future Antarctic sea ice loss under a changing climate is, at present, a largely unexplored question.

The recent literature has almost entirely focused on the atmospheric effects of Arctic sea ice loss (for recent reviews see e.g., Cohen et al. (2014) and Vihma (2014)), partly motivated by the recent dramatic reduction of Arctic SIE at a rate of over 4% per decade (Vaughan et al., 2013). The consequences of diminishing Arctic sea ice on the high latitudes are well established, with higher levels of warming in the Arctic than at lower latitudes, and increased

precipitation in that region (Deser et al., 2010; Screen and Simmonds, 2010). There is less agreement, however, on the impact of Arctic sea ice loss on the mid-latitudes (Barnes and Screen, 2015; Overland et al., 2015; Screen, 2017a). Evidence from climate models suggests that Arctic sea ice loss acts to shift the jet equatorward in winter (Butler et al., 2010; Deser et al., 2010; Peings and Magnusdottir, 2014; Sun et al., 2015) and the robustness among models has been documented in (Screen et al., 2018). However, many features of the mid-latitude response to sea ice loss identified from the recent historical trends (Screen et al., 2013; Mori et al., 2014; McCusker et al., 2016; Sun et al., 2016) seem to be model dependent.

For instance, there is disagreement over whether sea ice loss causes a weakening (Kim et al., 2014; Peings and Magnusdottir, 2014; Sun et al., 2015) or a strengthening (Cai et al., 2012; Screen et al., 2013; Sun et al., 2014) of the polar vortex. Sun et al. (2015) (hereafter S2015) demonstrate that part of the discrepancy can be reconciled by the competing effect from the sea ice loss in the Pacific and Atlantic sector: melting sea ice in the Atlantic sector is linked to enhanced wave propagation into the stratosphere and a weaker vortex whereas melting sea ice in the Pacific sector is linked to wave suppression and a stronger vortex. This cancellation, also reported in McKenna et al. (2018), is found to produce a muted stratospheric response when sea ice loss is imposed in both sectors.

Unlike the Arctic, there has been very little research concentrating on the atmospheric impacts of projected Antarctic sea ice loss. The Antarctic offers the opportunity to investigate the effects of future sea ice loss in a simpler setting than the Arctic because (1) most of the major land masses are found in the NH, (2) the SH atmospheric circulation is more zonally symmetric and (3) projected sea ice losses are much less regionally varying in the Antarctic. In the context of historical trends, it has been suggested that recent sea ice expansion might have resulted in a small poleward jet shift during the cold seasons (Smith et al., 2017). Results from Raphael et al. (2011) suggest that changes in Antarctic sea ice in austral summer may also have an effect on the atmospheric circulation. Complicating matters, Bracegirdle et al. (2018) suggest that the relationship between Antarctic SIE and the strength of the Southern jet is possibly stronger than the relationship with the latitu-

dinal position of the jet. On the subject of future Antarctic sea ice decline, we are aware of only three studies that have used comprehensive climate models, and their results are in disagreement; Kidston et al. (2011) find no significant effects when contracting the sea ice edge, whereas Bader et al. (2013) (while investigating the response in Austral winter alone) find an equatorward shift of the tropospheric jet, in agreement with an earlier study by Menendez et al. (1999). The effect of the changing Antarctic sea ice on the mid-latitudes is still largely an unresolved question.

In this paper, we examine the atmospheric response to future reduced Antarctic SIE, and contrast it with its Arctic counterpart, using a state of the art climate model. Following S2015, we use the CESM WACCM, a model with a well-resolved stratosphere and interactive chemistry for stratospheric ozone. We find that projected Antarctic sea ice losses have a clear and robust effect on the tropospheric circulation throughout the year, albeit with an amplitude that is somewhat smaller compared to the Arctic response.

This chapter is organised as follows. In Section 4.2, we describe the model and experimental design used in this study. In Section 4.3, we compare and contrast the atmospheric response, in the troposphere, stratosphere and at the surface, to future Antarctic and Arctic sea ice loss. The chapter is concluded with a summary and discussion in Section 4.4.

4.2 Data and Methods

4.2.1 Model

For this study we employ WACCM4, a high top model which participated in the CMIP5, and was fully documented by Marsh et al. (2013). It has a horizontal resolution of 1.9° latitude by 2.5° longitude, with 66 vertical levels and a model lid extending up to the lower thermosphere, near 140 km. In addition to enhanced vertical resolution in the stratosphere and mesosphere, WACCM incorporates an interactive stratospheric chemistry package, and special gravity wave parametrizations for the upper atmosphere. These features give this model a much improved representation of the stratosphere than low top models. Employing

a high top model is important because recent research has identified the stratosphere as a possible pathway for interactions between the polar climate and mid-latitude weather (Peings and Magnusdottir, 2014; Zhang et al., 2017).

4.2.2 Experiments

We investigate the effect of Antarctic and Arctic sea ice loss on the atmospheric circulation by performing three numerical experiments, each 151 years long, using WACCM; a control run and two perturbed sea ice runs. The control experiment is forced with a repeating seasonal cycle of SIC and SST, averaged over the period 1955-69 (the reason for this choice is discussed below), obtained from the mean of a six-member ensemble of historical twentieth-century simulations with the corresponding fully coupled version of WACCM (Marsh et al., 2013). The two perturbation experiments are specified with repeating seasonal cycles of polar SIC in one hemisphere, averaged over the period 2085-99, from the mean of a six-member ensemble of twenty-first-century simulations of the fully coupled version of WACCM, forced by RCP8.5. The perturbed Antarctic experiment has prescribed 2085-99 values for Antarctic SIC, but Arctic SIC is unchanged from the control. Similarly, the perturbed Arctic experiment has prescribed 2085-2099 values for Arctic SIC, but Antarctic SIC is left unchanged from the control. The SSTs in the perturbation experiments are handled using the same method as S2015: in the perturbation experiments, SSTs are changed to end of the century values, averaged from the six WACCM RCP8.5 runs, only in grid cells where SIC is projected to decrease. Following convention (e.g., Peings and Magnusdottir (2014)), sea ice thickness is specified to be 2 m in the Arctic and 1 m in the Antarctic.

While it is common to use the year 2000 (or present conditions) for the control runs, in our experiments all forcings (including ozone-depleting substances) are fixed at 1955 year levels, except for SIC. In all other aspects, the design of these experiments is similar to the Arctic runs performed by S2015. However, we have chosen to use an earlier period for the control because we are primarily focusing on the SH. By fixing all forcings at 1955 values, we can avoid including a perpetual stratospheric ozone hole in the simulations (recall that the

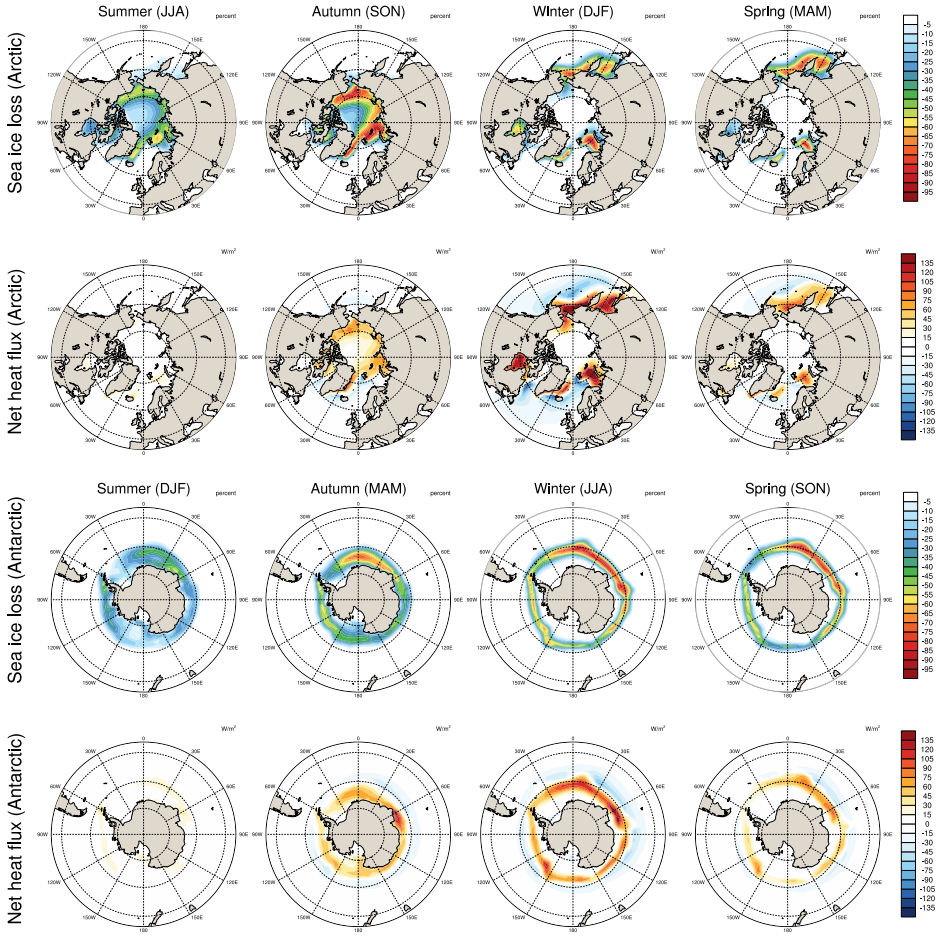

Figure 4.1: Seasonally averaged sea ice loss (difference between 1955-1969 and 2085-2099 averages) imposed for the Arctic (first row) and Antarctic (third row) experiment, and the associated net surface heat fluxes in the Arctic (second row) and Antarctic (fourth row). Positive heat fluxes correspond to the ocean releasing heat to the atmosphere and negative heat fluxes correspond to the atmosphere losing heat to the ocean. Note that seasons have been shifted to align northern and austral seasons.

Antarctic polar stratosphere is severely perturbed at present, but the ozone hole is expected to recover by 2060-2080 (WMO, 2014)). To avoid complicating matters with the recovery of stratospheric ozone, we have selected the SIC from the middle of the 20th century, before the ozone hole over Antarctica was ever formed. This choice results in a slightly larger amount of sea ice loss than the one imposed by S2015; however, since the vast majority of the loss is projected to occur in the 21st century, the results of these two studies are broadly comparable in the Arctic.

4.2.3 The imposed sea ice forcing

Given our experiment design, it should be clear that differences found in the atmospheric circulation between the Antarctic perturbation experiment and the control experiment can be attributed to Antarctic sea ice loss, although a small remnant of internal variability might be present, even with such long integrations (150 years). Similarly, differences found in atmospheric circulation between the Arctic perturbation experiment and the control experiment can be attributed to Arctic sea ice loss. Therefore we start by examining the SIC forcing, and contrasting the Antarctic and Arctic losses of sea ice.

Figure 4.1 shows the differences between the perturbation experiments and the control experiment for the Arctic SIC (first row) and Antarctic SIC (third row). SIC is projected to diminish in all seasons in both hemispheres by the end of the century. In the NH, significant sea ice loss is found in the Arctic circle in summer and autumn. In the winter and spring, sea ice loss is restricted to the marginal zones, especially the Bering Sea, Hudson Bay, the Sea of Okhotsk and the Barents Sea. In comparison, the predicted sea ice loss in the SH appears far more zonally symmetric. In austral winter and spring the projected sea ice loss is an annulus completely encircling the Antarctic continent, whereas in austral autumn future sea ice loss is confined to the Antarctic coastline. The net heat flux (the sum of the long wave flux, the sensible heat flux and the latent heat flux) associated with these sea ice changes is also shown (second and fourth row) with, as expected, areas of sea ice melt losing energy to the atmosphere. Equatorward of the sea ice loss region, the atmosphere can be warmed by thermal advection while SSTs are fixed by experimental design. This leads to a downward heat flux response, a common feature in similar modelling studies (e.g. Deser et al., 2010).

The area integrated quantities of sea ice and net heat flux, and their variations throughout the year, are presented in Figure 4.2. The seasonal cycle of sea ice area for the control (averaged 1955-1969) and the perturbed experiments (averaged 2085-2099) are shown for the Arctic (a) and the Antarctic (b). Consistent with the theory of Eisenman et al. (2011), sea ice area becomes less seasonally varying in the Antarctic by the end of the century,

Table 4.1: Details of the three WACCM timeslice experiments and the sea ice conditions imposed in them. Sea ice conditions averaged averaged the years 1955-1969 are from the ensemble mean of six WACCM historical runs. Sea ice conditions averaged over the years 2085-2099 are from the ensemble mean of six WACCM RCP8.5 runs.

Experiment	Antarctic sea ice	Arctic sea ice	Years	All other forcings
Control (C)	1955-1969	1955-1969	151	Fixed at 1955 values
Future Antarctic (A1)	2085-2099	1955-1969	151	Fixed at 1955 values
Future Arctic (A2)	1955-1969	2085-2099	151	Fixed at 1955 values

whereas the seasonal cycle of Arctic sea ice becomes larger. This is more easily interpreted by considering the timing of the maximum Arctic sea ice loss (c) which aligns with the Arctic September minimum (a), whereas the minimum Antarctic sea ice loss (c) coincides with the Antarctic February minimum (b).

The annual cycle of net surface flux (d) and total forcing to the atmosphere (e), arising from the SIC changes, are lagged by a few months after the timing of the maximum sea ice loss in the Arctic, but this does not seem to be the case in the Antarctic. Recall that changes in heat flux need not be in phase with changes in sea ice loss; for example, in the Arctic, the energy transport from the ocean to the atmosphere is highest in winter even though sea ice loss peaks in the autumn. The details of how the net surface flux and the total forcing to the atmosphere were calculated are included in the Appendix. We expect to see the largest atmospheric circulation response to sea ice loss in months where the net surface flux peaks, so winter for the Arctic, and autumn and winter for the Antarctic. In addition to the role played by the net surface fluxes, the basic climatological state of the atmosphere is also important, as shown by Smith et al. (2017).

The experimental setup for the experiments is summarised in Table 4.1. The following figures will all show the difference (future - past) between the perturbation and the control experiments: we will refer to these as the 'response' to sea ice loss. In all of the following figures the months have been aligned so that boreal and austral seasons correspond with

each other. To calculate the strength and latitudinal position of the tropospheric jet, we use the approach of Bracegirdle et al. (2018). The zonally averaged zonal wind between 75°S and 15°S (SH jet) and 15°N and 75°N (NH jet) is interpolated with a cubic spline onto a 0.1° latitude grid; from this interpolated curve, the maximum wind speed and its location is determined for each month. A two-sided Student's t-test is used to estimate the statistical significance of all responses. We discard the first year of each 151 year simulation from our analysis.

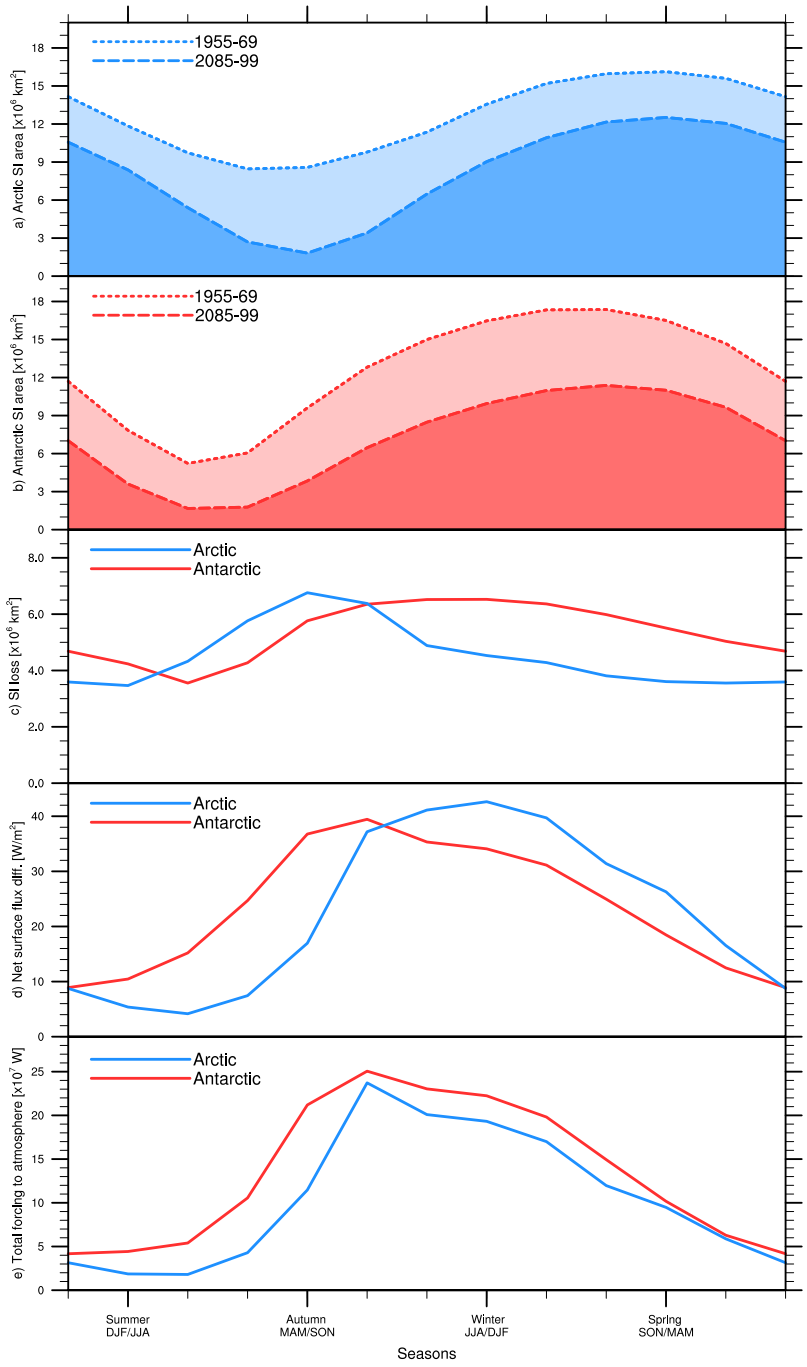

Figure 4.2: The seasonal cycle of 1955-1969 and 2085-2099 total sea ice area for (a) the Arctic and (b) the Antarctic, from historical and RCP8.5 WACCM runs respectively. For both the Arctic and Antarctic the monthly sea ice loss between these two periods is shown in (c). Resulting from this sea ice loss are the net surface flux differences (d) and the total forcing to the atmosphere (e) [values in (c) multiplied by values in (d)]. Note that the months have been shifted to align northern and austral seasons.

4.3 The atmospheric response to future sea ice loss

4.3.1 Tropospheric response

Figure 4.3 show the zonally averaged temperature response (shading) throughout the whole atmosphere to Arctic (top row) and Antarctic (bottom row) projected future sea ice losses in the four seasons, overlayed on to the climatological temperature structure from the control experiment (contours). High levels of local warming are evident at high latitudes over the regions of sea ice loss. In both hemispheres, the response peaks in winter and is smallest in summer: this corresponds to the seasonal cycle of the net surface flux. It can be seen that, in the troposphere, the response in the Arctic shows larger seasonal variations whereas, in the Antarctic, the temperature response is more similar throughout the year. Examining the first harmonic of the area averaged temperature response in the lower troposphere, the Arctic response has a seasonal cycle amplitude which is 2.1x larger than that for the Antarctic response, and is significant at a 99% level.

The local warming is clearly confined, both latitudinally and vertically. In neither hemisphere we find a large mid-to-upper tropospheric warming, although the warming extends slightly higher in the Arctic (up to 400 hPa) compared to the Antarctic (up to 600 hPa). Note also a small cooling response above 600 hPa in the Antarctic for most of the year. The largest stratospheric temperature changes are found in the Arctic in winter, but the stratospheric response is examined in Section 4.3.2 below.

Figure 4.4 shows the zonally averaged zonal wind response throughout the whole atmosphere to projected Arctic and Antarctic sea ice loss (shaded). Again, it is clear that the tropospheric zonal wind response to Antarctic sea ice loss is less seasonally confined than for the Arctic case, although the biggest response occurs in spring. In the Arctic, the largest wind changes are seen in the stratosphere: however, even with our century long integrations, most of the stratospheric response is *not* statistically significant because of the high variability in the Arctic stratosphere. In agreement with most previous studies, we find that melting

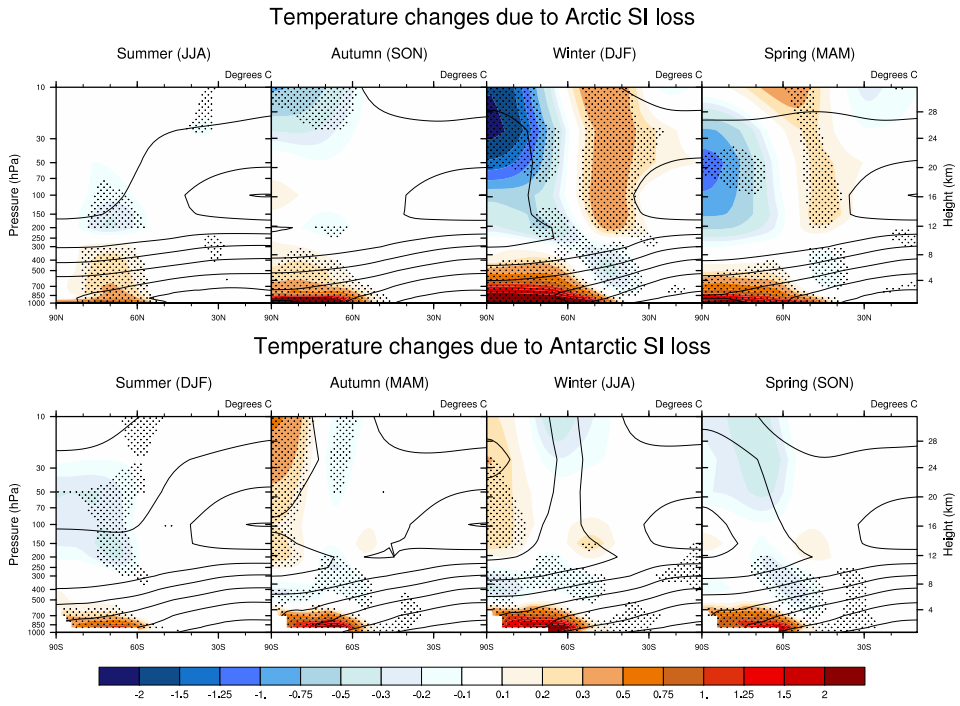

Figure 4.3: Zonally averaged temperature changes throughout the atmosphere for the four seasons in response to Arctic and Antarctic future sea ice loss (shaded contours) on top of the control climatological temperature structure (black contours) with contour increments of 15°C. Stippling denotes a statistically significant response at the 95% confidence level. Note that for ease of comparison, the latitudes for the NH have been reversed.

sea ice causes an equatorward shift in the tropospheric jet in both hemispheres. This agrees with the recent finding of Baker et al. (2017) who suggest that, as long as it is located on the jet's poleward flank, a local source of heating will move the tropospheric jet equatorwards. The key point is that both Arctic and Antarctic projected sea ice losses would provide a negative feedback on the poleward tropospheric jet shift associated with increasing greenhouse gases in each hemisphere (Yin, 2005; Lorenz and DeWeaver, 2007; Barnes and Polvani, 2013; Grise and Polvani, 2014). Comparing to WACCM RCP8.5 simulations, according to these simulations sea ice losses would reduce the end of the century poleward winter jet shift by roughly 30-40% (assuming the relationship remains linear (McCusker et al., 2017)).

The tropospheric zonal wind response to future sea ice loss throughout the year is illustrated in Figure 4.5, which shows the entire seasonal cycle of zonal wind response at 700 hPa. This plot best conveys the difference in the seasonality of the response to future Arctic and

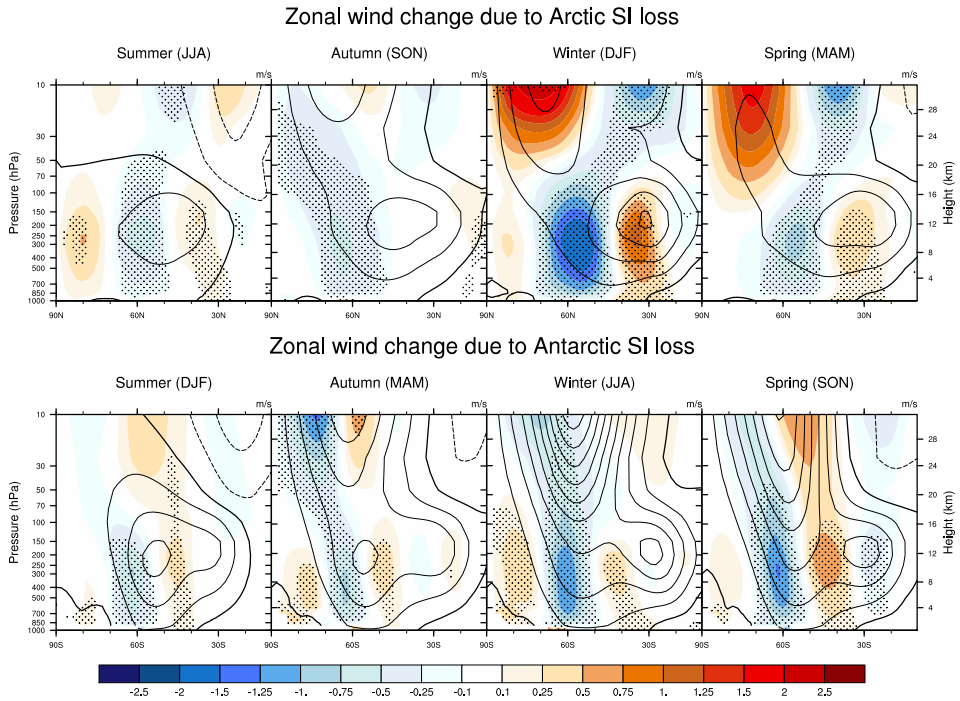

Figure 4.4: As in Figure 4.3 but for zonally averaged zonal wind. Contour increments of the control climatological zonal wind structure have increments of 10m/s with the bold line being zero and the dashed lines indicating negative values.

Antarctic sea ice loss. The latitudinal position of the maximum zonal wind of the control run is indicated by the black dots, to demonstrate that both Arctic and Antarctic sea ice loss result in jet shifts, although as discussed later Antarctic sea ice loss also causes a weakening of the jet. These results disagree with the findings of Kidston et al. (2011) who find no apparent effect on the zonal wind. The major difference between the atmospheric responses in the two hemispheres is that Antarctic sea ice losses causes an equatorward shift of the eddy-driven jet throughout the entire calendar year, whereas the Arctic response is largest between December and May and not significant at all in the autumn. Lastly, we note that the peak response to future Antarctic sea ice loss is somewhat smaller than in the Arctic, albeit statistically significant for every month of the year.

To further elucidate the response of the tropospheric jet, the top panel of Figure 4.6 compares the effect of Arctic and Antarctic sea ice on two important parameters describing the jet: the jet maximum speed and its latitudinal location (details about how these parameters

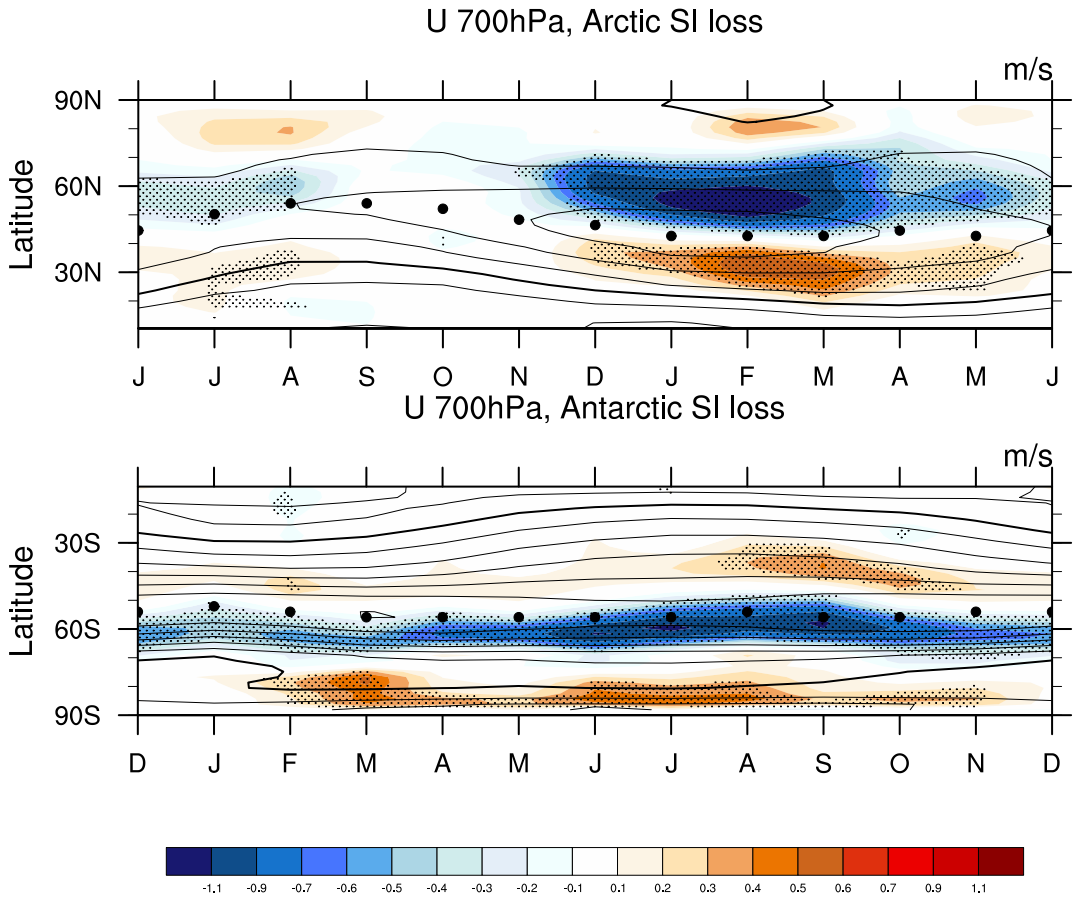

Figure 4.5: Seasonal cycle of zonally averaged zonal wind changes at 700hPa in response to Arctic and Antarctic future sea ice loss (shaded contours) on top of the control climatological zonal wind structure (black contours). Contour increments of the control climatological zonal wind structure have increments of 3 m/s with the bold line being zero. Stippling denotes a statistically significant response at the 95% confidence level. The latitudinal location of the maximum zonal wind is shown with the black circles. Note that months have been shifted to align northern and austral seasons.

are calculated are included in Section 4.2). Consistent with Figure 4.5, the response of the SH tropospheric jet is a small but significant equatorward shift in every month, whereas the jet response to Arctic sea ice loss is not statistically significant for roughly a third of the year. The amplitude of the seasonal cycle of the response to Arctic sea ice loss is roughly double that of the Antarctic response, similar to the response of near-surface temperature discussed previously.

Interestingly, one important feature where Antarctic sea ice loss seems to have a larger impact on than Arctic sea ice loss is the jet strength, shown in the bottom panel of Figure

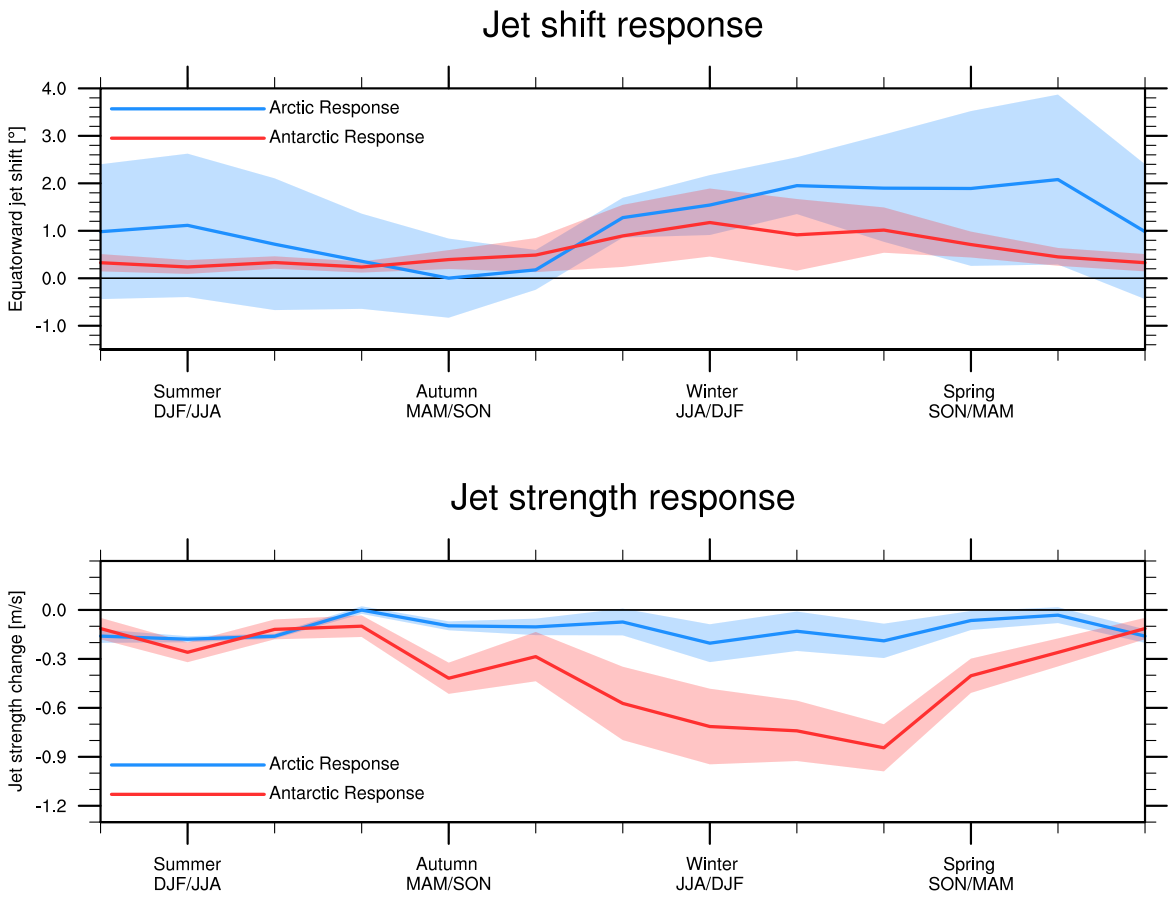

Figure 4.6: Seasonal cycle of response of the NH and SH tropospheric jet (at 700 hPa) to sea ice loss. The top panel shows the equatorward jet shift response and the bottom panel shows the change in jet strength, with the negative values indicating a slowdown of the jet. For information on how these parameters were calculated, refer to Section 4.2. Shading indicates the $+/-2\sigma$ envelope. Note that months have been shifted to align northern and austral seasons.

4.6. While the impact of sea ice loss is to weaken the tropospheric jet in both hemispheres, Antarctic sea ice loss has a significantly larger effect. This is consistent with Bracegirdle et al. (2018) who reported a stronger relationship between Antarctic SIE and jet strength, than between SIE and the latitudinal location of the jet. Although Bader et al. (2013) do not decompose the jet response into the strength and location, it seems that their results tell a similar story (although their experiment only examines the summertime). The role of jet strength could offer a partial explanation of why, even though the seasonal cycle of total forcing to the atmosphere is the same in both hemispheres, the response of the SH jet latitude varies less seasonally than the NH jet latitude; rather, these seasonal variations

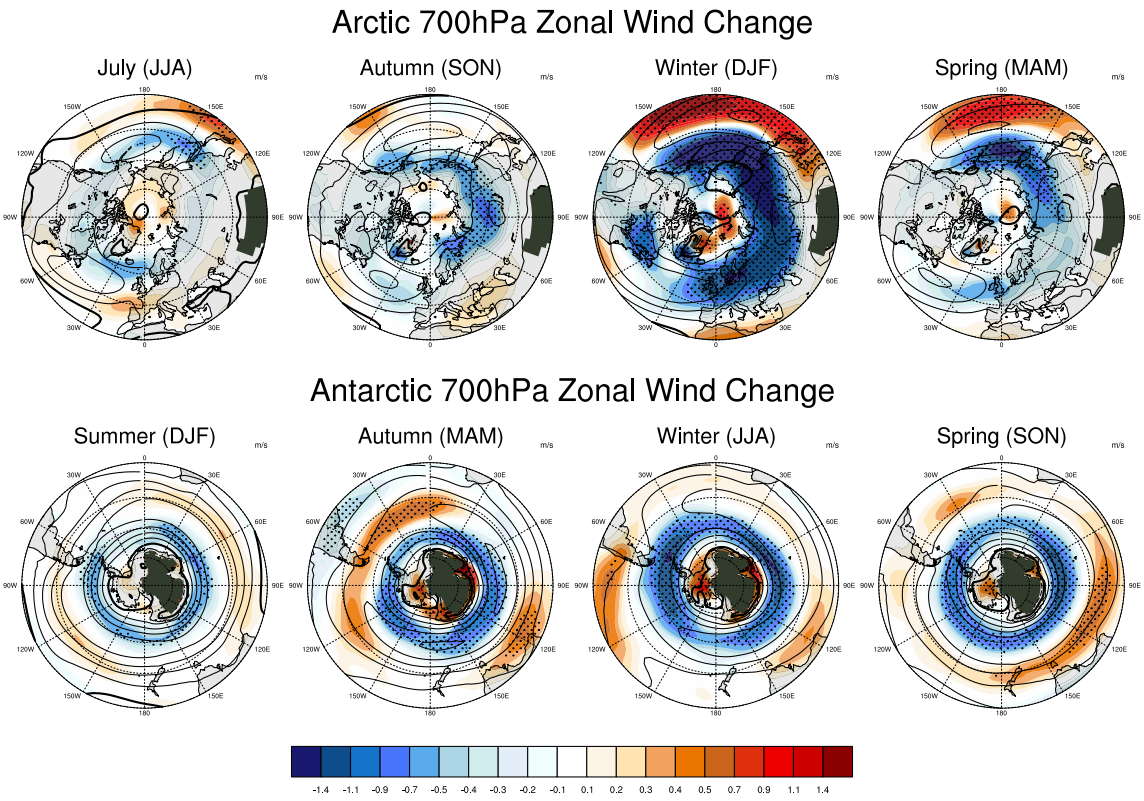

Figure 4.7: 700 hPa zonal wind response to Arctic and Antarctic future sea ice loss (contours) on top of the control climatological 700 hPa zonal wind structure (black contours) with contour intervals of 4m/s. Stippling denotes a statistically significant response at the 95% confidence level. Some values are not plotted because of topography.

manifest themselves in a weakening of the jet.

Figure 4.7 shows the zonal wind response at 700hPa for each of the four seasons. The tropospheric zonal wind response due to future Antarctic sea ice loss is largely zonally symmetric, unlike the regional response to Arctic sea ice loss. One would have predicted a more zonal response in the SH for two reasons: 1) the projected end of the century sea ice losses, seen in Figure 4.1, are approximately zonally symmetric in the Antarctic and regionally confined in the Arctic, and 2) the effects are acting upon a climatological state is which is far more zonally symmetric in the SH (Kushner et al., 2000). In contrast, in response to melting Arctic sea ice, WACCM's primary centre of action seems to be over the Pacific basin (not the North Atlantic): this is a common feature of many climate models (Gong et al., 2017).

4.3.2 Stratospheric response

Figure 4.8 shows the seasonal cycle of the stratospheric zonal wind response to future sea ice loss, the same as Figure 4.5 but at 10hPa rather than 500hPa. One can easily see that while the tropospheric responses to Arctic and Antarctic sea ice loss are quite similar, the stratospheric responses are not. Arctic sea ice loss results in a strengthening of the polar vortex in our model between December and March, although the reader should note that much of it is not statistically significant. Our findings differ from many other modelling studies (Kim et al., 2014; Peings and Magnusdottir, 2014), and perhaps most interestingly, S2015, who used a very similar experimental design and the same model as we do. Although the stratospheric response in boreal spring is the same, S2015 find a slowdown of the polar vortex in winter. We offer two possible explanations of this discrepancy: (1) given that the changes are small relative to the climatological conditions and much of the changes are not statistically significant, the differences could simply arise from the large levels of internal variability in the stratosphere or (2) our study imposes slightly more sea ice loss in the Pacific sector (for example in the sea of Okhotsk in winter) than S2015 and, as a consequence, wave suppression could be more pronounced, leading to a stronger polar vortex. If the 150 year integration is broken down into three 50-year chunks, one out those three time periods shows a large weakening of the winter statospheric vortex in the NH, rather than a strengthening (not shown). The fact that the sign of the response is not consistent throughout the integration suggests that internal variability might be the most important fator behind these differences.

The largest, and robust, stratospheric response to Antarctic sea ice loss, in Figure 4.8, is seen in austral autumn (MAM): it consists of a weakening of the polar vortex on its poleward flank and a slight strengthening on its equatorward flank. Although these responses are statistically significant, their amplitudes are small and consitute only a few percent of the climatological state, with the SH polar vortex being much stronger than its northern counterpart. It is possible that this small stratospheric response could be intensified when the atmospheric model is coupled to an interactive ocean (Smith et al., 2017), but that

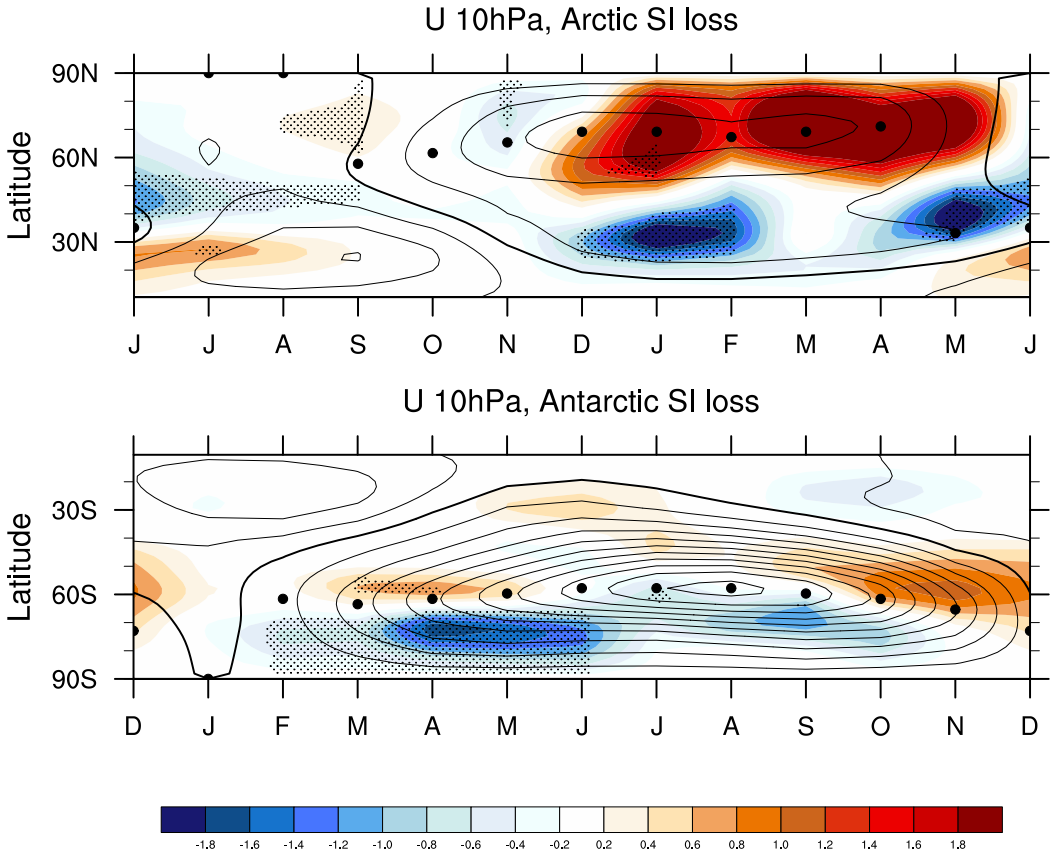

Figure 4.8: As in Figure 4.5 but for zonally averaged zonal wind changes at 10hPa. Contour increments of the control climatological zonal wind structure have increments of 10m/s with the bold line being zero.

remains to be established for our model.

To investigate the stratospheric responses further, Figure 4.9 shows the stratospheric Eliassen-Palm (E-P) flux divergence response to Arctic and Antarctic sea ice loss. E-P flux divergence quantifies wave dissipation. Consistent with the stratospheric wind response, the largest change E-P flux divergence in the stratosphere is during boreal winter in response to Arctic sea ice loss. The increase in E-P flux divergence (reduced wave dissipation) is related to a suppression of upward wave propagation into the stratosphere (not shown), and thus a strengthened stratospheric jet. The E-P flux divergence response in the Antarctic, largest in austral spring and autumn, is weaker and does not impact the strength of the stratospheric jet. Projected sea ice losses in the Antarctic are highly zonally symmetric, and thus might

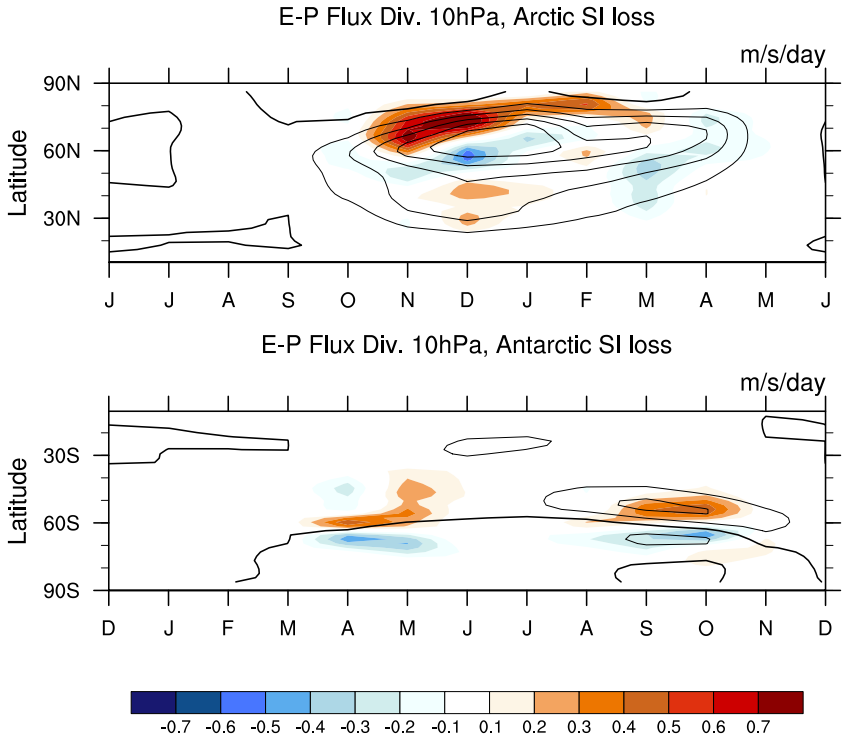

Figure 4.9: Seasonal cycle of E-P flux divergence response (shaded contours) [m/s/day] at 10hPa in response to Arctic (top) and Antarctic (bottom) future sea ice loss overlayed on E-P flux divergence climatology (contours). Contour increments of the control climatological values have increments of 1 m/s/day with the bold line being zero and thin lines being negative. Only statistically significant responses have been shown. Negative values correspond to convergence and positive values correspond to divergence.

not cause large changes in planetary waves and the stratospheric circulation.

Leveraging the fact that WACCM has interactive stratospheric chemistry, we now investigate the impact of sea ice loss on stratospheric ozone concentrations. Changes in stratospheric ozone have been shown to have an important impact upon the climate system (Previdi and Polvani, 2014). Analysing the same set of runs as S2015, Sun et al. (2014) find that Arctic sea ice loss causes a significant reduction of total column ozone in the spring, by over 30 Dobson Units. Figure 4.10 shows the response of total column ozone to Arctic and Antarctic sea ice loss in our runs. In agreement with Sun et al. (2014), we find a reduction of total column ozone in the spring (although of roughly half their magnitude), and this reduction extends back through the winter to November. This response is consistent with the

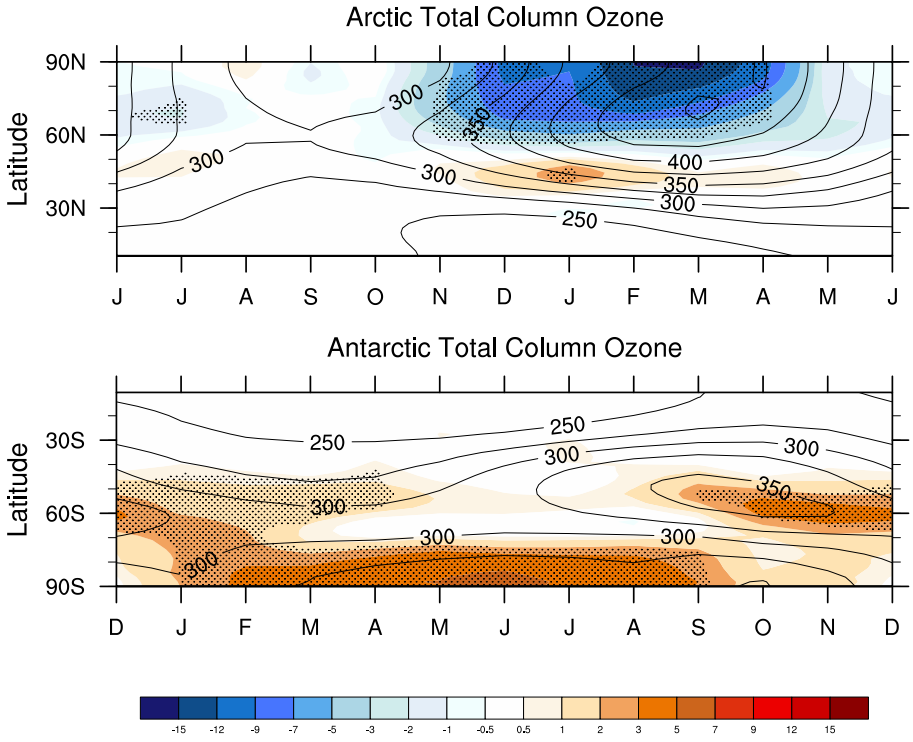

Figure 4.10: As in Figure 4.5 but for zonally averaged total column ozone, in Dobson units, in response to Arctic and Antarctic future sea ice loss. Contour increments of the control zonally averaged total column ozone structure have increments of 25DU. Stippling denotes a statistically significant response at the 95% confidence level.

stratospheric cooling seen in these seasons. The differences in the amplitude of stratospheric ozone seen in these two set of experiments might be linked to the different climatological conditions in the control runs; Sun et al. (2014) analyse a base period with reduced Arctic stratospheric ozone owing to the high levels of hydrocarbons in their simulations (Manney et al., 2011). These results further highlight how sensitive the stratospheric response is to the experimental design of these sea ice loss experiments.

In contrast to the reduction in stratospheric ozone seen in response to Arctic sea ice, Figure 4.10 demonstrates that Antarctic sea ice loss will actually cause an increase in stratospheric ozone, throughout much of the year. The response of ozone in the two hemispheres is consistent with the stratospheric temperature changes and their effect on ozone production rates. Another difference between the two hemispheres is that the response to Antarctic sea ice loss does not coincide with the season of maximum ozone depletion (SON, (WMO, 2014));

austral spring actually exhibits the smallest response of any season. Note that in both hemispheres the response of stratospheric ozone concentrations to sea ice loss is small compared to the climatological values (especially in the Antarctic where the response constitutes only 1-2%). Long integrations are required to detect statistically significant differences (see Figure 2b of Sun et al. (2014) for an indication of the large internal variability). These changes in ozone are not considered large enough to influence the dynamics. Nevertheless, stratospheric ozone offers another instance with interesting differences between the atmospheric response to Antarctic and Arctic sea ice loss.

4.3.3 Surface response

Of potential societal and ecological importance, it is important to understand the surface response to Antarctic sea ice loss, starting from the surface temperature response which is shown in Figure 4.11. First, note that the amplitude of warming in both hemispheres is similar with a maximum of roughly 10°C in the wintertime. Second, note that surface temperature changes in both hemispheres are broadly confined to the polar regions, with Arctic sea ice loss having a slightly larger effect towards the equator because the sea ice loss extends to lower latitudes. Third, our model shows that projected sea ice losses in the SH have negligible impact upon the surface temperatures of the interior of the Antarctic continent; however, we note a warming over the Peninsula and the West Antarctic, which might have profound impacts upon the stability of Antarctic ice shelves (Trusel et al., 2015). It is probable that coupling to an interactive ocean would intensify the local warming further into the continent, and extend it in height (Smith et al., 2017), but we find it surprising how trapped near to the surface the response is in these runs, given the magnitude of the sea ice loss imposed. We also point out that Arctic sea ice loss causes a clear winter Eurasian cooling in these model integrations, between 1 and 2°C, in agreement with other studies (Cohen et al., 2014; Mori et al., 2014; Sun et al., 2015; Wu and Smith, 2016); however this response is not found by all studies (Screen et al., 2013; McCusker et al., 2016; Sun et al., 2016) and it may partly depend on the magnitude of the sea ice forcing.

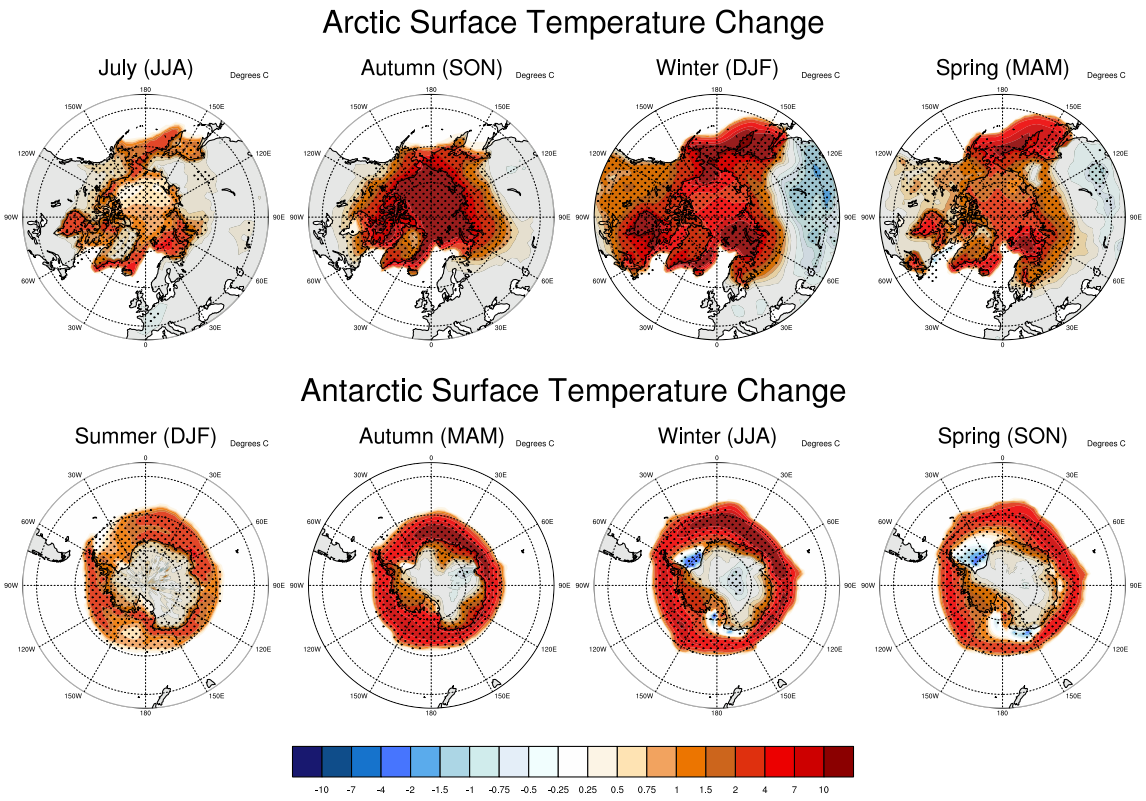

Figure 4.11: Surface temperature response to Arctic and Antarctic future sea ice loss. Stippling denotes a statistically significant response at the 95% confidence level.

We conclude by examining how precipitation responds to Arctic and Antarctic sea ice loss (Figure 4.12). It can be seen that precipitation changes correspond to changes in the net heat flux, shown in Figure 4.1. Areas in which the net heat flux is positive (where the ocean is releasing energy into the atmosphere) are co-located with an increase in precipitation. Conversely, areas in which the net heat flux is negative (where the atmosphere is losing energy to the ocean) experience a decrease in precipitation. This similarity between the net heat flux and local precipitation is in agreement with the findings of Deser et al. (2010), who show that the seasonal cycle of the averaged net heat flux and the integrated precipitation are completely in phase with one another. In the SH, changes in precipitation at low latitudes, which could be affected by the mid-latitude jet are not significant. There is no significant change in precipitation over populated landmasses in the SH, such as Australia or South

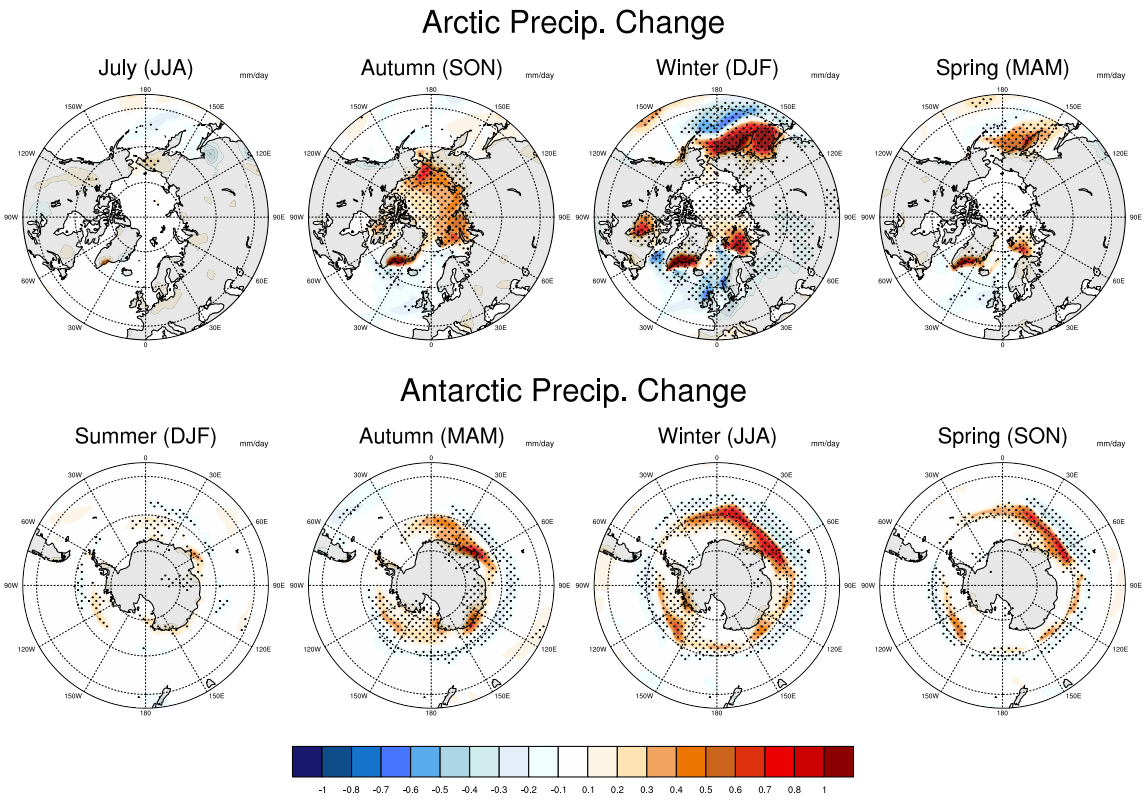

Figure 4.12: Precipitation response to Arctic and Antarctic future sea ice loss, with units of mm/day. Stippling denotes a statistically significant response at the 95% confidence level.

America, as the response is confined near the regions of sea ice loss. These results suggest a small impact of Antarctic sea ice loss on the mid-latitudes in the SH, either through changes in temperature or precipitation. Including ocean coupling, however, could alter this conclusion, because ocean dynamics could act as a pathway to extend the impacts to the lower latitudes (Deser et al., 2016). Over the period 1979-2009, Smith et al. (2017) only find significant changes in precipitation near Australia or South America when the atmosphere is coupled to an interactive ocean.

4.4 Summary and Discussion

4.4.1 Summary

We have performed a comprehensive set of model experiments to compare the atmospheric response to projected late twenty-first- century Arctic and Antarctic sea ice loss. There has been very little research on the effects of Antarctic sea ice loss, so our aim was to place the findings in the context of the Arctic, for which a vast literature exists. Our main conclusion is that future Antarctic sea ice loss is likely to have a significant impact on the atmospheric circulation throughout the year, with comparable magnitude to the impact of Arctic sea ice loss. We find that in both hemispheres, sea ice loss is associated with considerable surface and lower tropospheric warming in the polar regions: however this localised warming is more confined in height and in latitude in the Antarctic case. Interestingly, the surface warming response in the Antarctic is unable to penetrate the interior of the Antarctic continent in these runs. Similarly, changes in precipitation are also confined to the polar regions. One possible reason for these two results, which motivates further study, is the lack of ocean coupling in these experiments. Sea ice loss in both hemispheres causes the tropospheric jet to shift equatorwards; this is a negative feedback on the poleward jet shift associated with increased concentrations of greenhouse gases. The stratospheric response to Antarctic sea ice loss is smaller than the response to Arctic sea ice loss, and has a different seasonality. Comparison of our results with S2015 suggests that stratospheric response to Arctic sea ice loss could be dominated by the large levels of internal variability in the stratosphere.

Perhaps the largest difference between the atmospheric effects of Arctic and Antarctic sea ice loss is their seasonal variability, even though the seasonal cycles of the net surface fluxes are similar. The peak response in the atmospheric circulation is seen in winter, but the amplitude of that response is significantly larger for Arctic sea ice loss than for Antarctic sea ice loss. However, the tropospheric response in the Antarctic is seen throughout the calendar year, whereas the response in the Arctic is mostly confined to winter and spring.

The only impact of Antarctic sea ice loss which is of larger amplitude than of its Arctic counterpart, is a weakening of the tropospheric jet, which peaks in winter. A key difference between two hemispheres is found in the zonality of the response to sea ice loss. For the Antarctic, the response of the atmospheric circulation is approximately zonally-symmetric, whereas for the Arctic sea ice loss the response shows an important regional structure, with much of it located over the Pacific basin.

4.4.2 Discussion

One important caveat of these findings is that they are derived from a single climate model, so they are only as reliable as our model can be. It is obviously desirable to repeat our exercise with other models, to confirm these results and estimate the spread across models. One would want to understand why the results of Kidston et al. (2011) are in stark contrast to the findings of this study and that of Bader et al. (2013). Recent results from studies investigating the response to Arctic sea ice loss have highlighted the dependence of the results on the mean state of the atmosphere (Screen and Francis, 2016; Osborne et al., 2017; Smith et al., 2017). Any biases in the background state of the control run, or the period chosen for the control run, could impact the results. This may explain some discrepancies between the results of this study and Sun et al. (2015), even though the same model was used with a very similar experimental set-up; the choice of 1955 rather than 2000 forcing could contribute to any differences. Further complicating the issue, there is evidence suggesting that the atmospheric response has a non-linear relationship to the magnitude and location of the sea ice loss (Chen et al., 2016; Screen, 2017b).

It is important to recall that recent observed sea ice trends in the Antarctic look very different to those simulated in WACCM, and in all other current-generation climate models; models show significant levels of high latitude warming and a decline in SIE in the last several decades. The literature is divided on whether the reason for this discrepancy is due to high levels of internal variability (Polvani and Smith, 2013; Zunz et al., 2013; Gagne et al., 2015) or to, yet to be robustly identified, major flaws in the models (Marshall et al.,

2014; Kostov et al., 2017; Rosenblum and Eisenman, 2017). Whatever may be the case, it is hard to imagine that there will not be significant melting of Antarctic sea ice by the end of the century, in response to increasing greenhouse gases; so our exercise is still informative. For instance, from our study we can learn something about possible circulation errors in the future projections. If, in the future, Antarctic sea ice loss occurs at a slower rate than projected by the current generation of climate models, then model projections are also likely to overestimate the future local warming and underestimate the poleward shift of the jet as well as the jet strength. Our results offer an initial estimate of the magnitude of these potential errors.

An important finding from our study is that, in our model, surface temperatures over the interior of the Antarctic continent appear not to respond to changes in sea ice conditions (even with the substantial end of the century sea ice loss imposed). In recent decades, the West Antarctic regions have been warming in the autumn (Schneider et al., 2012; Bromwich et al., 2013) but the eastern part of the continent has experienced a small cooling trend (Nicolas and Bromwich, 2014). The extent to which these regional trends are due to internal variability (Smith and Polvani, 2017) or are part of an anthropogenically-forced response (Steig et al., 2009) is an open question. Our study suggests that cooling of the interior of Antarctica may be unrelated to changing sea ice conditions, but further investigations which couple an interactive ocean to the atmosphere are necessary to validate this hypothesis.

The next step to further our understanding of the effects of Antarctic sea ice loss, which we aim to complete soon, will be to repeat the same experiment using WACCM with a coupled ocean rather than fixed SSTs, using the approach of Deser et al. (2015). Literature on the Arctic suggests that including a coupled ocean can allow sea ice loss to have an impact on the low latitudes (Deser et al., 2016; Tomas et al., 2016; Blackport and Kushner, 2017) and have a amplified effect on the high latitudes because of feedbacks (Deser et al., 2015; Smith et al., 2017). One would want to investigate whether this amplifying effect is as large in the SH given the different configuration of oceans and land masses in the SH. In addition, it is important to understand how a coupled ocean might affect the difference in seasonality

of the atmospheric response to Arctic and Antarctic sea ice loss that we have shown in this study.

CHAPTER 5

REMARKABLY SIMILAR TROPICAL RESPONSE TO ARCTIC AND ANTARCTIC SEA ICE LOSS

5.1 Introduction

By the end of this century, a considerable decline in the sea ice cover in both the Arctic and the Antarctic is expected. Over the past four decades, observed Arctic sea ice cover has already dramatically decreased; September SIE has nearly halved since 1979 (NSIDC, 2019), having lost an estimated 8,000 km^3 of sea ice volume over that period (Schweiger et al., 2011). In addition, 2017 and 2018 were the two lowest years for Antarctic SIE since satellite observations began in 1979 (Ludescher et al., 2018; NSIDC, 2019), indicating a potential turning point toward a continued decrease in Antarctic SIE over the coming decades. In each of the RCPs examined by the Intergovernmental Panel on Climate Change's Fifth Assessment Report, both Arctic and Antarctic SIE are projected to decrease by 2100 (Collins et al., 2013), and, under a business-as-usual scenario, models predict that the first ice-free Arctic summer will occur by the middle of this century (Liu et al., 2013; Overland and Wang, 2013; Jahn et al., 2016). To understand the full effect of these dramatic changes on the climate system, we here study the impact of future Arctic and Antarctic sea ice loss both separately and together.

The NH high latitude response to Arctic sea ice loss involves an intense warming and moistening of the polar atmosphere (Deser et al., 2010; Liu et al., 2012; Screen et al., 2018), especially near the surface. The mounting body of modeling work on Arctic sea ice loss

indicates that the likely impacts also include a weakening and equatorward shift of the tropospheric jet (Screen et al., 2013; Peings and Magnusdottir, 2014; Sun et al., 2015; England et al., 2018) and a potential slowdown in the Atlantic Meridional Overturning Circulation (AMOC) (Blackport and Kushner, 2016; Tomas et al., 2016; Sevellec et al., 2017; Sun et al., 2018; Liu and Fedorov, 2019). When these experiments are run in an atmosphere-only configuration, the effects of sea ice loss are confined to the mid- and high-latitudes (Smith et al., 2017; England et al., 2018): however when coupled to an interactive ocean, sea ice loss can have global effects (Deser et al., 2015; Tomas et al., 2016; Smith et al., 2017), with important impacts in the tropics (Sun et al., 2018; Wang et al., 2018; Chemke et al., 2019). So far studies examining the effects of projected Antarctic sea ice loss have been limited to atmosphere-only models (Kidston et al., 2011; Bader et al., 2013; England et al., 2018), and therefore have not captured the full extent of the response. In this study, we are the first to examine the far-flung effects of Antarctic sea ice loss using model simulations with a coupled, dynamic ocean. Under this framework, we are able to investigate the impact of Arctic and Antarctic sea ice loss on the tropics.

Arctic sea ice loss has been shown to impact tropical SSTs, the position of the Intertropical Convergence Zone (ITCZ) and the strength and location of the Hadley Cell (Chiang and Bitz, 2005; Deser et al., 2015; Tomas et al., 2016; Sun et al., 2018; Chemke et al., 2019; Liu and Fedorov, 2019). Zonally asymmetries in the tropical SST response are linked to ocean dynamics, with enhanced warming in the Eastern Equatorial Pacific (Tomas et al., 2016). This response is detectable less than 25 years after a large instantaneous amount of sea ice loss is imposed (Wang et al., 2018), but when a more realistic, transient change in Arctic sea ice is imposed, it takes significantly longer to detect this robust pattern of warming (Sun et al., 2018). This warming is accompanied by an increase in rainfall over the Equatorial Pacific, roughly symmetric about the equator, which intensifies the equatorward edge of the ITCZ (Deser et al., 2015; Tomas et al., 2016; Sun et al., 2018; Wang et al., 2018). In this study we address the following questions: (i) Will future Antarctic sea ice loss have an important impact on the tropics? and, if so, (ii) Does Antarctic sea ice loss act to reinforce or

oppose the tropical response to Arctic sea ice loss?

5.2 Methods

5.2.1 Sea Ice Extent

SIE is defined as the total area of the gridboxes in the Arctic/Antarctic which are covered with 15% or more of sea ice. For an observational estimate of the seasonal cycle of Arctic and Antarctic SIE, we use the U.S. National Snow and Ice Data Center's (NSIDC) Sea Ice Index (NSIDC, 2019).

5.2.2 WACCM4

To investigate the effect of Arctic and Antarctic sea ice loss, we performed experiments using the WACCM4, a high top model that participated in phase 5 of the Coupled Model Intercomparison Project. WACCM4 has been fully documented by Marsh et al. (2013). It has a horizontal resolution of 2 latitude by 2.6 longitude, with 66 vertical levels and a model lid extending up to the lower thermosphere, near 140 km. In addition to enhanced vertical resolution in the stratosphere and mesosphere, WACCM incorporates an interactive stratospheric chemistry package, and special gravity wave parametrizations for the upper atmosphere. These features give this model a much improved representation of the stratosphere than low top models. Employing a high top model is important because recent research has identified the stratosphere as a possible pathway for interactions between the polar climate and mid-latitude weather (Peings and Magnusdottir, 2014; Zhang et al., 2018; De and Wu, 2018). It also allows us to compare these results with previous atmosphere-only experiments using the same model (England et al., 2018). We run WACCM4 coupled to the CICE4 ice model (Holland et al., 2012) and the POP2 ocean model (Danabasoglu et al., 2012).

5.2.3 WACCM experiments with constrained sea ice conditions

We investigate the effect of Antarctic and Arctic sea ice loss on the climate system by performing four numerical experiments (outlined in Table 5.1), each 350 years long, using WACCM: a control run and three perturbed sea ice runs. There is the control experiment CONTROL where sea ice conditions in both hemispheres are kept at mid-20th century values, MELT-A where only Arctic sea ice is melted to end-of-21st century values and Antarctic sea ice is unperturbed from the control run, MELT-AA where only Antarctic sea ice is melted to end-of-21st century values and Arctic sea ice is unperturbed from the control run, and MELT-BOTH where both Arctic and Antarctic sea ice is melted to end-of-21st century values. The control period is chosen to be the sea ice conditions averaged over the years 1955-69 obtained from the mean of a six-member ensemble of historical twentieth-century simulations with the fully coupled version of WACCM. The future period is chosen to be the sea ice conditions averaged over the years 2085-99 obtained from the mean of a six-member ensemble of 21st-century simulations of the fully coupled version of WACCM, forced by RCP8.5. We note that WACCM4 is able to well simulate the climatological seasonal cycle of sea ice in each hemisphere (Fig. 5.1).

To achieve the desired seasonal cycle of sea ice conditions in each hemisphere, we follow the 'ghost forcing' method outlined in Deser et al. (2015). This involves specifying a seasonally varying longwave radiative flux to the ice model at each grid box and time step. 'Ghost forcing' refers to the fact that the additional longwave forcing is invisible to other model components, except indirectly through changes in sea ice. This flux is only applied to areas where sea ice is present, but for simplicity does not vary spatially. The longwave radiative flux necessary to replicate the desired sea ice conditions was calibrated through 5-10 iterations of shorter runs. The process is outlined in the appendix of Deser et al. (2015). We note that the change in SIE has a linear relationship with additional long wave forcing except for in the summer months (when the relationship is non-linear); this requires additional iterations before the experiments are within an acceptable tolerance of the target SIE values.

Figure 5.2 shows how close the constrained sea ice experiments are to their target values from the historical or RCP8.5 integrations. We also note that the 'ghost flux' method used in this study is one of a few techniques commonly used in this type of experiment (Screen et al., 2018).

In all of our experiments, all forcings (including ozone-depleting substances) are fixed at 1955 year levels, except for the added longwave radiative flux used to constrain the SIC. As in England et al. (2018), we use this period for the control because we are largely focussed on the SH and want to avoid including a perpetual stratospheric ozone hole in the simulations [recall that the Antarctic polar stratosphere is severely perturbed at present (see England et al. (2016a) for the stratospheric ozone depletion in the WACCM historical runs), but the ozone hole is projected to recover before the end of this century (WMO, 2018)]. We have selected periods before and after the existence of the ozone hole, so as to simplify the interpretation of our results. Our choice results in a slightly larger amount of sea ice loss than similar studies, but the results are still broadly comparable because the vast majority of the sea ice loss is projected to occur in the 21st century.

It should be clear that differences between the experiments arise from differences in SIC alone, assuming that the integrations are long enough to minimise the effect of internal variability. The effect of Arctic sea ice loss can be found from MELT-A – CONTROL. Similarly, the effect of Antarctic sea ice loss can be found from MELT-AA – CONTROL. Lastly, the effect of Arctic and Antarctic sea ice loss together can be found from MELT-BOTH – CONTROL. From the 350-year long integrations, we discard the first 100 years and average over the remaining 250 years in order to capture the equilibrium response to sea ice loss (Wang et al., 2018).

5.2.4 Calculating the atmospheric and oceanic northward heat transport

The oceanic Northward Heat Transport (NHT) is diagnosed directly from the N_HEAT variable in the ocean history file. The atmospheric net NHT is calculated using the method

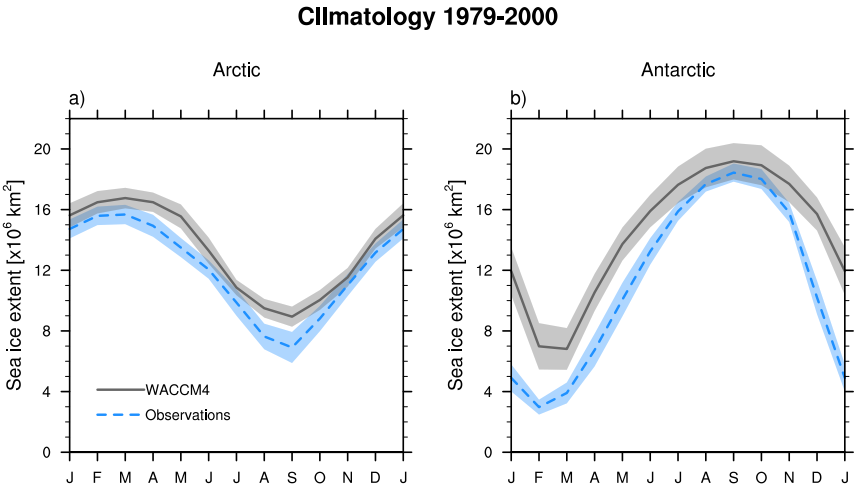

Figure 5.1: The seasonal cycle of (a) Arctic and (b) Antarctic SIE averaged over the years 1979-2000 from six WACCM historical runs (grey) and observational data from the NSIDC Sea Ice database (NSIDC, 2019) (blue). The shading show the $+/-2\sigma$ envelope.

Table 5.1: Details of perturbed sea ice experiments using the fully coupled version of WACCM.

Experiment name	Length (yrs)	Arctic sea ice	Antarctic sea ice
CONTROL	350	1955-1969	1955-1969
MELT-A	350	2085-2099	1955-1969
MELT-AA	350	1955-1969	2085-2099
MELT-BOTH	350	2085-2099	2085-2099

outlined in the appendix of Kay et al. (2012). As an input, this calculation requires the net longwave and net shortwave flux at top of atmosphere, as well as the net shortwave, net longwave, latent heat and sensible heat at the surface.

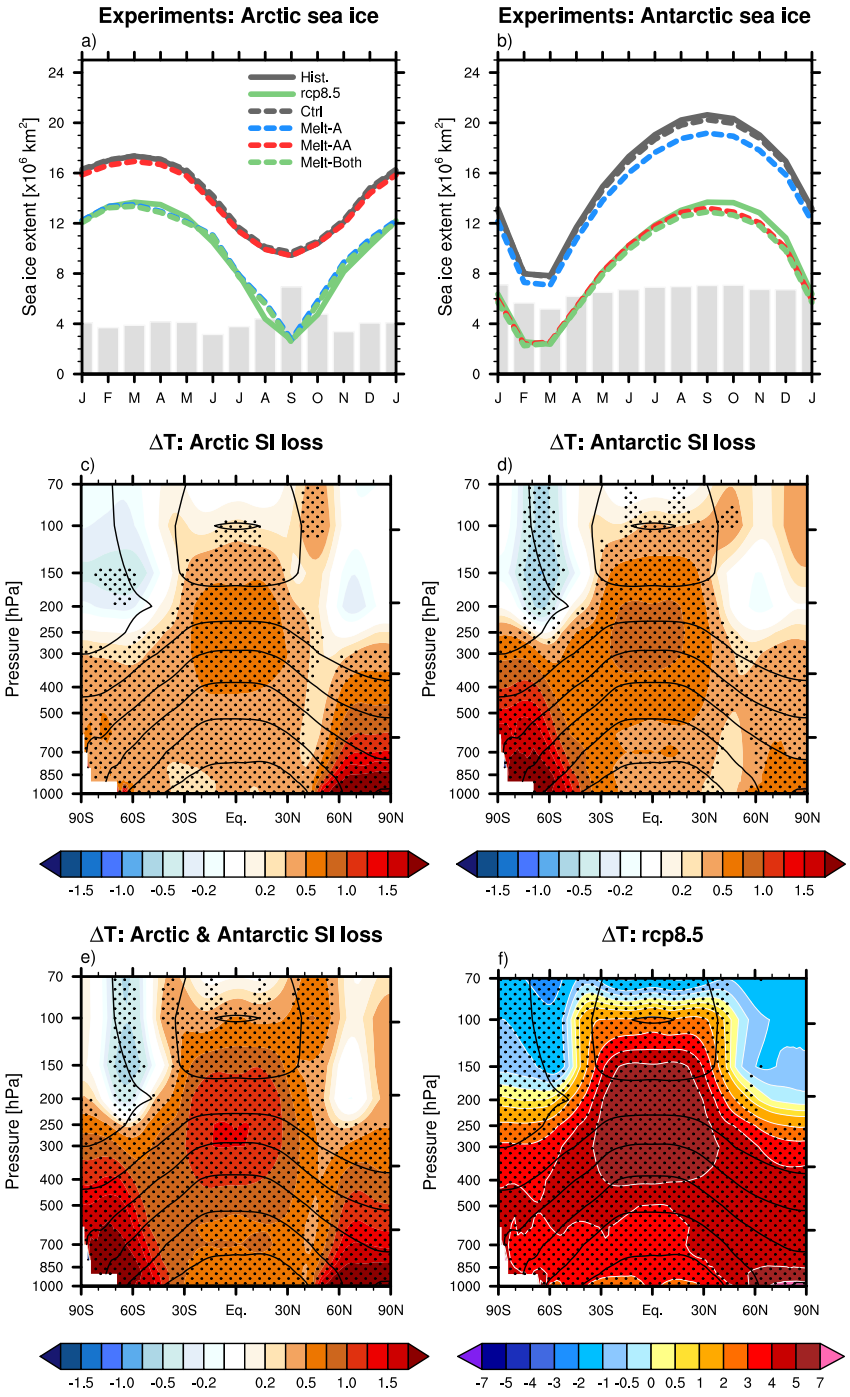

Figure 5.2: The seasonal of cycle Arctic (a) and Antarctic (b) SIE in the four experiments (dashed lines): CONTROL = Ctrl, MELT-A = A, MELT-AA = AA and MELT-BOTH = A+AA. The full lines show the target SIE values from the historic runs, averaged 1955-1969, and the RCP8.5 runs, averaged 2085-2099. We show the zonally averaged atmospheric temperature response to (c) Arctic sea ice loss, (d) Antarctic sea ice loss and (e) both Arctic and Antarctic sea ice loss. As a comparison we include the (f) RCP8.5 temperature change, 1955-1969 to 2085-2099, averaged from six WACCM historical and RCP8.5 runs. Note that the colorbar values have been made considerably higher. Stippled regions indicate a significant change at 95% significance.

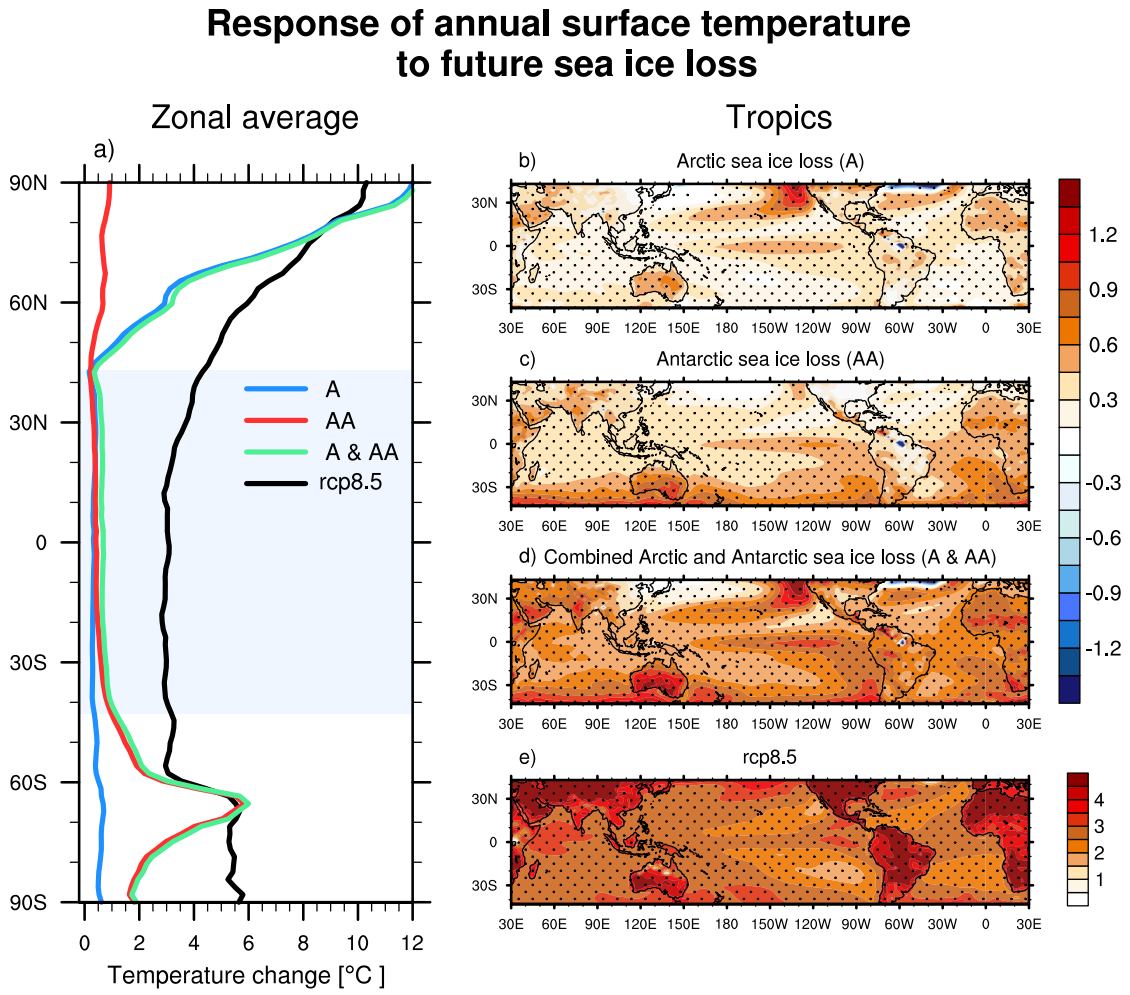

Figure 5.3: Left: (a) The zonally averaged annual mean surface temperature response to Arctic sea ice loss (blue), Antarctic sea ice loss (red) and both Arctic and Antarctic sea ice loss (green). The black line shows the RCP8.5 change, 1955-1969 to 2085-2099, averaged from six WACCM historical and RCP8.5 runs. The shaded region shows the latitudes of interest for the panels on the right. Right: The annual mean surface temperature response to (b) Arctic sea ice loss, (c) Antarctic sea ice loss and (d) both Arctic and Antarctic sea ice loss compared to the projected changes under RCP8.5, 1955-1969 to 2085-2099. Note that the colorbar values are considerably higher for the lower panel. Stippled regions indicate regions which have a significant difference at 95% significance.

5.3 Isolating the tropical response to Arctic and Antarctic sea ice loss

The atmospheric temperature response to Arctic sea ice loss (Fig. 5.2c), similar to the one found in previous studies (Deser et al., 2015; Blackport and Kushner, 2016; Oudar et al., 2017; Screen et al., 2018; Sun et al., 2018), features strong warming in the lower parts of the Arctic atmosphere and a 'mini global warming' signal which can even impact the Southern high latitudes. The tropical response to Arctic sea ice loss is robust across different models and different sea ice perturbation methods (Deser et al., 2015; Screen et al., 2018; Sun et al., 2018). This study is the first to demonstrate that the response to projected Antarctic sea ice loss (Fig. 5.2d) will have a similar structure, except of course from enhanced warming at the opposite pole, and a larger magnitude than its Arctic counterpart, although this is likely dependent on the amount of projected Antarctic versus Arctic sea ice loss. When both Arctic and Antarctic sea ice loss are imposed simultaneously (Fig. 5.2e), the increase in tropical upper tropospheric temperature is 1-1.5°C which accounts for roughly 20% of the warming projected under RCP8.5 (Fig. 5.2f). It is important to note that the response to Arctic sea ice loss and Antarctic sea ice loss are roughly additive (panels $c + d \approx e$ in Fig. 5.2), a result which also holds for the other quantities examined in this study.

Zonally averaged, the tropical (30°S-30°N) surface temperature response to Antarctic sea ice loss is as large as the response to Arctic sea ice loss (both approximately 0.3°C) (Fig. 5.3a). Together this 0.6°C accounts for roughly 20% of the tropical surface warming projected under RCP8.5, a contribution, which is consistent throughout the year. However, the zonal average masks important regional features of the surface temperature response (Fig. 5.3b,c,d). There is enhanced warming in the eastern Pacific with warm tongues from the North American coastline, largely linked to Arctic sea ice loss (Fig. 5.3b), and in the southeast tropical Pacific, mostly linked to Antarctic sea ice loss (Fig. 5.3c), which are very similar to the Pacific Meridional Modes (Zhang et al., 2014a,b). Interestingly, sea ice loss

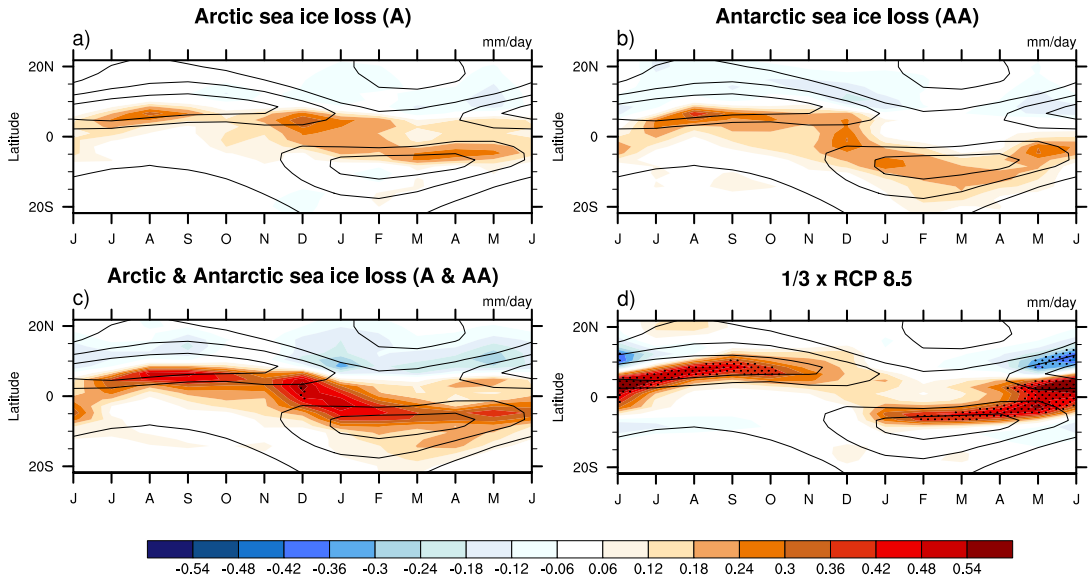

Figure 5.4: The seasonal cycle of the zonally averaged tropical precipitation response (shaded) to (a) Arctic sea ice loss, (b) Antarctic sea ice loss, and (c) Arctic and Antarctic sea ice loss. (d) The projected change in the seasonal cylce of zonally averaged tropical precipitation under RCP8.5, from 1955-1969 to 2085-2099. Note that the response in panel (d) is scaled by dividing by three to fit on the same colorbar. The response is overlaid on the climatological values with contours of 1mm/day and 3 mm/day.

in one hemisphere acts to reinforce the warming pattern from sea ice loss in the opposite hemisphere (Fig. 5.3d). We note that surface temperature response to Antarctic sea ice loss resembles the pattern (with the opposite sign) which Hwang et al. (2017) find when investigating the effect of increased Southern Ocean heat uptake using a GCM coupled to a slab ocean model. This suggests that the same mechanisms they diagnose, namely the wind-evaporation-SST feedback and the shortwave cloud feedback, are likely to be important in determining the structure of the response to sea ice loss in the southern tropics.

Both Arctic and Antarctic sea ice loss are found to significantly increase precipitation over the equatorial Pacific throughout the year but the response is seasonally dependent (Fig. 5.4), unlike for surface temperature, with the largest effect occurring in DJF (Fig.5.5). Interestingly, the months for which the tropical precipitation response is highest (December and January) are also the months in which the RCP8.5 projected response is weakest (Fig. 5.4, compare panels c and d). We first note how similar the latitudinal structure of tropical precipitation change is when comparing the response to Arctic and Antarctic sea ice loss with

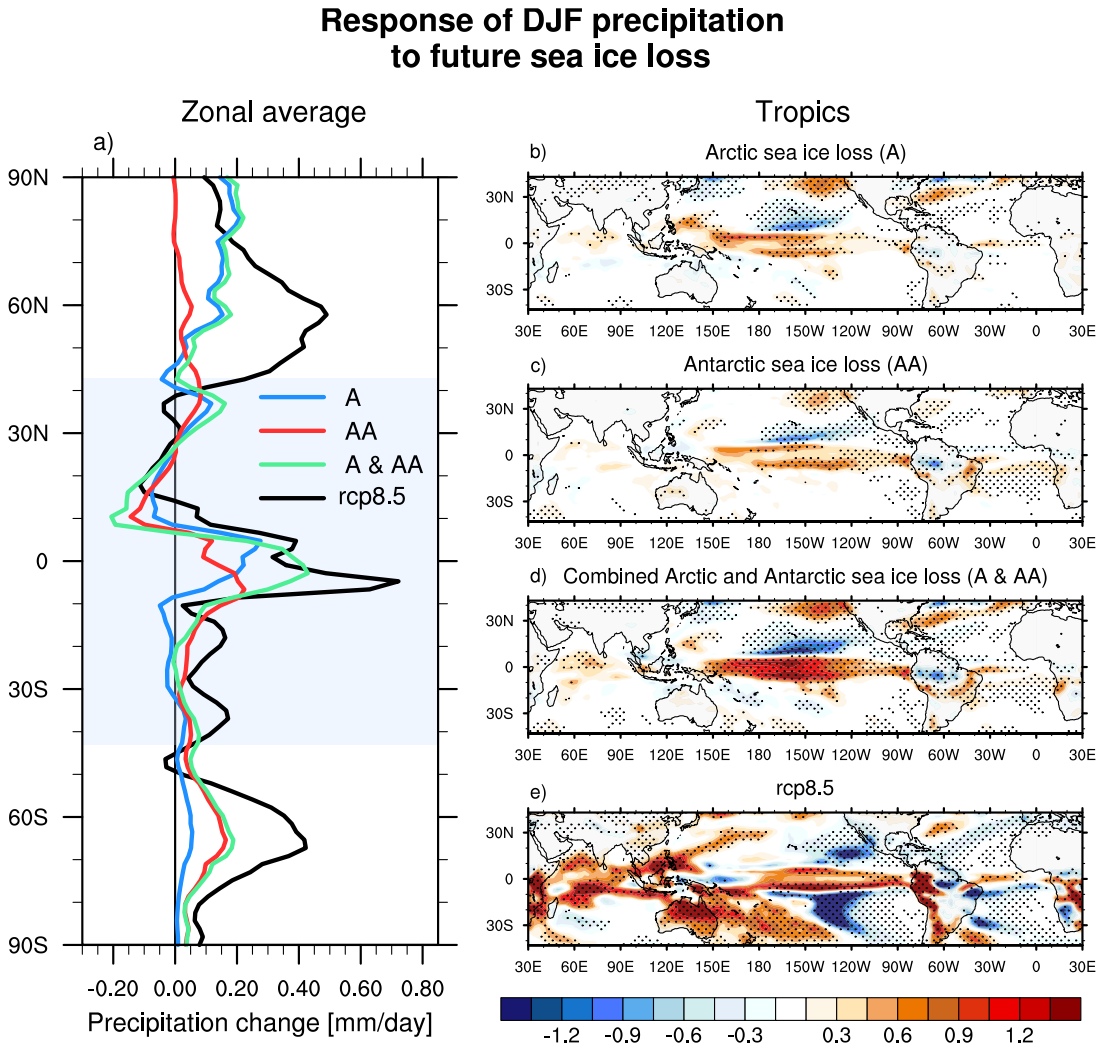

Figure 5.5: Same as Figure **??** but for DJF precipitation. Note that the colorbar is the same for the all panels on the right. The stippled regions show changes significant at 95% significance.

projected RCP8.5 changes (Fig. 5.5a); increases close to the equator and small changes, possibly a reduction, in the NH off-equatorial regions. The hemispherically asymmetric precipitation pattern in the Pacific looks nearly identical for both Arctic and Antarctic sea ice loss (Fig. 5.5b,c). This suggests that Antarctic sea ice loss has important cross-equatorial effects, consistent with the idea that the north-of-the-equator location of the ITCZ may preferentially permit cross-equatorial transport from the south (Zhang et al., 2014a,b). Both Arctic and Antarctic sea ice loss intensify the equatorward edge of the ITCZ in the Pacific with a combined increase of nearly 1mm/day in DJF (Fig. 5.5d). This is roughly equal to

the entire change in DJF, and its location, projected under RCP8.5 scenario (Fig. 5.5e) (note that the colorbar is the same for in all four panels). In the yearly average, the precipitation response to sea ice loss is roughly one third of the RCP8.5 projected changes. The magnitude of the precipitation response, and its similarity in regional structure to RCP8.5 projections, underlines the important impact Arctic and Antarctic sea ice loss will have on the tropics.

The tropical response to both Arctic and Antarctic sea ice loss is largest in magnitude in the upper troposphere (Fig. 5.2c,d,e). Consistent with results from Deser et al. (2015), sea ice loss in either hemisphere is found to increase the atmospheric condensational heating in the upper troposphere, resulting in an upward shift of the climatological heating maxima (Fig. 5.6a,b,c). Both Arctic and Antarctic sea ice loss act to intensify the heating maxima near the equator in the mid-troposphere, associated with the increased precipitation discussed previously. The reduction in the condensational heating rate at 10°N in response to both Arctic sea ice loss and Antarctic sea ice loss is consistent with reduced precipitation at this latitude in the Pacific (Fig. 5.5). Again, we find that the tropical response to Arctic sea ice loss and Antarctic sea ice loss are remarkably similar (comparing Fig. 5.6a and Fig. 5.6b). The structure of the response to both Arctic and Antarctic sea ice loss is very similar to changes projected under RCP8.5 (comparing Fig. 5.6c and Fig. 5.6d). One of the differences between the response in the two hemispheres is the condensational heating rate increase in the troposphere of the Southern mid- and high-latitudes (seen in Fig. 5.6b and Fig. 5.6c) which is not present in the NH. This hemispherically asymmetrical signature of sea ice loss is clearly present in the RCP8.5 projections.

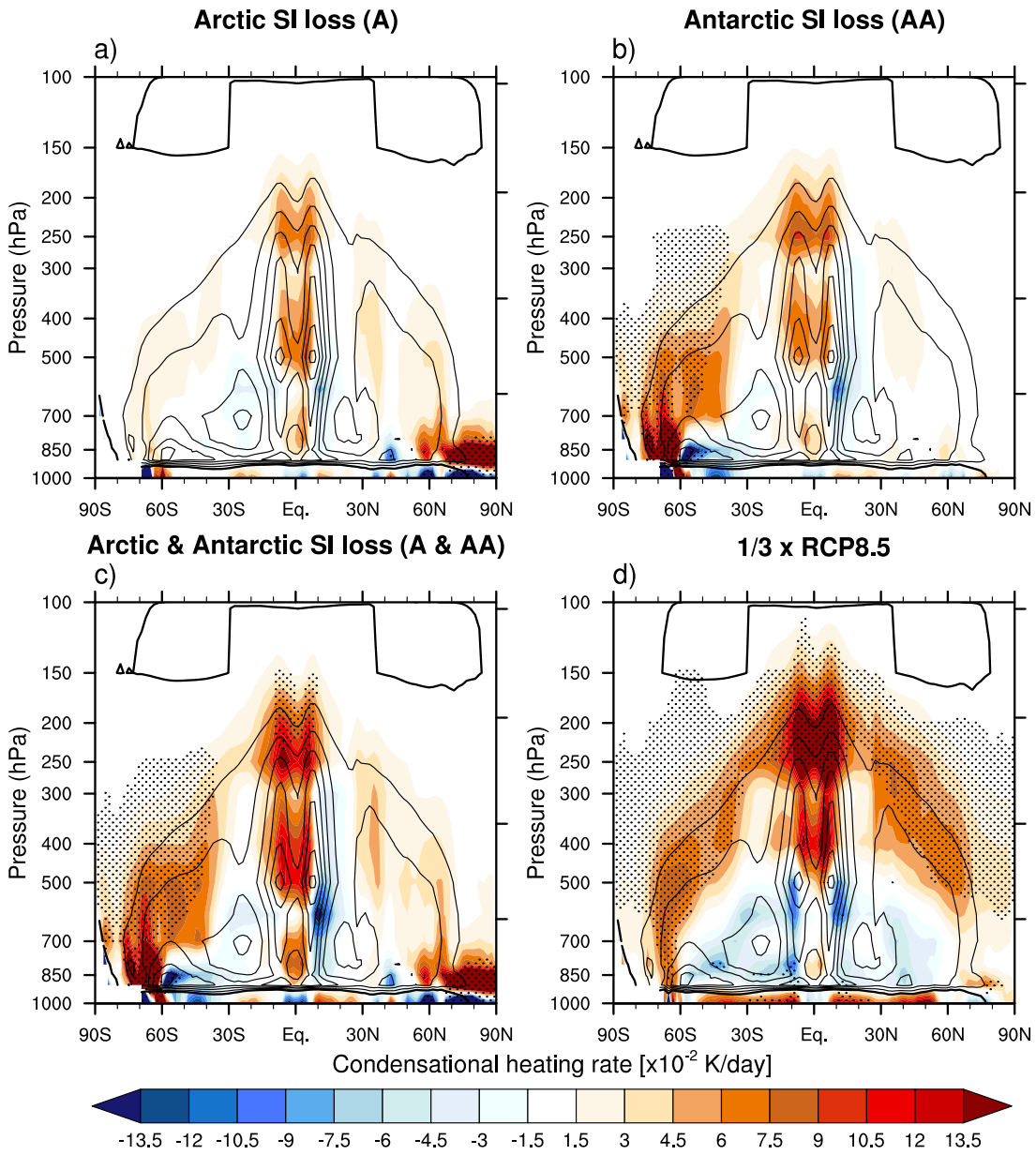

Figure 5.6: The response of annual mean condensational heating rate to (a) Arctic sea ice loss, (b) Antarctic sea ice loss and (c) both Arctic and Antarctic sea ice loss. (d) The projected change in annual mean condensational heating rate under RCP8.5, from 1955-1969 to 2085-2099. Note that the response in panel (d) is scaled by dividing by three to fit on the same colorbar.

5.4 Connecting sea ice loss to the tropics

In the absence of atmosphere-ocean coupling, the climate system is not able to transport energy to the tropics and the response to sea ice loss is confined to the mid- and high-latitudes (Deser et al., 2015; Smith et al., 2017; England et al., 2018) (Fig. 5.7b). The position of the ITCZ responds to changes in the cross-equatorial atmospheric NHT (Kang et al., 2008; Donohoe et al., 2012). Therefore, how models partition the cross-equatorial NHT response between the atmospheric and oceanic components (Cabre et al., 2017) has important implications for changes in the ITCZ position. We find that Arctic sea ice loss and Antarctic sea ice loss both transport similar amounts of energy away from the pole and across the equator (Fig. 5.7a). Thus, when both Arctic and Antarctic sea ice loss are imposed, the net effect is to transport heat to the equator from both hemispheres. The tropical response to Arctic sea ice loss is solely due to oceanic energy transport (Fig. 5.7c) because the atmosphere transports energy southwards only to 20°N (Fig. 5.7d). In contrast, the tropical response to Antarctic sea ice loss is facilitated by both energy transport in the atmosphere and ocean (Fig. 5.7c,d), although primarily through the ocean. In these model runs, the atmosphere is able to transport energy cross-equatorially in response to Antarctic sea ice loss, potentially impacting the ITCZ position, but not in response to Arctic sea ice loss. The ocean heat transport response to Arctic sea ice loss is partly achieved by the slowdown of the AMOC. In our runs, the slow-down is approximately 2 Sv which is in line with similar experiments (Blackport and Kushner, 2016; Tomas et al., 2016), but smaller than some other estimates (Oudar et al., 2017; Sun et al., 2018). Furthermore, in our runs, Antarctic sea ice loss has only a small impact on the AMOC and so the ocean heat transport response must come from other changes in ocean circulation.

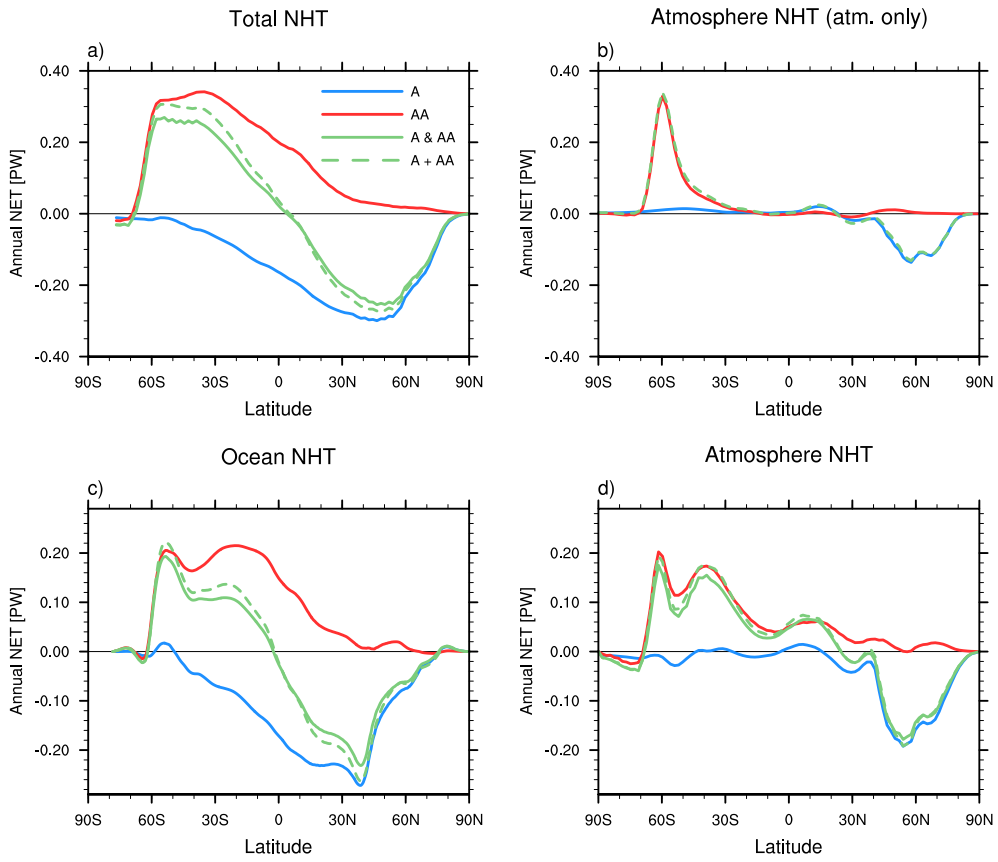

Figure 5.7: The northward heat transport (NHT) in the (a) atmosphere + ocean, (c) ocean, and (d) atmosphere. We plot the NHT response to Arctic sea ice loss (blue), Antarctic sea ice loss (red) and both Arctic and Antarctic sea ice loss (green). The green dashed line shows the sum of the response to Arctic sea ice loss and Antarctic sea ice loss. The NHT response found from atmosphere-only runs from England et al. (2018) using the same model and sea ice loss is shown in (b). The calculation for NHT is outlined in the methods section.

5.5 Conclusions

In this study we have shown that the tropical response to end-of-century Antarctic sea ice loss is large and as important as the response to Arctic sea ice loss. We isolated the response using fully coupled climate model simulations with perturbed sea ice conditions. We find that Antarctic sea ice loss will have important global effects, as found for Arctic sea ice loss, with each causing a 'mini global warming' signal. Upper tropospheric tropical warming is consistent among the experiments, and the combined effect amounts to roughly 20% of the warming projected under RCP8.5. The tropical response to Antarctic sea ice loss is

remarkably similar to, and hence acts to strengthen, the tropical response to Arctic sea ice loss. This response involves enhanced warming in the Eastern Tropical Pacific and increased precipitation over the Pacific ITCZ region. We demonstrate that the tropical impacts of both Arctic and Antarctic sea ice loss are largely mediated by ocean energy transport. In some ways, Antarctic sea ice loss may have even further-reaching effects than Arctic sea ice loss. The north-of-the-equator location of the ITCZ preferentially permits cross-equatorial transport from the south; in our runs, the signal of Antarctic sea ice loss is clearly seen in the North Pacific.

Although this study uses only one coupled climate model, its tropical response to Arctic sea ice loss is very similar to the one found in GFDL-CM3 (Sun et al., 2018) and CCSM4 (Deser et al., 2015; Tomas et al., 2016; Wang et al., 2018) (with two different methods used to perturb the sea ice) models. We note, however, that Liu and Fedorov (2019), using CCSM4 in a different configuration, find the tropical effects of Arctic sea ice loss to be mostly concentrated in the Atlantic sector rather than the Pacific. One possible reason for this discrepancy could be that their model was run over a different time period at a coarser resolution, with a less realistic sea ice climatology. As we are the first to investigate the tropical effects of future Antarctic sea ice loss, we will have to wait to see if the effects we have identified are robust across different models. The upcoming Polar Amplification Model Comparison Project (Smith et al., 2019) will offer the invaluable opportunity to explore the impact of Antarctic sea ice loss, with a standard methodology, across a range of different climate models.

CHAPTER 6

SUMMARY

6.1 Summary and Discussion

In Chapters 2 and 3, we investigated the drivers of Antarctic climate change over the observational period. Specifically, we examined the influence of the stratosphere on the southern high latitude surface climate, through stratospheric ozone depletion (Chapter 3) and stratosphere-troposphere dynamic coupling (Chapter 2).

The main finding of Chapter 2 is that stratospheric heat flux extremes are linked to high latitude tropospheric anomalies in the Amundsen Sea region. During extreme negative (positive) events there is a westward (eastward) shift of the ASL, a warming (cooling) and increase (decrease) of geopotential height over the Amundsen and Bellingshausen Seas. We showed that most CMIP5 models are not able to capture this relationship. Models with biased stratospheric heat flux extremes significantly under-estimate mean sea level pressure variability over the Antarctic Peninsula. The main limitation of this study was that nearly all CMIP5 models are biased in the mean circulation and this hindered finding a robust effect on the mean tropospheric climate, as found for the NH (Shaw et al., 2014).

We demonstrated in Chapter 3 that, since 1965, stratospheric ozone depletion has acted to deepen the ASL in austral summer by 1 hPa per decade. This result was consistent across two different comprehensive climate models, each with very different model physics and climate sensitivity. It must be noted that the ozone depletion signal on the ASL is small compared to the internal climate variability in this region. Using ensembles of model

integrations and analysing them over the full period of ozone depletion (which started a couple of decades before the satellite era) was necessary to detect a robust signal. Therefore, one may not expect to see this trend in the observed record (which is relatively short and is only one realisation). These results highlight that, even though stratospheric ozone depletion is the main driver of recent SH climate change, the ozone signal may be difficult to detect in regional circulation features.

In Chapters 4 and 5, we investigated the effects of future Antarctic climate change, specifically the effects of projected sea ice loss over the coming century. Climate model simulations were used to isolate the effect of end-of-the-century Antarctic sea ice loss which was compared and contrasted with the effects of projected Arctic sea ice loss.

In Chapter 4, we studied the effects of projected Antarctic sea ice loss using atmosphere-only simulations with WACCM. As for the Arctic, results indicated that Antarctic sea ice loss will act to shift the tropospheric jet equatorward, an internal negative feedback to the poleward shift associated with increased greenhouse gases. Antarctic sea ice loss was shown to have an important effect throughout the year whereas Arctic sea ice loss had more seasonally varying impacts.The obvious limitation of this study was that no coupling to a dynamic ocean was included in the experiments and so the response to sea ice loss was largely confined to the high latitudes. This limitation was the motivation for Chapter 5.

Building upon the results from Chapter 4, in Chapter 5 we used the same model (WACCM) but in a fully coupled setup to study the effects of projected Antarctic sea ice loss on the climate system. We showed that both Arctic and Antarctic sea ice loss will have important global effects, causing a 'mini global warming' signal. In this Chapter, we demonstrated that the tropical response to Antarctic sea ice loss is remarkably similar to that of Arctic sea ice loss, with warming in the Eastern Tropical Pacific and increased precipitation throughout much of the equatorial Pacific. One potential criticism of the method we applied to perturb sea ice conditions is energy isn't conserved (although water is conserved). However, methods which do conserve energy, give very similar results for Arctic sea ice loss experiments (Screen et al., 2018). Furthermore, we are adding substantially less energy into the system than the

energy of the total response so there must be some feedbacks involved which amplify the response.

Diagnosing the response solely to sea ice loss might seem like an academic exercise. After all, the climate system is a complex, fully coupled system so why is it important to understand the role of individual components? Firstly, in Chapter 5 we have demonstrated how connected Antarctic climate change will be to the rest of the globe. Secondly, much of the attention has been on the effect of Arctic sea ice loss on the lower latitudes. For those interested in tropical climate change, however, these results suggest that Antarctic sea ice loss will be just as important as Arctic sea ice loss. Finally, the RCP projections already include the effects of Antarctic sea ice loss. If, in fact, the pace of Antarctic sea ice loss is much slower than projected, then these results give us a way of understanding and adjusting the full projections accordingly.

6.2 Future Work

Using output from the perturbed sea ice experiments outlined in Chapters 4 and 5, the next step will be to directly compare how coupling to an interactive ocean mediates the response to Antarctic sea ice loss. This has only previously been examined for the case of Arctic sea ice loss (Deser et al., 2015, 2016). Preliminary results suggest that including ocean coupling is vital to get the correct strength of the high-latitude response to Antarctic sea ice loss. Polar warming is roughly 50% greater in the fully coupled runs compared to the atmosphere only runs. The assumption is that this extra warming is due an enhanced poleward transport of water vapour from the lower latitudes. We also have the tools available to compare results from the two hemispheres using one climate model in a clean and precise way. It seems likely that ocean coupling may be even more important for the response to Antarctic sea ice loss, given that the continent is entirely surrounded by the Southern Ocean.

We also need to improve our understanding of the processes which are facilitating the tropical response to Antarctic. In Chapter 5, we demonstrated that Antarctic sea ice loss will

drive important changes in the tropics, however the mechanisms linking the southern high latitudes to the tropics need to be elucidated. It seems likely that the wind-evaporation-SST feedback is important in driving the zonally asymmetric response seen in the tropics. One key issue which remains relates to how the tropics responds to high latitude forcing: Wang et al. (2018) find that a dynamic ocean is necessary to simulate this zonally asymmetric warming pattern in the Pacific whilst Hwang et al. (2017) are able to simulate this asymmetry with only a slab ocean model. Therefore, we plan to investigate this potential discrepancy and explore the role of ocean dynamics further. We also aim to provide a mechanistic explanation of why the tropical response to Arctic and Antarctic sea ice loss are so similar.

BIBLIOGRAPHY

Andrews, D., J. Holton, and C. Leovy, 1987: *Middle Atmosphere Dynamics*, International Geophysics Series, Vol. 40. Academic Press.

Arblaster, J., G. Meehl, and D. Karoly, 2011: Future climate change in the Southern Hemisphere: Competing effects of ozone and greenhouse gases. *Geophysical Research Letters*, **38 (L02701)**, doi:10.1029/2010GL045384.

Armour, K., J. Marshall, J. Scott, A. Donohoe, and E. Newsom, 2016: Southern Ocean warming delayed by circumpolar upwelling and equatorward transport. *Nature Geoscience*, **9**, 549–554, doi:10.1038/ngeo2731.

Bader, J., M. Flugge, N. Kvamsto, M. Mesquita, and A. Voigt, 2013: Atmospheric winter response to a projected future Antarctic sea ice reduction: a dynamical analysis. *Climate Dynamics*, **40**, 2710–2718, doi:10.1007/s00382-012-1507-9.

Baines, P., and K. Fraedrich, 1989: Topographic effects on the mean tropospheric flow patterns around Antarctica. *Journal of Atmospheric Sciences*, **46 (22)**, 3401–3415, doi:10.1175/1520-0469(1989)046⟨3401:TEOTMT⟩2.0.CO;2.

Baker, H., T. Woollings, and C. Mbengue, 2017: Eddy-driven jet sensitivity to diabatic heating in an idealised GCM. *Journal of Climate*, **30**, 6413–6431, doi:10.1175/JCLI-D-16-0864.1.

Baldwin, M., and T. Dunkerton, 2001: Stratospheric harbingers of anomalous weather regimes. *Science*, **294**, 581–584, doi:10.1126/science.1063315.

Baldwin, M., D. Stephenson, D. Thompson, T. Dunkerton, A. Charlton, and A. O'Neil, 2003: Stratospheric memory and skill of extended range weather forecasts. *Science*, **301**, 636–640, doi:10.1126/science.1087143.

Barnes, E., and L. Polvani, 2013: Response of the midlatitude jets, and of their variability, to increased greenhouse gases in the CMIP5 models. *Journal of Climate*, **26**, 7117–7135, doi:10.1175/JCLI-D-12-00536.1.

Barnes, E., and J. Screen, 2015: The impact of Arctic warming on the midlatitude jet-stream: Can it? Has it? Will it? *WIRES*, **6**, 277–286, doi:10.1002/wcc.337.

Bintanja, R., S. van Oldenborgh, B. Wouters, and C. Katsman, 2013: Important role for ocean warming and increased ice-shelf melt in Antarctic sea ice expansion. *Nature Geoscience*, **6**, 376–379, doi:10.1038/NGEO1767.

Blackport, R., and P. Kushner, 2016: The transient and equilibrium climate response to rapid summertime sea ice loss in CCSM4. *Journal of Climate*, **29**, 401–417, doi:10.1175/JCLI-D-15-0284.1.

Blackport, R., and P. Kushner, 2017: Isolating the atmospheric circulation response to Arctic sea ice loss in the coupled climate system. *Journal of Climate*, **30**, 2163–2185, doi:10.1175/JCLI-D-16-0257.1.

Boville, B., and X. Cheng, 1988: Upper boundary effects in a general circulation model. *Journal of Atmospheric Sciences*, **45 (18)**, 2591–2606, doi:10.1175/1520-0469(1988)045⟨2591:UBEIAG⟩2.0.CO;2.

Bracegirdle, T., P. Hyder, and C. Holmes, 2018: CMIP5 diversity in southern westerly jet projections related to historical sea ice area: strong link to strengthening and weak link to shift. *Journal of Climate*, **31**, 195–211, doi:10.1175/JCLI-D-17-0320.1.

Bracegirdle, T., and G. Marshall, 2012: The reliability of Antarctic tropospheric pressure

and temperature in the latest global reanalyses. *Journal of Climate*, **25 (20)**, 7138–7146, doi:10.1175/JCLI-D-11-00685.1.

Bracegirdle, T., D. Stephenson, J. Turner, and T. Phillips, 2015: The importance of sea ice area biases in 21st century multimodel projections of Antarctic temperature and precipitation. *Geophysical Research Letters*, **42**, 10,832–10,839, doi:10.1002/2015GL067055.

Bracegirdle, T., E. Suckburgh, J. Salee, Z. Wang, A. Meijers, N. Bruneau, T. Phillips, and L. Wilcox, 2013: Assessment of surface winds over the Atlantic, Indian and Pacific Ocean sectors of the Southern Ocean in CMIP5 models: historical bias, forcing response and state dependence. *Journal of Geophysical Research*, **118**, 547–562, doi:10.1002/jgrd.50153.

Bromwich, D., J. Nicolas, A. Monaghan, M. Lazzara, L. Keller, G. Weidner, and A. Wilson, 2013: Central West Antarctica among the most rapidly warming regions on earth. *Nature Geoscience*, **6**, 139–145, doi:10.1038/NGEO1671.

Budd, W., 1991: Antarctica and global change. *Climatic Change*, **18**, 271–299.

Butler, A., D. Thompson, and R. Heikes, 2010: The steady-state atmospheric circulation to climate change-like thermal forcings in a simple general circulation model. *Journal of Climate*, **23**, 3474–3496, doi:10.1175/2010JCLI3228.1.

Cabre, A., I. Marinov, and A. Gnanadesikan, 2017: Global atmospheric teleconnections and multidecadal climate oscillations driven by Southern Ocean convection. *Journal of Climate*, **30**, 8,107–8,126, doi:10.1175/JCLI-D-16-0741.1.

Cai, D., M. Dameris, H. Garny, and T. Runde, 2012: Implications of all season arctic sea ice anomalies on the stratosphere. *Atmospheric Chemistry and Physics*, **12**, 11 819–11 831, doi:10.5194/acp-12-11819-2012.

Catchpole, D., S. Kopylov, and D. Verdonik, 2010: Montreal protocol on substances that deplete the ozone layer. Tech. rep., United Nations Environment Programme.

Ceppi, P., Y. Hwang, D. Frierson, and D. Hartmann, 2012: Southern Hemisphere jet latitude biases in CMIP5 models linked to shortwave cloud forcings. *Geophysical Research Letters*, **39 (L19708)**, doi:10.1029/2012GL053115.

Charlton-Perez, A., and Coauthors, 2013: On the lack of stratospheric dynamic variability in low-top versions of the CMIP5 models. *Journal of Geophysical Research*, **118**, 2494–2505, doi:10.1002/jgrd/50125.

Charney, J., and P. Drazin, 1961: Propogation of planetary scale disturbances from the lower into the upper atmosphere. *Journal of Geophysical Research*, **66 (1)**, 83–109, doi:10.1029/JZ066i001p00083.

Chemke, R., L. Polvani, and C. Deser, 2019: The effect of Arctic sea-ice loss on the Hadley circulation. *Geophysical Research Letters*, **46**, 963–972, doi:10.1029/2018GL081110.

Chen, H., F. Zhang, and R. Alley, 2016: The robustness of midlatitude weather pattern changes due to Arctic sea ice loss. *Journal of Climate*, **29**, 7831–7849, doi:10.1175/JCLI-D-16-0167.1.

Chiang, J., and C. Bitz, 2005: Influence of high latitude ice cover on the marine intertropical convergence zone. *Climate Dynamics*, **25**, 477–496, doi:10.1007/s00382-005-0040-5.

Cohen, J., and Coauthors, 2014: Recent Arctic amplification and extreme mid-latitude weather. *Nature Geoscience*, **7**, 627–637, doi:10.1038/NGEO2234.

Collins, M., and Coauthors, 2013: Climate Change: The Physical Science Basis. Contribution of Working Group I to the Fifth Assessment Report of the Intergovernmental Panel on Climate Change. Cambridge University Press.

Comiso, J., 2000: Variability and trends in Antarctic surface temperatures from in situ and satellite infrared measurements. *Journal of Climate*, **13 (1674-1696)**.

Comiso, J., R. Gersten, L. Stock, J. Turner, G. Perez, and K. Cho, 2017a: Positive trend in the Antarctic sea ice cover and associated changes in surface temperature. *Journal of Climate*, **30**, 2251–2267, doi:10.1175/JCLI-D-16-0408.1.

Comiso, J., C. Meier, and R. Gersten, 2017b: Variability and trends in the Arctic sea ice cover: Results from different techniques. *Journal of Geophysical Research*, **122 (8)**, 6883–6900, doi:10.1002/2017JC012768.

Danabasoglu, G., S. Bates, B. Briegleb, S. Jayne, M. Jochum, W. Large, S. Peacock, and S. Yeager, 2012: The CCSM4 ocean component. *Journal of Climate*, **25**, 1,361–1,389, doi:10.1175/JCLI-D-11-00091.1.

De, B., and Y. Wu, 2018: Robustness of the stratospheric pathway in linking the Barents-Kara Sea sea ice variability to the mid-latitude circulation in CMIP5 models. *Climate Dynamics*, doi:10.1007/s00382-018-4576-6.

DeConto, R., and D. Pollard, 2016: Contribution of Antarctica to past and future sea-level rise. *Nature*, **531**, 591–597, doi:10.1038/nature17145.

Dee, D., and Coauthors, 2011: The ERA-Interim reanalysis: configuration and performance of the data assimilation system. *Quarterly Journal of the Royal Meterological Society*, **137**, 553–597, doi:10.1002/qj.828.

Deser, C., L. Sun, R. Tomas, and J. Screen, 2016: Does ocean coupling matter for the northern extratropical response to projected Arctic sea ice loss? *Geopysical Reseach Letters*, **43**, 2149–2157, doi:10.1002/2016GL067792.

Deser, C., R. Tomas, M. Alexander, and D. Lawrence, 2010: The seasonal atmospheric response to projected Arctic sea ice loss in the late twenty-first century. *Journal of Climate*, **23**, 333–351, doi:10.1175/2009JCLI3053.1.

Deser, C., R. Tomas, and L. Sun, 2015: The role of ocean-atmosphere coupling in the zonal-

mean atmospheric response to Arctic sea ice loss. *Journal of Climate*, **28**, 2168–2186, doi:10.1175/JCLI-D-14-00325.1.

Ding, Q., and E. Steig, 2013: Temperature change on the Antarctic Peninsula linked to the tropical Pacific. *Journal of Climate*, **26**, 7570–7585, doi:10.1175/JCLI-D-12-00729.1.

Ding, Q., E. Steig, D. Battisti, and M. Kuttel, 2011: Winter warming in West Antarctica caused by central tropical Pacific warming. *Nature Geoscience*, **4**, 398–403, doi:10.1038/ngeo1129.

Donohoe, A., J. Marshall, D. Ferreira, and D. McGee, 2012: The relationship between ITCZ location and cross-equatorial atmospheric heat transport: From the seasonal cycle to the last glacial maximum. *Journal of Climate*, **26**, 3,597–3,618, doi:10.1175/JCLI-D-12-00467.1.

Dunn-Sigouin, E., and T. Shaw, 2015: Comparing and contrasting extreme stratospheric events, including their coupling to the troposheric circulation. *Journal of Geophysical Research*, **120**, 1374–1390, doi:10.1002/2014JD022116.

Eisenman, I., T. Schneider, D. Battisti, and C. Bitz, 2011: Consistent changes in the sea ice seasonal cycle in response to global warming. *Journal of Climate*, **24**, 5325–5335, doi:10.1175/2011JCLI4051.1.

England, M., A. Jahn, and L. Polvani, 2019: Non-uniform contribution of internal variability to recent Arctic sea ice loss. *Journal of Climate*, **(In press)**, doi:10.1175/JCLI-D-18-0864.1.

England, M., L. Polvani, K. Smith, L. Landrum, and M. Holland, 2016a: Robust response of the Amundsen Sea Low to stratospheric ozone depletion. *Geophysical Research Letters*, **43**, 8207–8213, doi:10.1002/2016GL070055.

England, M., T. Shaw, and L. Polvani, 2016b: Troposphere-stratosphere dynamical coupling

in the Southern high latitudes, and its linkage to the Amundsen Sea. *Journal of Geophysical Research*, **121**, 3776–3789, doi:10.1002/2015JD024254.

England, M., L. Sun, and L. Polvani, 2018: Contrasting the antarctic and arctic atmospheric response to projected sea ice loss in the late 21st century. *Journal of Climate*, **31**, 6353–6370, doi:10.1175/JCLI-D-17-0666.1.

Ferreira, D., J. Marshall, C. Bitz, S. Solomon, and A. Plumb, 2014: Antarctic Ocean and sea ice response to ozone depletion: A two-time-scale problem. *Journal of Climate*, **28**, 1206–1226, doi:10.1175/JCLI-D-14-00313.1.

Fogt, R., D. Bromwich, and K. Hines, 2011: Understanding the SAM influence on the South Pacific ENSO teleconnection. *Climate Dynamics*, **36**, 1555–1576, doi:10.1007/s00382-010-0905-0.

Fogt, R., J. Jones, and J. Renwick, 2012a: Seasonal zonal asymmetries in the Southern Annular Mode and their impact on regional temperature anomalies. *Journal of Climate*, **25**, 6253–6270, doi:10.1175/JCLI-D-11-00474.1.

Fogt, R., and A. Wovrosh, 2015: The relative influence of tropical sea surface temperatures and radiative forcing on the Amundsen Sea Low. *Journal of Climate*, **28**, 8540–8555, doi:10.1175/JCLI-D-15-0091.1.

Fogt, R., A. Wovrosh, R. Langen, and I. Simmonds, 2012b: The characteristic variability and connection to the underlying synoptic activity of the Amundsen-Bellingshausen Seas Low. *Journal of Geophysical Research*, **117 (D07111)**, doi:10.1029/2011JD017337.

Fogt, R., and E. Zbacnik, 2014: Sensitivity of the Amundsen Sea Low to stratospheric ozone depletion. *Journal of Climate*, **27**, 9383–9400, doi:10.1175/JCLI-D-13-00657.1.

Gagne, M., N. Gillett, and J. Fyfe, 2015: Observed and simulated changes in Antarctic sea ice extent over the past 50 years. *Geopysical Reseach Letters*, **42**, 90–95, doi:10.1002/2014GL062231.

Gent, P., and Coauthors, 2011: The Community Climate System Model version 4. *Journal of Climate*, **24**, 4973–4991, doi:10.1175/2011JCLI4083.1.

Gerber, E., and Coauthors, 2012: Understanding the impact of stratospheric dynamics and variability on the earth system. *Bulletin of the American Meteorological Society*, **93 (6)**, 845–859, doi:10.1175/BAMS-D-11-00145.1.

Gettelman, A., J. Kay, and J. Fasullo, 2013: Spatial decomposition of climate feedbacks in the Community Earth System Model. *Journal of Climate*, **26**, 3544–3561, doi:10.1175/JCLI-D-12-00497.1.

Gong, H., L. Wang, W. Chen, X. Chen, and D. Nath, 2017: Biases of the wintertime Arctic Oscillation in CMIP5 models. *Environmental Research Letters*, **12 (014001)**, doi:10.1088/1748-9326/12/1/014001.

Grise, K., and L. Polvani, 2014: The response of midlatitude jets to increased co2: Distinguishing the roles of sea surface temperature and direct radiative forcing. *Journal of Geophysical Research*, **41**, 6863–6871, doi:10.1002/2014GL061638.

Grise, K., S. Son, G. Correa, and L. Polvani, 2014: The response of extratropical cyclones in the Southern Hemisphere to stratospheric ozone depletion in the 20th century. *Atmospheric Science Letters*, **15**, 29–36, doi:10.1002/asl2.458.

Harnik, N., J. Perlwitz, and T. Shaw, 2011: Observed decadal change in downward wave coupling between the stratosphere and troposphere in the Southern Hemisphere. *Journal of Climate*, **24**, 4558–4569, doi:10.1175/2011JCLI4118.1.

Hawkins, E., and R. Sutton, 2009: The potential to narrow uncertainty in regional climate predictions. *Bulletin of the American Meteorological Society*, **90 (8)**, 1,095–1,107, doi:10.1175/2009BAMS2607.1.

Holland, M., D. Bailey, B. Briegleb, B. Light, and E. Hunke, 2012: Improved sea ice short-

wave radiation physics in CCSM4: The impact of melt ponds and aerosols on Arctic sea ice. *Journal of Climate*, **25**, 1413–1430, doi:10.1175/JCLI-D-11-00078.1.

Holland, M., and R. Kwok, 2012: Wind-driven trends in Antartic sea-ice drift. *Nature Geoscience*, **5**, 872–875, doi:10.1038/NGEO1627.

Hosking, J., A. Orr, T. Bracegirdle, and J. Turner, 2016: Future circulation changes off West Antarctica: Sensitivity of the Amundsen Sea Low to projected anthropogenic forcing. *Geophysical Research Letters*, **43**, 367–376, doi:10.1002/2015GL067143.

Hosking, J., A. Orr, G. Marshall, J. Turner, and T. Phillips, 2013: The influence of the Amundsen-Bellingshausen Seas Low on the climate of West Antarctica and its representation in coupled climate model simulations. *Journal of Climate*, **26**, 6633–6648, doi:10.1175/JCLI-D-12-00813.1.

Hwang, Y., S. Xie, C. Deser, and S. Kang, 2017: Connecting tropical climate change with Southern Ocean heat uptake. *Geophysical Research Letters*, **44**, 9,449–9,457, doi:10.1002/2017GL074972.

Jacobs, S., C. Giulivi, and P. Mele, 2002: Freshening of the Ross Sea during the late 20th century. *Science*, **297 (5580)**, 386–389, doi:10.1126/science.1069574.

Jahn, A., J. Kay, M. Holland, and D. Hall, 2016: How predictable is the timing of a summer ice-free Arctic? *Geophysical Research Letters*, **43**, 1,029–1,136, doi:10.1002/2016GL070067.

Joughin, I., and R. Alley, 2011: Stability of the West Antarctic ice sheet in a warming world. *Nature Climate Change*, **4**, 506–513, doi:10.1038/ngeo1194.

Kanamitsu, M., W. Ebisuzaki, J. Woollen, S. Yang, J. Hnilo, M. Fiorino, and G. Potter, 2002: NCEP–DOE AMIP-II reanalysis (R-2). *Bulletin of the American Meteorological Society*, **83**, 1631–1644, doi:10.1175/BAMS-83-11-1631.

Kang, S., I. Held, D. Frierson, and M. Zhao, 2008: The response of the ITCZ to extratropical thermal forcing: Idealized slab-ocean experiments with a GCM. *Journal of Climate*, **21**, 3,521–3,532, doi:10.1175/2007JCLI2146.1.

Kang, S., L. Polvani, J. Fyfe, and M. Sigmond, 2011: Impact of polar ozone depletion on subtropical precipitation. *Science*, **332 (6032)**, 951–954, doi:10.1126/science.1202131.

Kay, J., M. Holland, C. Bitz, E. Blanchard-Wrigglesworth, A. Gettelman, A. Conley, and D. Bailey, 2012: The influence of local feedbacks and northward heat transport on the equilibrium Arctic climate response to increased greenhouse gas forcing. *Journal of Climate*, **25**, 5,433–5,450, doi:10.1175/JCLI-D-11-00622.1.

Kay, J., and Coauthors, 2015: The Community Earth System Model (CESM) large ensemble project: A community resource for studying climate change in the presence of internal climate variability. *Bulletin of the American Meteorological Society*, **96**, 1333–1349, doi:10.1175/BAMS-D-13-00255.1.

Kidston, J., and E. Gerber, 2010: Intermodel variability of the poleward shift of the austral jet stream in the CMIP3 integrations linked to biases in 20th century climatology. *Geophysical Research Letters*, **37 (L09708)**, doi:10.1029/2010GL042873.

Kidston, J., A. Scaife, S. Hardiman, D. Mitchell, N. Butchart, M. Baldwin, and L. Gray, 2015: Stratospheric influence on tropospheric jet streams, storm tracks and surface weather. *Nature Geoscience*, **8**, 433–440, doi:10.1038/ngeo2424.

Kidston, J., A. Taschetto, D. Thompson, and M. England, 2011: The influence of Southern Hemisphere sea ice extent on the latitude of the midlatitude jet stream. *Geopysical Reseach Letters*, **38 (L15804)**, doi:10.1029/2011GL048056.

Kim, B., S. Son, S. Min, J. Jeong, S. Kim, X. Zhang, T. Shim, and J. Yoon, 2014: Weakening of the stratospheric polar vortex by Arctic sea ice loss. *Nature Communications*, **5 (4646)**, doi:10.1038/ncomms5646.

Konrad, H., L. Gilbert, S. Cornford, A. Payne, A. Hogg, A. Muir, and A. Shepherd, 2017: Uneven onset and pace of ice-dynamical imbalance in the Amundsen Sea Embayment, West Antarctica. *Geophysical Research Letters*, **44 (2)**, 910–918, doi:10.1002/2016GL070733.

Kostov, Y., J. Marshall, U. Hausmann, K. Armour, D. Ferreira, and M. Holland, 2017: Fast and slow responses of Southern Ocean sea surface temperatures to SAM in coupled climate models. *Climate Dynamics*, **48**, 1595–1609, doi:10.1007/s00382-016-3162-z.

Kushner, P., I. Held, and T. Delworth, 2000: Southern Hemisphere atmospheric circulation response to global warming. *Journal of Climate*, **14**, 2238–2249, doi:10.1175/1520-0442(2001)014⟨0001:SHACRT⟩2.0.CO;2.

Kuttippurath, J., and P. Nair, 2017: The signs of Antarctic ozone hole recovery. *Scientific Reports*, **7 (585)**, doi:10.1038/s41598-017-00722-7.

Lachlan-Cope, T., W. Connolley, and J. Turner, 2001: The role of the non-axisymmetric Antarctic orography in forcing the observed pattern of variability of the Antarctic climate. *Geophysical Research Letters*, **28 (21)**, 4111–4114, doi:10.1029/2001GL013465.

Landrum, L., M. Holland, M. Raphael, and L. Polvani, 2017: Stratospheric ozone depletion: An unlikely driver of the regional trends in Antarctic sea ice in austral fall in the late twentieth century. *Geophysical Research Letters*, **44**, 11 062–11 070, doi:10.1002/2017/GL075618.

Lefebvre, W., H. Goosse, R. Timmermann, and T. Fichefet, 2004: Influence of the Southern Annular Mode on the sea ice-ocean system. *Journal of Geophysical Research*, **109 (C09005)**, doi:10.1029/2004JC002403.

Li, X., D. Holland, P. Gerber, and C. Yoo, 2015: Rossby waves mediate impacts of tropical oceans on West Antarctic atmospheric circulation in austral winter. *Journal of Climate*, **28**, 8151–8164, doi:10.1175/JCLI-D-15-0113.1.

Liu, J., J. Curry, H. Wang, M. Song, and R. Horton, 2012: Impact of declining Arctic sea ice

on winter snowfall. *Proceedings of the National Academy of Sciences of the United States of America*, **109**, 4,074–4,079, doi:10.1073/pnas.1114910109.

Liu, J., M. Song, R. Horton, and Y. Hu, 2013: Reducing spread in climate model projections of a September ice-free Arctic. *Proceedings of the National Academy of Sciences of the United States of America*, **110**, 12,571–12,576, doi:10.1073/pnas.1219716110.

Liu, W., and A. Fedorov, 2019: Timescales and mechanisms of global climate impacts of Arctic sea ice loss mediated by the Atlantic meridional overturning circulation. *Geophysical Research Letters*, **46**, 944–952, doi:10.1029/2018GL080602.

Lorenz, D., and E. DeWeaver, 2007: Tropopause height and zonal wind response to global warming in the ipcc scenario integrations. *Journal of Geophysical Research*, **112 (D10119)**, doi:10.1029/2006JD008087.

Ludescher, J., N. Yuan, and A. Bunde, 2018: Detecting the statistical significance of the trends in the antarctic sea ice extent: an indication for a turning point. *Climate Dynamics*, doi:10.1007/s00382-018-4579-3.

Maksym, T., S. Stammerjohn, S. Ackley, and R. Massom, 2012: Antarctic sea ice - a polar opposite? *Oceanography*, **25 (3)**, 140–151, doi:10.5670/oceanog.2012.88.

Manney, G., M. Santee, and coauthors, 2011: Unprecedented arctic ozone loss in 2011. *Nature*, **478**, 469–475, doi:10.1038/nature10556.

Marsh, D., M. Mills, D. Kinnison, J. Lamarque, N. Calvo, and L. Polvani, 2013: Climate change from 1850 to 2005 simulated in CESM1(WACCM). *Journal of Climate*, **26**, 7372–7391, doi:10.1175/JCLI-D-12-00558.1.

Marshall, G., 2003: Trends in the Southern Annular Mode from observations and reanalysis. *Journal of Climate*, **16**, 4134–4143, doi:10.1175/1520-0442(2003)016⟨4134:TITSAM⟩2.0.CO;2.

Marshall, J., K. Armour, J. Scott, Y. Kostov, U. Hausmann, D. Ferreira, T. Shepherd, and C. Bitz, 2014: The ocean's role in polar climate change: asymmetric Arctic and Antarctic responses to greenhouse gas and ozone forcing. *Philosophical transactions of the royal society*, **372 (20130040)**, doi:10.1098/rsta.2013.0040.

Massom, R., S. Stammerjohn, W. Lefebvre, S. Harangozo, N. Adams, T. Scambos, M. Pook, and C. Fowler, 2008: West Antarctic Peninsula sea ice in 2005: Extreme ice compaction and ice edge retreat due to strong anomaly with respect to climate. *Journal of Geophysical Research*, **113 (C02S20)**, doi:10.1029/2007JC004239.

McCusker, K., J. Fyfe, and M. Sigmond, 2016: Twenty five winters of unexpected Eurasian cooling unlikely due to Arctic sea ice loss. *Nature Geoscience*, **9**, 838–843, doi:10.1038/NGEO2820.

McCusker, K., P. Kushner, J. Fyfe, M. Sigmond, V. Kharin, and C. Bitz, 2017: Remarkable separability of circulation response to Arctic sea ice loss and greenhouse gas forcing. *Geopysical Reseach Letters*, **44**, 7955–7964, doi:10.1002/2017GL074327.

McKenna, C., T. Bracegirdle, E. Shuckburgh, P. Haynes, and M. Joshi, 2018: Arctic sea ice loss in different regions leads to contrasting Northern Hemisphere impacts. *Geopysical Reseach Letters*, **45**, doi:10.1002/2017GL076433.

Meehl, G., J. Arblaster, C. Chung, M. Holland, A. DuVivier, L. Thompson, D. Yang, and C. Bitz, 2019: Sustained ocean changes contributed to sudden antarctic sea ice retreat in late 2016. *Nature Communications*, **10 (14)**, doi:10.1038/s41467-018-07865-9.

Menendez, C., V. Serafini, and H. LeTreut, 1999: The effect of sea ice on the transient atmospheric eddies of the Southern Hemisphere. *Climate Dynamics*, **15**, 659–671, doi:10.1007/s003820050308.

Min, S., and S. Son, 2013: Multimodel attribution of the Southern Hemisphere Hadley cell widening: Major role of ozone depletion. *Journal of Geophysical Research*, **118**, 3007–3015, doi:10.1002/jgrd.50232.

Mori, M., M. Watanabe, H. Shiogama, J. Inoue, and M. Kimoto, 2014: Robust Arctic sea ice influence on the frequent Eurasian cold winters in past decades. *Nature Geoscience*, **7**, 869–873, doi:10.1038/NGEO2277.

Nicolas, J., and D. Bromwich, 2014: New reconstruction of Antarctic near-surface temperatures: Multidecadal trends and reliability of global reanalyses. *Journal of Climate*, **27**, 8070–8093, doi:10.1175/JCLI-D-13-00733.1.

NSIDC, 2019: Sea ice index. URL https://nsidc.org/data/seaice_index.

Osborne, J., J. Screen, and M. Collins, 2017: Ocean-atmosphere state dependence of the atmospheric response to Arctic sea ice loss. *Journal of Climate*, **30**, 1537–1552, doi:10.1175/JCLI-D-16-0531.1.

Oudar, T., E. Sanchez-Gomez, F. Chauvin, J. Cattiaux, L. Terray, and C. Cassou, 2017: Respective roles of direct GHG radiative forcing and induced Arctic sea ice loss on the Northern Hemisphere atmospheric circulation. *Climate Dynamics*, **49**, 3,693–3,717, doi:10.1007/s00382-017-3541-0.

Overland, J., J. Francis, R. Hall, E. Hana, S. Kim, and T. Vihma, 2015: The melting Arctic and midlatitude weather patterns: Are they connected? *Journal of Climate*, **28**, 7917–7932, doi:10.1175/JCLI-D-14-00822.1.

Overland, J., and M. Wang, 2013: When will the summer Arctic be nearly sea ice free? *Geophysical Research Letters*, **40**, 2,097–2,101, doi:10.1002/grl.50316.

Parkinson, C., and D. Cavalieri, 2012: Antarctic sea ice variability and trends, 1979-2010. *Cryosphere*, **6**, 871–880, doi:10.5194/tc-6-871-2012.

Peings, Y., and G. Magnusdottir, 2014: Response of the wintertime Northern Hemisphere atmospheric circulation to current and projected Arctic sea ice decline: A numerical study with CAM5. *Journal of Climate*, **27**, 244–264, doi:10.1175/JCLI-D-13-00272.1.

Pezza, A., H. Rashid, and I. Simmonds, 2012: Climate links and recent extremes in Antarctic sea ice, high-latitude cyclones, Southern Annular Mode and ENSO. *Climate Dynamics*, **38**, 57–73, doi:10.1007/s00382-011-1044-y.

Plumb, A., 2010: Planetary waves. American Geophysical Union.

Polvani, L., 2011: Large cancellation, due to ozone recovery, of future Southern Hemisphere atmospheric circulation trends. *Geophysical Research Letters*, **38 (L04707)**, doi:10.1029/2011GL046712.

Polvani, L., and P. Kushner, 2002: Tropospheric response to stratospheric perturbations in a relatively simple general circulation model. *Geophysical Research Letters*, **29 (7)**, doi:10.1029/2001GL014284.

Polvani, L., and K. Smith, 2013: Can natural variability explain observed Antarctic sea ice trends? New modelling evidence from CMIP5. *Geopysical Reseach Letters*, **40**, 3195–3199, doi:10.1002/grl.50578.

Polvani, L., and D. Waugh, 2004: Upward wave activity flux as a precursor to extreme stratospheric events and subsequent anomalous surface weather regimes. *Journal of Climate*, **17**, 3548–3554, doi:10.1175/1520-0442(2004)017⟨3548:UWAFAA⟩2.0.CO;2.

Polvani, L., D. Waugh, G. Correa, and S. Son, 2011: Stratospheric ozone depletion: The main driver of twentieth-century atmospheric circulation changes in the Southern Hemisphere. *Journal of Climate*, **24**, 795–812, doi:10.1175/2010JCLI3772.1.

Previdi, M., and L. Polvani, 2014: Climate system response to stratospheric ozone depletion and recovery. *Quarterly Journal of the Royal Meterological Society*, **140**, 2401–2419, doi:10.1002/qj.2330.

Purich, A., and S. Son, 2012: Impact of Antarctic ozone depletion and recovery on Southern Hemisphere precipitation, evaporation and extreme changes. *Journal of Climate*, **25**, 3145–3154, doi:10.1175/JCLI-D-11-00383.1.

Quere, C. L., R. Andrews, and coauthors, 2018: Global carbon budget 2018. *Earth System Science Data*, **10**, 2141–2194, doi:10.5194/essd-10-2141-2018.

Ramaswamy, V., M. Schwarzkopf, and W. Randel, 1996: Letter — published: 15 august 1996 fingerprint of ozone depletion in the spatial and temporal pattern of recent lower-stratospheric cooling. *Nature*, **382**, 616–618, doi:10.1038/382616a0.

Randel, W., 1988: The seasonal evolution of planetary waves in the Southern Hemisphere stratosphere and troposphere. *Quarterly Journal of the Royal Meterological Society*, **114**, 1385–1409, doi:10.1002/qj.49711448403.

Raphael, M., 2001: Response of the large-scale, Southern Hemisphere extratropical atmospheric circulation to extremes of Antarctic sea ice concentration in general circulation model. *Polar Geography*, **25 (3)**, 218–238, doi:10.1080/10889370109377714.

Raphael, M., W. Hobbs, and I. Wainer, 2011: The effect of Antarctic sea ice on the Southern Hemisphere atmosphere during the southern summer. *Climate Dynamics*, **36**, 1403–1417, doi:10.1007/s00382-010-0892-1.

Raphael, M., and Coauthors, 2016: The Amundsen Sea Low. *Bulletin of Atmospheric Science*, **97 (1)**, 111–121, doi:10.1175/BAMS-D-14-00018.1.

Renwick, J., 2002: Southern Hemisphere circulation and relations with sea ice and sea surface temperature. *Journal of Climate*, **15**, 3058–3068, doi:10.1175/1520-0442(2002)015⟨3058:SHCARW⟩2.0.CO;2.

Rignot, E., J. Mouginout, B. Scheuchl, M. van den Broeke, M. van Wessem, and M. Morlighem, 2019: Four decades of Antarctic ice sheet mass balance from 1979-2017. *Proceedings of the National Academy of Sciences of the United States of America*, **116 (4)**, 1095–1103, doi:10.1073/pnas.1812883116.

Rintoul, S., 2000: *Southern Ocean currents and climate*, Vol. 133, 41–50. Academic Press, San Diego.

Riser, S., H. Freeland, and coauthors, 2016: Fifteen years of ocean observations with the global Argo array. *Nature Climate Change*, **6**, 145–153, doi:10.1038/nclimate2872.

Ritz, C., T. Edwards, G. Durand, A. Payne, V. Peyaud, and R. Hindmarsh, 2015: Potential sea-level rise from Antarctic ice-sheet instability constrained by observations. *Nature*, **528**, 115–118, doi:10.1038/nature16147.

Rosenblum, E., and I. Eisenman, 2017: Sea ice trends in climate models only accurate in runs with biased global warming. *Journal of Climate*, **30**, 6265–6278, doi:10.1175/JCLI-D-16-0455.1.

Salzmann, M., 2017: The polar amplication asymmetry: role of Antarctic surface height. *Earth System Dynamics*, **8**, 323–336, doi:10.5194/esd-80323-2017.

Scambos, T., and Coauthors, 2017: How much, how fast?: A science review and outlook for research on the instability of Antarctica's Thwaites Glacier in the 21st century. *Global and Planetary Change*, **153**, 16–34, doi:10.1016/j.gloplacha.2017.04.008.

Schneider, D., C. Deser, and Y. Okumura, 2012: An assessment and interpretation of the observed warming of West Antarctica in the austral spring. *Climate Dynamics*, **38**, 323–347, doi:10.1007/s00382-010-0985-x.

Schweiger, A., R. Lindsay, J. Zhang, M. Steele, and H. Stern, 2011: Uncertainty in modeled Arctic sea ice volume. *Journal of Geophysical Research*, **116 (C00D06)**, doi:10.1029/2011JC007084.

Screen, J., 2017a: Far-flung effects of Arctic warming. *Nature Geoscience*, **10**, 253–54, doi:10.1038/ngeo2924.

Screen, J., 2017b: Simulated atmospheric response to regional and pan-Arctic sea ice loss. *Journal of Climate*, **30**, 3945–3962, doi:10.1175/JCLI-D-16-0197.1.

Screen, J., and J. Francis, 2016: Contrubtion of sea ice loss to Arctic amplification is regulated by Pacific Ocean decadal variability. *Nature Climate Change*, **6**, 856–860, doi: 10.1038/nclimate3011.

Screen, J., and I. Simmonds, 2010: The central role of diminishing sea ice in recent Arctic temperature amplification. *Nature*, **464**, 1334–1337, doi:10.1038/nature09051.

Screen, J., I. Simmonds, C. Deser, and R. Tomas, 2013: The atmospheric response to three decades of observed Arctic sea ice loss. *Journal of Climate*, **26**, 1230–1248, doi:10.1175/JCLI-D-12-00063.1.

Screen, J., and Coauthors, 2018: Elucidating the effects of arctic sea ice loss on northern hemisphere climate. *Nature Geoscience*, **in press**.

Sevellec, F., A. Fedorov, and W. Liu, 2017: Arctic sea-ice decline weakens the Atlantic meridional overturning circulation. *Nature Climate Change*, **7**, 604–610, doi:10.1038/NCLIMATE3353.

Shaw, T., and J. Perlwitz, 2010: The impact of stratospheric model configuration on planetary scale waves in Northern Hemisphere winter. *Journal of Climate*, **23**, 6365–6381, doi:10.1175/2010JCLI3804.1.

Shaw, T., and J. Perlwitz, 2013: The life cycle of Northern Hemisphere downward wave coupling between the stratopshere and troposphere. *Journal of Climate*, **26**, 1745–1763, doi:10.1175/JCLI-D-12-00251.1.

Shaw, T., J. Perlwitz, and N. Harnik, 2010: Downward wave coupling between the stratosphere and troposphere: The importance of meridional wave guiding and comparison with zonal-mean coupling,. *Journal of Climate*, **23**, 6365–6381, doi:10.1175/2010JCLI3804.1.

Shaw, T., J. Perlwitz, N. Harnik, P. Newman, and S. Pawson, 2011: The impact of stratospheric ozone changes on downward wave coupling in the Southern Hemisphere. *Journal of Climate*, **24**, 4210–4229, doi:10.1175/2011JCLI4170.1.

Shaw, T., J. Perlwitz, and O. Weiner, 2014: Troposphere-stratosphere coupling: Links to North Atlantic weather and climate, including their representation in CMIP5 models. *Journal of Geophysical Research*, **119**, 5864–5880, doi:10.1002/2013JD021191.

Singh, H., C. Bitz, and D. Frierson, 2016: The global climate response to lowering surface orography of Antarctica and the importance of atmosphere-ocean coupling. *Journal of Climate*, **29**, 4137–4153, doi:10.1175/JCLI-D-15-0442.1.

Smith, D., N. Dunstone, A. Scaife, E. Fiedler, D. Copsey, and S. Hardiman, 2017: Atmospheric response to Arctic and Antarctic sea ice: The impotance of ocean-atmosphere coupling and the background state. *Journal of Climate*, **30**, 4547–4565, doi:10.1175/JCLI-D-16-0564.1.

Smith, D., and Coauthors, 2019: The Polar Amplification Model Intercomparison Project (PAMIP) contribution to CMIP6: investigating the causes and consequences of polar amplification. *Geoscientific Model Development*, **12**, 1,139–1,164, doi:10.5194/gmd-12-1139-2019.

Smith, K., and L. Polvani, 2017: Spatial patterns of recent Antarctic surface temperature trends and the importance of natural variability: lessons from multiple reconstructions and the CMIP5 models. *Climate Dynamics*, **48**, 2653–2670, doi:10.1007/s00382-016-3230-4.

Smith, K., L. Polvani, and D. Marsh, 2012: Mitigation of 21st century Antarctic sea ice loss by stratospheric ozone recovery. *Geophysical Research Letters*, **39 (L20701)**, doi:10.1029/2012GL053325.

Solomon, A., L. Polvani, K. Smith, and R. Abernathey, 2015: The impact of ozone depleting substances on the circulation, temperature, and salinity of the Southern Ocean: An attribution study with CESM1(WACCM4). *Geophysical Research Letters*, **42**, 5547–5555, doi:10.1002/2015GL064744.

Solomon, S., D. Ivy, D. Kinnison, M. Mills, R. Neely, and A. Schmidt, 2016: Emergence of

healing in the Antarctic ozone layer. *Science*, **353 (6296)**, 269–274, doi:10.1126/science.aae0061.

Son, S., and Coauthors, 2010: Impact of stratospheric ozone on Southern Hemisphere circulation change: A multimodel assessment. *Journal of Geophysical Research*, **115 (D00M07)**, doi:10.1029/2010JD014271.

Stearns, C., L. Keller, G. Weidner, and M. Sievers, 1997: *Antarctic meteorology and climatology*, Vol. 61, chap. 1, 1–21. American Geophysical Union.

Steig, E., D. Schneider, S. Rutherford, M. Mann, J. Comiso, and D. Shindell, 2009: Warming of the Antarctic ice-sheet surface since the 1957 International Geophysical Year. *Nature*, **457**, 459–463, doi:10.1038/nature07669.

Stroeve, J., and D. Notz, 2018: Changing state of Arctic sea ice across all seasons. *Environmental Research Letters*, **13 (10)**, 103 001, doi:10.1088/1748-9326/aade56.

Stuecker, M., C. Bitz, and K. Armour, 2017: Conditions leading to the unprecedented low Antarctic sea ice extent during the 2016 austral spring season. *Geophysical Research Letters*, **44**, 9008–9019, doi:10.1002/2017GL074691.

Sun, L., M. Alexander, and C. Deser, 2018: Evolution of the global coupled climate response to Arctic sea ice loss during 1990–2090 and its contribution to climate change. *Journal of Climate*, **31**, 7,823–7,843, doi:10.1175/JCLI-D-18-0134.1.

Sun, L., C. Deser, L. Polvani, and R. Tomas, 2014: Influence of projected Arctic sea ice loss on polar stratospheric ozone and circulation in spring. *Environmental Research Letters*, **9 (084016)**, doi:10.1088/1748-9326/9/084016.

Sun, L., C. Deser, and R. Tomas, 2015: Mechanisms of stratospheric and tropospheric circulation response to projected Arctic sea ice loss. *Journal of Climate*, **28**, 7824–7845, doi:10.1175/JCLI-D-15-0169.1.

Sun, L., J. Perlwitz, and M. Hoerling, 2016: What caused the recent "Warm Arctic, cold continents" trend pattern in winter temperatures? *Geopysical Reseach Letters*, **43**, 5345–5352, doi:10.1002/2016GL069024.

Swart, N., and J. Fyfe, 2013: The influence of recent Antarctic ice sheet retreat on simulated sea ice area trends. *Geophysical Research Letters*, **40**, 4328–4332, doi:10.1002/grl.50820.

Taylor, K., R. Stouffer, and G. Meehl, 2012: Overview of CMIP5 and the experiment design. *Bulletin of the American Meteorological Society*, **93**, 485–498, doi:10.1175/BAMS-D-11-00094.1.

Thompson, D., and S. Solomon, 2002: Interpretation of recent Southern Hemisphere climate change. *Science*, **296**, 895–899, doi:10.1126/science.1069270.

Thompson, D., S. Solomon, P. Kushner, M. England, K. Grise, and D. Karoly, 2011: Signatures of the Antarctic ozone hole in Southern Hemisphere surface climate change. *Nature Geoscience*, **4**, 741–749, doi:10.1038/NGEO1296.

Ting, M., K. Yochanan, R. Seager, and C. Li, 2009: Forced and internal twentieth-century SST trends in the North Atlantic. *Journal of Climate*, **22 (5)**, 1469–1481, doi:10.1175/2008JCLI2561.1.

Tomas, R., C. Deser, and L. Sun, 2016: The role of ocean heat transport in the global climate response to projected Arctic sea ice loss. *Journal of Climate*, **29**, 6841–6859, doi:10.1175/JCLI-D-15-0651.1.

Trusel, L., K. Frey, S. Das, K. Karnauskas, P. Munneke, E. van Meijgaard, and M. van den Broeke, 2015: Divergent trajectories of Antarctic surface melt under two twenty first century climate scenarios. *Nature Geoscience*, **8**, 927–932, doi:10.1038/NGEO2563.

Turner, J., T. Bracegirdle, T. Phillips, G. Marhall, and J. Hosking, 2013a: An initial assessment of Antarctic sea ice extent in the CMIP5 models. *Journal of Climate*, **26**, 1473–1484, doi:10.1175/JCLI-D-12-00068.1.

Turner, J., S. Colwell, and S. Harangozo, 1997: Variability of precipitation over the coastal western Antarctic Peninsula from synoptic observations. *Journal of Geophysical Research*, **102 (D12)**, 13 999–14 007, doi:10.1029/96JD03359.

Turner, J., J. Hosking, G. Marshall, T. Phillips, and T. Bracegirdle, 2015: Antarctic sea ice increase consistent with intrinsic variability of the Amundsen Sea Low. *Climate Dynamics*, **46**, 2391–2402, doi:10.1007/s00382-015-2708-9.

Turner, J., T. Phillips, S. Hosking, G. Marshall, and A. Orr, 2013b: The Amundsen Sea low. *International Journal of Climatology*, **33**, 1818–1829, doi:10.1002/joc.3558.

Turner, J., T. Phillips, G. Marshall, J. Hosking, J. Pope, T. Bracegirdle, and P. Deb, 2017: Unprecedented springtime retreat of Antarctic sea ice in 2016. *Geophysical Research Letters*, **44**, 6868–6875, doi:10.1002/2017GL073656.

Turner, J., and Coauthors, 2009a: Antarctic climate change and the environment. Tech. rep., Scientific Committee on Antarctic Research, Cambridge.

Turner, J., and Coauthors, 2009b: Non-annular atmospheric circulation change induced by stratospheric ozone depletion and its role in the recent increase of Antarctic sea ice extent. *Geophysical Research Letters*, **36 (L08502)**, doi:10.1029/2009GL037524.

Uotila, P., A. Lynch, J. Cassano, and R. Cullather, 2007: Changes in Antarctic net precipitation in the 21st century based on Intergovernmental Panel on Climate Change (IPCC) model scenarios. *Journal of Geophysical Research*, **112 (D10107)**, doi:10.1029/2006JD007482.

van Loon, H., and R. Jenne, 1972: The zonal harmonic standing waves in the Southern Hemisphere. *Journal of Geophysical Research*, **77 (6)**, 992–1003.

Vaughan, D., and Coauthors, 2013: *Climate Change: The Physical Science Basis. Contribution of Working Group I to the Fifth Assessment Report of the Intergovernmental Panel on Climate Change*. Cambridge University Press.

Vihma, T., 2014: Effects of Arctic sea ice decline on weather and climate: A review. *Surv Geophys*, **35**, 1175–1214, doi:10.1007/s10712-014-9284-0.

Walsh, K., I. Simmonds, and M. Collier, 2000: Sigma-coordinate calculation of topographically forced baroclinicity around antarctica. *Dynamics of Atmospheres and Oceans*, **33**, 1–29, doi:10.1016/S0377-0265(00)00054-3.

Wang, G., H. Hendon, J. Arblaster, E. Lim, S. Abhik, and P. van Rensch, 2019: Compounding tropical and stratospheric forcing of the record low Antarctic sea-ice in 2016. *Nature Communications*, **10 (13)**, doi:10.1038/s41467-018-07689-7.

Wang, K., C. Deser, L. Sun, and R. Tomas, 2018: Fast response of the tropics to an abrupt loss of Arctic sea ice via ocean dynamics. *Geophysical Research Letters*, **45**, 4,264–4,272, doi:10.1029/2018GL077325.

Wingham, D., D. Wallis, and A. Shepherd, 2009: Spatial and temporal evolution of Pine Island Glacier thinning, 1995–2006. *Geophysical Research Letters*, **36 (L17501)**, doi:10.1029/2009GL039126.

WMO, 2014: Scientific assessment of ozone depletion: 2014. Tech. Rep. 55, WMO Global Ozone Research and Monitoring Project.

WMO, 2018: Scientific assessment of ozone depletion: 2018. Tech. Rep. 58, WMO Global Ozone Research and Monitoring Project.

Wu, X., I. Simmonds, and W. Budd, 1996: Southern Hemisphere climate system recovery from instantaneous sea-ice removal. *Quarterly Journal of the Royal Meterological Society*, **122**, 1501–1520, doi:10.1002/qj.49712253503.

Wu, Y., and K. Smith, 2016: Reponse of Northern Hemisphere midlatitude circulation to Arctic amplification in a simple atmospheric general circulation model. *Journal of Climate*, **29**, 2041–2058, doi:10.1175/JCLI-D-15-0602.1.

Yettella, V., and M. England, 2018: The role of internal variability in 21st century projections of the seasonal cycle of northern hemisphere surface temperature. *Journal of Geophysical Research*, **123**, 13 149–13 167, doi:10.1029/2018JD029066.

Yin, J., 2005: A consistent poleward shift of the storm tracks in simulations of 21st century climate. *Geopysical Reseach Letters*, **32 (L18701)**, doi:10.1029/2005GL023684.

Zhang, H., A. Clement, and P. DiNezio, 2014a: The South Pacific meridional mode: A mechanism for ENSO-like variability. *Journal of Climate*, **27**, 769–783, doi:10.1175/JCLI-D-13-00082.1.

Zhang, H., C. Deser, A. Clement, and R. Tomas, 2014b: Equatorial signatures of the Pacific Meridional modes: Dependence on mean climate state. *Geophysical Research Letters*, **41**, 568–574, doi:10.1002/2013GL058842.

Zhang, P., Y. Wu, I. Simpson, K. Smith, X. Zhang, and P. Callaghan, 2018: A stratospheric pathway linking a colder Siberia to Barents-Kara Sea sea ice loss. *Science Advances*, **4 (7)**, doi:10.1126/sciadv.aat6025.

Zhang, P., Y. Wu, and K. Smith, 2017: Prolonged effect of the stratospheric pathway in linking Barents-Kara Ssea sea ice variability to the midlatitude circulation in a simplified model. *Climate Dynamics*, doi:10.1007/s00382-017-3624-y.

Zunz, V., H. Goosse, and F. Massonnet, 2013: How does internal variability infleunce the ability of CMIP5 models to reproduce the recent trend in Southern Ocean sea ice extent. *The Cryosphere*, **7**, 451–468, doi:10.5194/tc-7-451-2013.